

MASS, HEAT, OXYGEN AND NUTRIENT FLUXES AT  
30°S AND THEIR IMPLICATIONS FOR THE  
PACIFIC-INDIAN THROUGH FLOW AND THE  
GLOBAL HEAT BUDGET

by

**Alison Marguerite Macdonald**

B.A. Bryn Mawr College, Bryn Mawr Pa.  
(1981)

Submitted in partial fulfillment of the  
requirements for the degree of

Master of Science

at the

MASSACHUSETTS INSTITUTE OF TECHNOLOGY

and the

WOODS HOLE OCEANOGRAPHIC INSTITUTION

July 1991

© Alison M. Macdonald 1991

The author hereby grants to MIT and to WHOI permission to reproduce  
and to distribute copies of this thesis document in whole or in part.

Signature of Author .....

Joint Program in Physical Oceanography  
Massachusetts Institute of Technology  
Woods Hole Oceanographic Institution

July 3, 1991

Certified by .....

Carl Wunsch  
Cecil and Ida Green Professor of Physical Oceanography  
Thesis Supervisor

Accepted by .....

Lawrence J. Pratt  
Chairman, Joint Committee for Physical Oceanography  
Massachusetts Institute of Technology  
Woods Hole Oceanographic Institution

WITHDRAWN  
FROM  
MIT LIBRARIES  
AUG 14 1991



# MASS, HEAT, OXYGEN AND NUTRIENT FLUXES AT 30°S AND THEIR IMPLICATIONS FOR THE PACIFIC-INDIAN THROUGH FLOW AND THE GLOBAL HEAT BUDGET

by

Alison Marguerite Macdonald

Submitted in partial fulfillment of the requirements for the degree of  
Master of Science at the Massachusetts Institute of Technology  
and the Woods Hole Oceanographic Institution

July 2, 1991

## Abstract

Six hydrographic basinwide sections, two in each of the three major ocean basins, are employed in a set of inverse calculations to determine the extent of exchange between the Pacific and Indian Oceans through the Indonesian Archipelago and the net global oceanic heat flux at 30°S.

Using a model which combines the data for the South Pacific and South Indian Oceans, it is found that even the largest existing estimates of Indonesian Passage through flow (20 Sv) are consistent with the data. However, the available information cannot limit the extent of the exchange, *i.e.* both smaller and larger through flows produce physically reasonable circulation patterns. The seasonal and interannual variations which have been found by other investigators and which we are incapable of resolving, lead us to conclude that in the long term mean an estimate of  $\sim 10$  Sv for the through flow is most reasonable.

Globally, at 30°S, we find a net oceanic heat flux of  $-1.1 \pm 1.7$  PW, which is not significantly different from zero. It is dominated by a large ( $>1$  PW) southward heat flux in the Indian Ocean. Large equatorward ( $\sim 0.8$  PW) heat flux values in the South Atlantic Basin are not consistent with our data. We therefore conclude that although our data are consistent with some water following the warm water return path for NADW (Gordon 1986), the cold water path must play the dominant role in the maintenance of the global thermohaline cell associated with the formation process of NADW.

Thesis Supervisor: Carl Wunsch,  
Cecil and Ida Green Professor of Physical Oceanography  
Department of Earth, Atmospheric and Planetary Sciences  
Massachusetts Institute of Technology

## Acknowledgements

I would first like to thank my thesis advisor, Carl Wunsch, not only for suggesting this thesis topic, but also for allowing me the freedom to explore the subject and field of scientific research independently, while always giving patiently of his time and guidance when I needed it. I would also like to thank the other members of my thesis committee, John Toole (who graciously provided the CTD section in the Indian Ocean), Harry Bryden and Paola Malanotte-Rizzoli, for their ideas and criticisms. I am indebted to Bud Brown for his technical assistance in producing the figures. Barbara Grant, I cannot thank enough. She has withstood my constant barrage of programming and data questions with great patience and those beautiful plots of velocity fields could not have been done without her. I wish her the best of luck in her future travels to faraway places. Last, but by no means least, I would like to thank my husband, Fran for his love and support.

This research was supported by NASA under contract NAGW-1048.

# Contents

<b>Abstract</b>	<b>3</b>
<b>Acknowledgements</b>	<b>4</b>
<b>Introduction</b>	<b>7</b>
<b>1 The South Pacific Ocean</b>	<b>11</b>
1.1 Introduction . . . . .	11
1.1.1 Water Masses and Circulation . . . . .	11
1.1.2 Review of Previous Results . . . . .	17
1.1.3 Description of the Data Used . . . . .	22
1.2 Comparison with 1983 Study . . . . .	25
1.3 Extension of Model S4-91 . . . . .	42
<b>2 The South Indian Ocean</b>	<b>77</b>
2.1 Introduction . . . . .	77
2.1.1 Water Masses and Circulation . . . . .	78
2.1.2 Review of Previous Results . . . . .	83
2.1.3 Description of the Data Used . . . . .	84
2.2 Indian Ocean Models . . . . .	89

<b>3</b>	<b>The South Atlantic Ocean</b>	<b>114</b>
3.1	Introduction . . . . .	114
3.1.1	Water Masses and Circulation . . . . .	115
3.1.2	Review of Previous Heat Flux Results . . . . .	118
3.1.3	Description of the Data Used . . . . .	120
3.2	Atlantic Ocean Models . . . . .	125
<b>4</b>	<b>Conclusions</b>	<b>145</b>
<b>A</b>	<b>Formulation of the Inverse Problem</b>	<b>152</b>
A.1	Introduction . . . . .	152
A.2	Inverse Basics . . . . .	153
A.3	Formulation of the Equations . . . . .	157
A.3.1	Data Preparation . . . . .	157
A.3.2	Choice of Isopycnal Layers . . . . .	158
A.3.3	Choice of Equation Weightings . . . . .	159
A.3.4	Choice of Initial Reference Levels . . . . .	161
A.3.5	Choice of the Best Estimate of the Solution . . . . .	162
<b>B</b>	<b>Error Analysis</b>	<b>166</b>
<b>C</b>	<b>Column Weighting for 18°S Section</b>	<b>174</b>
	<b>References</b>	<b>177</b>

## Introduction

The field of physical oceanography has its foundation in the desire to understand how the waters of the world ocean move, interact and evolve to affect the environment in which we live. Yet it seems that in many ways even the basic understanding of the general circulation escapes us. The oceans we explore are enormous in extent, variable in time and do not exist in isolation, but rather as part of an even more complex environment which drives the ocean system at all its boundaries. The measurements with which we interpret this system are often crude in comparison to its complexities; sparse, rarely synoptic and never complete enough to isolate all the competing processes.

We can contemplate the dynamics of such a system by breaking it down into smaller pieces ( *e.g.* into specific geographical regions, physical processes or scales of motion ); looking at the individual parts. However, in recent years as questions have been raised concerning changes in the world climate, it has become increasingly evident that a knowledge of the ocean circulation on global scales is paramount to our understanding of the role it plays in the evolution of the climate.

This thesis will address two different, but related aspects of how the waters of the three major ocean basins (Pacific, Indian and Atlantic) work together as part of the global system known as the world ocean. The first is the extent of exchange between the basins, with emphasis upon the exchange occurring between the Pacific and Indian Oceans through the Indonesian Archipelago. The second is their relative importance in balancing the global heat budget, particularly at 30°S. This will be done in three steps, each involving the application of inverse techniques to hydrographic and nutrient data.

In the first step we will concentrate on the exchange between the Pacific and Indian Oceans. The Scorpio sections at 43°S and 28°S in the Pacific Ocean will be used to determine a limit on the transport through the Indonesian Archipelago.

In the second step, sections across the Indian Ocean at 18°S and 31°S will be included to focus on how the constraints provided by the connecting ocean affect the problem and the results.

In the final step, sections across the Atlantic at approximately 15°S and 30°S allow us to effectively cut off the entire southern ocean. To the north, the Atlantic's sole connection to the other major ocean basins is the relatively narrow and shallow Bering Straits. The advantage to including the Atlantic basin in this work is that it allows the oceanic fluxes of mass, heat and nutrients to be calculated in a consistent manner across a complete latitudinal circle.

In the annual global mean, there is a net gain of radiation at the equator while at the poles, there is a net loss of radiation. How the ocean and atmosphere act as a system to equilibrate this imbalance is an important outstanding question which concerns both meteorologists and physical oceanographers looking at climate evolution. The large difference in the mass between air and water, implies a large difference in heat capacity. Because the oceans have a comparatively large capacity for storing heat the role the oceans play in balancing the global heat budget is expected to be at least as important as that of the atmosphere. The second reason for expecting the oceans to play a significant role in the equilibration process is that the thermohaline circulation of the oceans is driven by the non-uniformity in the heating of the waters over the globe. Especially in the Atlantic, the thermohaline circulation appears to be dominated by a meridional vertically overturning cell in which the warm surface waters heated in the tropical regions move poleward and sink in the polar regions as they lose heat and undergo evaporation increasing their salinity. The cold, dense water masses which result, make the return journey



towards the equator at depth. As heat is lost to the north in the evaporation process, this type of thermohaline circulation suggests that it is a large poleward heat flux which equilibrates the imbalance in surface heating. Recently, it has been found that in the North Pacific, there is a horizontal circulation cell which may be at least as important as the vertical cell (Talley 1984, Bryden *et al.* 1990) in transporting heat.

Historically, the ocean heat transport was taken to be what was left over once the atmospheric transport had been calculated. An early attempt to compute ocean heat transport was made by Oort and Vander Haar (1976). Through the use of satellite data for the incoming and outgoing radiation, radiosonde data for the atmosphere and heat storage of the ocean they were able to indirectly compute the ocean heat transport as a residual of the incoming radiation and the atmospheric transport. Another indirect method of computing heat fluxes is the use of bulk formulas. A number of studies have made *direct* calculations of the ocean heat transport at a assortment of latitudes in the different oceans, using hydrographic measurements.

The present research produces estimates of ocean heat flux, at approximately 30°S in all the ocean basins as computed from hydrographic measurements. The inverse technique applied allows a variety of datasets and known constraints to be used, with assumptions written explicitly into the problem. It also allows some conclusions to be drawn about how the exchange between the oceans basins can affect the results.

We begin in Chapter 1 with the inversion analysis of the South Pacific Ocean. This first chapter contains more details than the other chapters as it not only describes the South Pacific inversion results, but also discusses how the various constraint assumptions and matrix weights affect the solutions. Chapters 3 and 4 present the results of the inverse models run for the Indian and Atlantic Oceans, as

well as, for the combined ocean Indian-Pacific model. The discussion in Chapter 5 will focus on the transports of mass, heat and nutrients within each of the ocean basins and the exchanges which occur between them. Appendix A presents the formulation of the inverse problem as it is used in this work. It is divided into two sections. The first discusses the basic design of the problem and the singular value decomposition solution. The second explains how the equations for this particular problem are set up and how the best estimate solution is chosen. Appendix B contains a discussion of the inversion error analysis. This analysis will allow us to draw some conclusions concerning the ways in which the various types of data from the different ocean basins constrain and/or drive the solution and the global circulation.

## **Chapter 1**

### **The South Pacific Ocean**

#### **1.1 Introduction**

##### **1.1.1 Water Masses and Circulation**

The Pacific Ocean is easily the largest and deepest of the three major ocean basins. It is bounded to the east by the west coasts of North and South America. In the north it is virtually cutoff at approximately  $60^{\circ}\text{N}$ , with only the narrow and relatively shallow exit allowed by the Bering Straits. The western boundary in the north is furnished by the the coast of Asia, in the south by Australia, but between these two the islands of the Indonesian Archipelago provide a complicated set of passages through which the waters of the Pacific flow into the southern Indian Ocean. To the south below Australia and Cape Horn, the Pacific is open to the rest of the world ocean.

We begin our study in the South Pacific with a description of the major water masses and circulation as they are currently understood, for later comparison with our results. The surface circulation of the South Pacific is described by a huge counter-clockwise subtropical gyre bounded by the South Equatorial Current

(SEC), the East Australia Current, the Antarctic Circumpolar Current (ACC) and the Peru Current.

It is known that the SEC displays fairly large seasonal variations but retains a consistent westward flow, with most of the seasonal variation due to the monsoons limited to the region north of 10°S. The East Australia Current, on the other hand, is part of an extremely variable region. It appears that not only is the current transient and not continuous along the coast, but that its southwesterly flow is associated with an offshore northwesterly flow and large (200-300 km) anticyclonic eddies moving to the south (Boland and Hamon 1970, Pickard and Emery 1982). Not surprisingly, the mean transport of the East Australia Current is not well determined. Estimates of its transport range from essentially zero (Thompson and Veronis 1980) to as high as 57 Sv, relative to 3500 db at 32°S (Boland and Hamon, 1970). On the eastern side of the Pacific the Peru Current flows equatorward carrying with it the relatively fresh, cool waters of the Southern Ocean. Below and shoreward of this eastern boundary current is the somewhat more saline, poleward flow of the Peru-Chile Current which appears to be of subequatorial origin (Fonesca 1989). Due to the winds, this east coast is a region of upwelling and therefore, overall low salinity.

The South Pacific circulation is discussed at length in Reid (1986). A detailed description of the characteristics of the South Pacific above about 2000 m. is given in Reid (1973). The main features of the waters are briefly reviewed here. The color plates of Stommel *et al.* (1973) are extremely useful in identifying the features discussed here, as are the many sections which illustrate the Reid (1986) article. Fig. 1.1 presents the zonally integrated plots of temperature, salinity and nutrient concentrations along the 28°S and 43°S sections used later in this chapter.

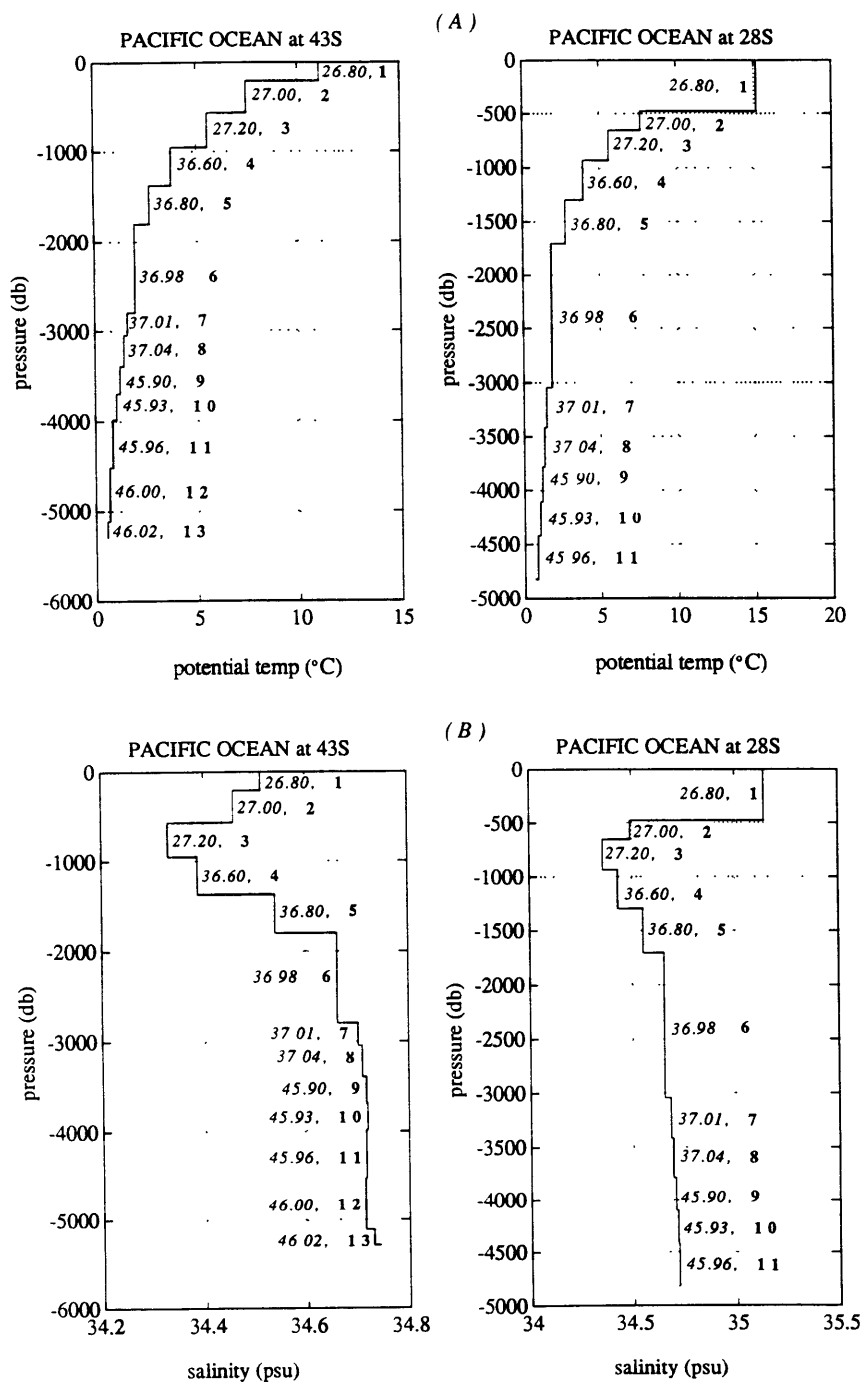
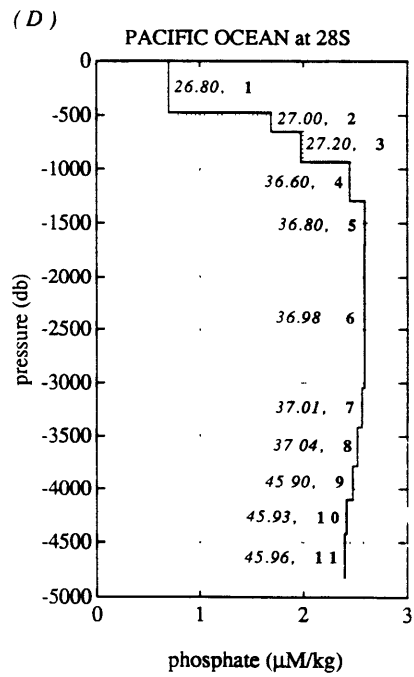
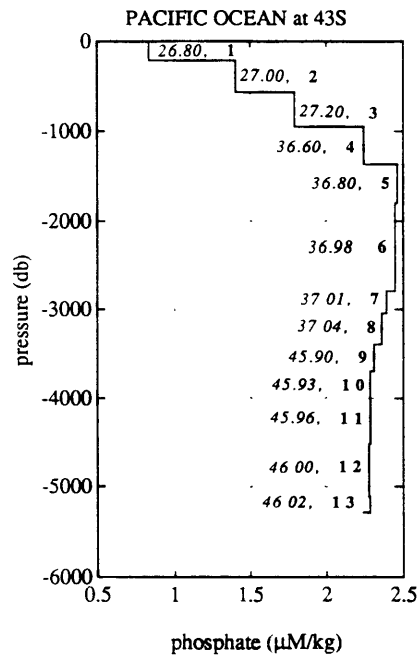
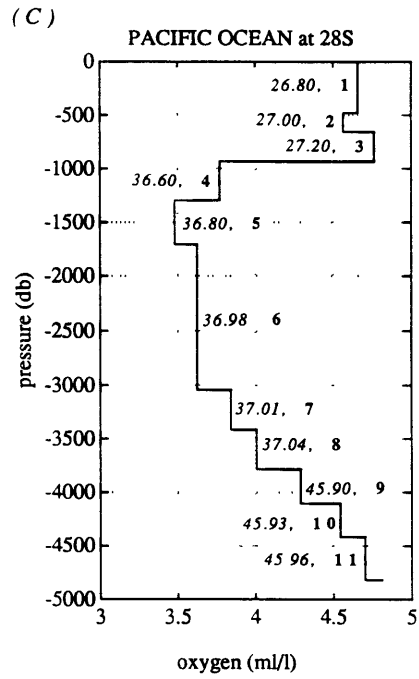
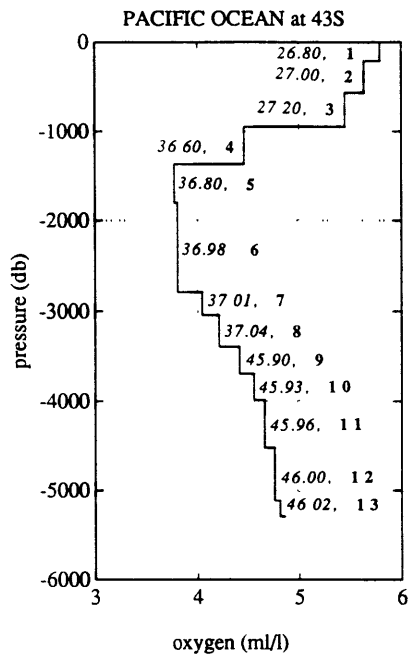
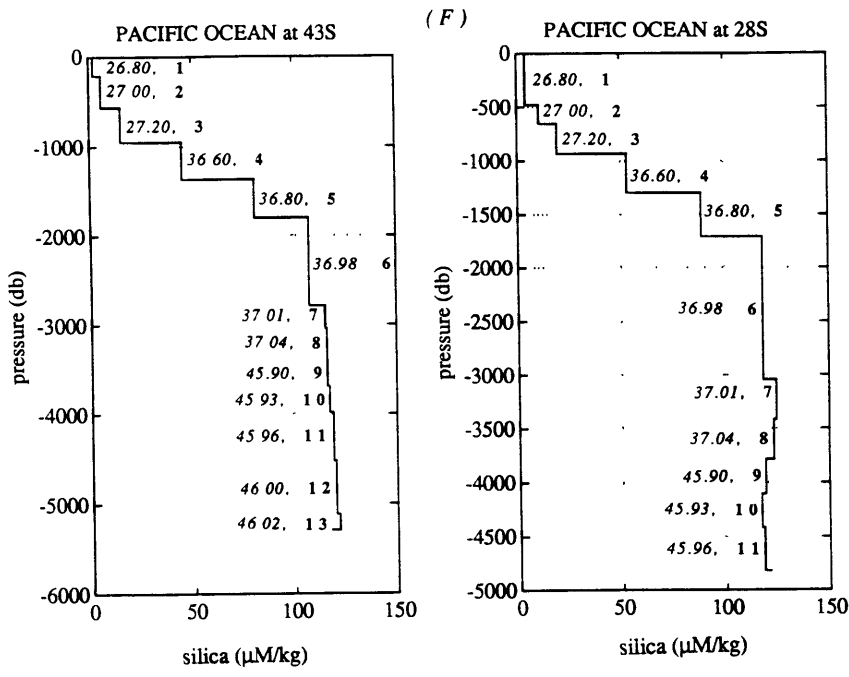


Figure 1.1: Zonally averaged profiles of temperature (a), salinity (b), oxygen (c), phosphate (d) and silica (e) for the Scorpio sections using the 14 layer model.





The waters on the two coasts of the South Pacific are quite different in character because the eastern equatorward flow of cold, fresh waters, high in nutrients is warmed, made more saline and modified in oxygen content before returning poleward, in the western regions. In the east there is a subsurface salinity minimum, associated with Intermediate Water which reaches from high southern latitudes around the main gyre. This feature is seen between about 600 db and 950 db in Fig. 1.1b. Near New Zealand, returning poleward, there is a weak subsurface salinity maximum which is due the excessive amount of evaporation over the central region of the South Pacific. Spanning the breadth of the ocean there is an small oxygen maximum at about 100-150 m, suspected of being a left over from the even higher concentrations of the winter mixed layer. Oxygen decreases below this forming a minimum at about 150-400 m between the maximum above and the underlying Intermediate Water. This minimum expresses itself to a greater degree in the eastern poleward flow. Further below is a deep oxygen minimum. In the pycnocline the oxygen minimum is also a nutrient maximum, but the Intermediate water, although high in nutrients and a region of strong biological production, appears as a minimum. The deeper oxygen minimum is also a nutrient maximum, but the silica only has a deep maximum in the central region.

In the deep waters of the Pacific (described in detail by Warren 1973,1981a) one of the most notable features of the cyclonic gyre circulation is the northward flow of the deep western boundary current through the south western Pacific basin<sup>1</sup>, carrying about 20 Sv (Warren 1981a). According to Reid (1986), this flow is not completely confined to the western boundary region but in fact spreads out across the entire central basin. The East Pacific Rise separates the eastern and central basins and weak poleward flow also exists east of the East Pacific Rise. Still further east there is a northward flow which can be seen at 43°S, but is not nearly as

---

<sup>1</sup>The effective western boundary of the deep South Pacific is not Australia, but New Zealand and the Tonga-Kermadec Ridge.



discernable at 28°S. The deep Tasman Sea is not a region of through flow as it is closed off to the north at depths greater than 2850 m.

Unlike the Atlantic, there is thought to be no deep water formation in the North Pacific, which implies that any deep water in the Pacific must originate in the Antarctic and North Atlantic. The coldest water is found in the west. There is a weak salinity maximum between 3000-4000 m, last remnants of the deep water from the North Atlantic which began its journey flowing into the South Atlantic and then circumnavigated the globe flowing eastward around Antarctica in the Antarctic Circumpolar Current before finally travelling northward into the Pacific. This saline water is also associated with a slight silica minimum. The region between 3000-4000 m appears to separate the equatorward bottom flow from the overlying poleward flow and represents a layer of high stability (Reid 1986). There is a mid-depth (1000 m to 3000 m across most of the basin) region which is an oxygen minimum, high in phosphates and silica. Near the western boundary this oxygen minimum layer is stronger and deeper (2000-2500 m) than it is in the Central Pacific. Reid (1973) saw this as an indication of southward flow at these depths from the North Pacific.

### **1.1.2 Review of Previous Results**

In the Atlantic warm, salty water spreads northward. It is cooled and becomes more saline through evaporation and as it becomes denser and sinks into the deep oceans the water mass known as North Atlantic Deep Water (NADW) is formed. The NADW spreads southward at depth, into the South Atlantic where it becomes entrained in the ACC which carries into the Indian and Pacific Oceans so that eventually it influences all the waters of the World Ocean. According to Gordon (1986), whose theory is based upon the nutrient concentrations of NADW,

the feed water for this process of NADW water formation is derived from within the main thermocline. His hypothesis is that the upper layer return flow is accomplished in the main thermocline of the oceans, *i.e.* that NADW upwells within the World Ocean and is returned to the Atlantic in the upper layer. He proposes two possible return paths for the feed water. The cold water path allows the water to return through the Drake Passage into the South Atlantic at the relatively cold temperatures of AAIW and Subantarctic Mode Water. Gordon estimated that less than 25% of the water returned through this route. In the warm water path the water is returned from the Pacific to the Indian Oceans through the Indonesian Archipelago, across the the Indian Ocean in the South Equatorial Current, poleward through the Mozambique Current and eventually around the southern tip of Africa from the retroflexion region of the Agulhas Current into the South Atlantic. This return water is warmer, coming mainly from the Indian Ocean thermocline. In this chapter we will explore the first connection in the warm water route, the exchange between the Pacific and Indian Oceans through the Indonesian Archipelago.

The Indonesian Archipelago is made up of the chain of Suma Islands, which is divided by numerous deep basins, a few deep passages and a variety of shallower straits and sills (see Fig 1.2). In the last thirty years a number of estimates of the flow through the Indonesian Archipelago, from the Pacific to the Indian Ocean have been made (Table 1.1). The range in these values is broad. Much of the earlier work in this region was performed by Wyrcki (1961). Under the assumption that the narrower and shallower straits would restrict the overall through flow to a fairly low value, Wyrcki estimated the average annual through flow value to be 1.7 Sv, confined to the upper 200 m. Since that time, most transport estimates have been much higher than this one, but all appear to have in common the stipulation or expectation that the major portion of the through flow occurs in the relative fresh upper layers.

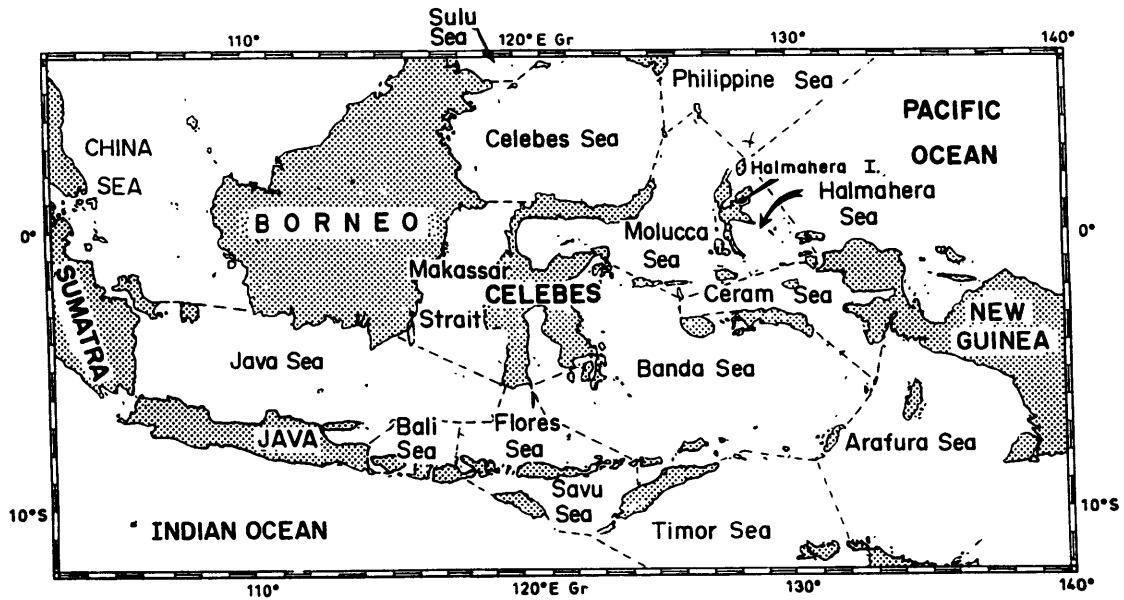


Figure 1.2: Geography of the Indonesian Archipelago between the Pacific and Indian Oceans (from Tchernia 1980).

Date	Reference	$10^6 \text{ m}^3/\text{s}$	Comment	Method
1961	Wyrtki	1.7	in upper 200 m	Dynamic height
1981	Godfrey & Golding	10-20	in upper 400 m	Geostrophically balanced through flow
1983	Piola & Gordan	10-14	at 33-33.6‰	Pacific, Indian salinity budget in the upper layer
1983	Wunsch	negligible		Inverse in Pacific Ocean
1985	Godfrey & Ridgeway	5		Steric Height
1985	Fine	$5 \pm 50\%$	in upper 300 m	Tritium data
1986	Fu	6.6		Inverse in Indian Ocean
1988	Murray & Arief	10-15		From estimate of 1.7 in Lombok Strait from current meters

Table 1.1: Estimates of westward transport through the Indonesian Archipelago.

In 1981, Godfrey and Golding, using the assumption that the Pacific-Indian through flow was geostrophically balanced, produced an estimate on the order of 10 Sv, with an upper limit of 25 Sv. The error associated with the upper value was fairly large, 21 Sv and they reasoned that it seemed unlikely that a transport as great as 20 Sv would have been previously missed. It would produce upper layer velocities as great as 1 m/sec in some of the Indonesian passages (Fine 1985). Piola and Gordon's 1983 estimate of 14 Sv at less than  $33.6\text{‰}$  is based on a requirement to balance their advective box model which produced a salinity in the upper layer outflow too low compared to the Pacific and too high compared to the Indian Ocean. As Table 1.1 shows, there have also been number of somewhat lower estimates in recent years, ranging from negligible to 6.6 Sv. The Murray and Arief (1988) estimate of 10-15 Sv for the total through flow transport is based upon current meter measurements in the Lombok Strait where velocities reaching nearly 1 m/sec (as would be expected for such high estimates) were found in the upper levels.

On the west coast of Australia the Leeuwin Current, unlike other eastern boundary currents flows poleward. The poleward nature of the current and the lack of upwelling which is common on the eastern shores of the other southern oceans may be due to the existence of the Indonesian through flow. The theory at present is that it is the sea-level slope between the Pacific and Indian Ocean basins which drives a net flux westward into the Indian Ocean (Wyrтки 1987, Murray and Arief 1988). This transport contains both annual and interannual variations, and although it does not appear to be affected by El Niño (Wyrтки 1987), it is affected by the monsoonal cycle (Wyrтки 1987, Murray and Arief 1988). Murray and Arief saw an annual cycle within the Lombok Strait with a range of 1-4 Sv. They compared this with the annual cycle for the entire through flow found by J. Kindle from the reduced-gravity Global Ocean Model of the Naval Ocean Research and Development Activity which ranged from 4 to 12 Sv. Such an annual cycle

Lat.	Date	Type	Reference	$10^{15}$ W
20°S	1989	i	Hsiung <i>et al.</i>	-2.1 to 0.5
28°S-32°S	1980	i	Hastenrath	-1.92
28°S	1983	d	Wunsch	$-0.18 \pm 0.22$
30°S	1984	i	Talley	$\sim -2.2$ to $\sim -0.3$
30°S	1985	i	Hsuing	$\sim -0.24$
32°S	1978	d	Bennett	-0.17 to -1.16
40°S	1982	d,i	Georgi & Toole	+0.043 to -0.089
40°S	1984	i	Talley	$\sim -2.3$ to $\sim -0.2$
40°S	1985	i	Hsuing	$\sim 0.09$
43°S	1978	d	Bennett	+0.15 to -0.42
43°S	1983	d	Wunsch	$0.03 \pm 0.35$

Table 1.2: Estimates of northward heat transport in the Pacific Ocean. Type 'd' implies a direct estimate. Type 'i' implies an indirect estimate.

may be partly responsible for the tremendous range in the through flow transports estimated thus far. It could also, no doubt, affect our calculation of an upper limit as we combine data sets from different seasons.

Let us now turn to role played by the South Pacific Ocean in balancing the global heat budget. The circulation in the Pacific Ocean in which there is a strong northward flow of deep and bottom water with a poleward return flow further up in the water column implies that there should be a poleward flow of heat in this basin, to balance the input of heat in the tropics. Estimates of the heat transports in the South Pacific present a range of values (Table 1.2). As would be expected from the need to balance the large heat gains in the region of the equator, most estimates indicate a southward transport of heat<sup>2</sup> in the South Pacific, but Hsuing (1985), Hsiung *et al.* (1989), Georgi and Toole (1982) and Bennett (1978) include the possibility of a northward heat transport. As pointed out by Talley (1984), the indirect estimates, either made from surface heat budget calculations or atmospheric measurement residuals tend to be larger than those which came from direct ocean

---

<sup>2</sup>Throughout this thesis positive values indicate northward motion, while negative values indicate southward motion.

measurements. In the Talley estimates, the large poleward transport at southern latitudes can be traced to apparent large heat gains in the eastern tropical Pacific and along the coast of South America. The estimates, however, when possible systematic errors are accounted for, have a range which includes most of the direct estimates. The heat transport is also expected to express a fairly large annual cycle. Hsiung *et al.* (1989) found extrema at 20°S of 0.5 PW in November-December and -2.1 PW in January. The error associated with these measurements was 1.5 PW which is not unusual for heat transport estimates in the South Pacific.

In this ocean basin we will be reworking the estimates of Wunsch *et al.* (1983) of Indonesian Passage through flow and heat transport in the South Pacific using the same data and similar techniques. We wish not only to confirm the 1983 results but also to extend them to include an upper limit estimate of Pacific-Indian through flow, which at the time of the initial study did not appear to be as great an issue as it is today.

### 1.1.3 Description of the Data Used

We will be using the two Scorpio hydrographic sections obtained in the spring and summer of 1967 for our study of the South Pacific Ocean. Table 1.3 shows the exact dates and summarizes other pertinent information about all the cruises used in this thesis. Fig. 1.3 illustrates the cruise tracks used. Rather than reproducing sections of potential temperature, salinity, oxygen, phosphate and silicate, the reader is once again referred to the colour plates of Stommel *et al.* (1973).

These Pacific sections at 43°S and 28°S were originally performed in order to obtain some good quality data in a region of the world ocean where data was, and still is, relatively scarce. As such, the data set has reasonable resolution with station spacings nominally 160 km in mid-ocean and 80 km over shallow topography. The

Data Name	Ship Name	Cruise #	Start Date	Stop Date	Ocean	Approx. Lat.	Start Long.	End Long.	Avg Sta. Spacing	Minimum Spacing	Maximum Spacing
Scorpio	Eltanin	28	3/12/67	5/8/67	Pacific	43°S	148.2	-75.1	132 km	9 km	209 km
Scorpio	Eltanin	29	6/4/67	7/31/67	Pacific	28°S	153.8	-71.2	134 km	6 km	203 km
AT93	Atlantis	93	7/7/76	8/9/76	Indian	18°S	51.0	117.3	126 km	14 km	208 km
CD29	RRS Darwin	29	11/12/87	12/17/87	Indian	31°S	30.4	114.8	81 km	2 km	188 km
SAVE	Knorr	leg 2	12/28/87	1/21/88	Atlantic	-15°S	322.1	12.7	117 km	9 km	168 km
SAVE	Knorr	leg 3	1/29/88	2/16/88	Atlantic	-30°S	356.2	318.7	110 km	12 km	188 km
SAVE	Melville	leg 4c	1/4/89	2/13/89	Atlantic	-30°S	357.5	15.3	110 km	12 km	188 km

Table 1.3: Details on the six sections used in this thesis.

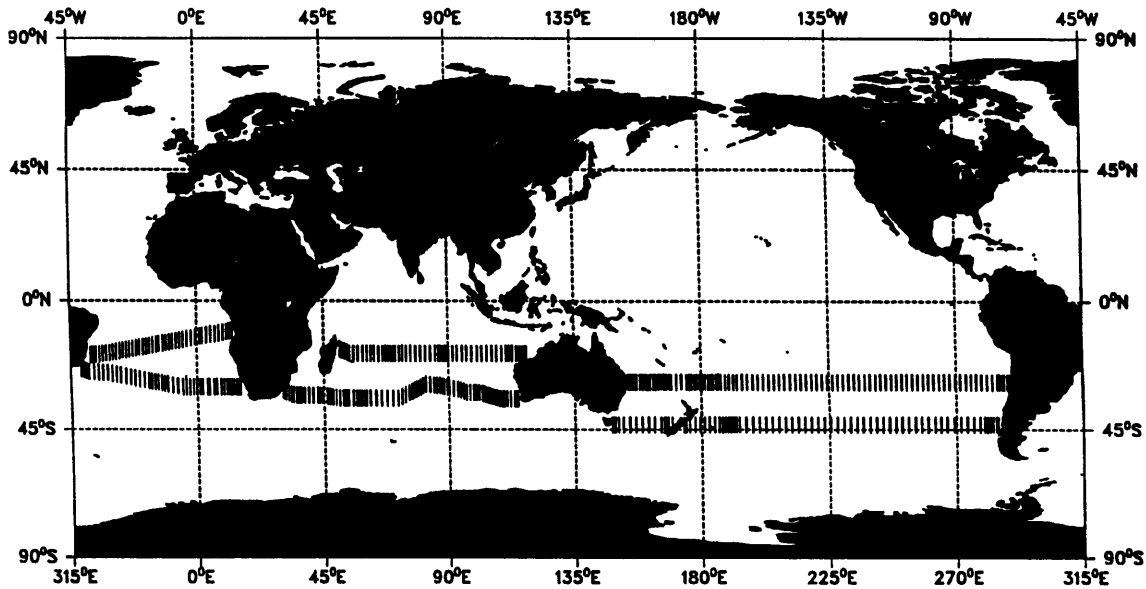


Figure 1.3: The station positions in each of the 6 sections used in this thesis. The northern lines are referred to as 15°S, 18°S and 28°S in the Atlantic, Indian and Pacific Oceans, respectively. The southern lines, in the same order, are 30°S, 31°S and 43°S.

duration of each of the individual cruises was about two months. Together, they span two seasons. In this study, we will eventually be combining data from all the major oceans, taken from different years and different seasons. There is a detailed description of the cruises, the station procedure and raw data analysis in Stommel *et al.* (1973).

The mass, heat, salt and nutrient fluxes in the South Pacific Ocean, determined using the Scorpio data set and inverse modelling, were calculated nearly ten years ago by Wunsch, Hu and Grant (1983) (Henceforth WHG). Summarizing the major results of what shall henceforth be referred to as the '1983' study:

- The zonally integrated results were insensitive to variations in the model assumptions (eg. initial reference level, variations in constraints)
- The interior flow is characterized by:
  - a large ( $12 \times 10^9$  kg/sec ) equatorward flux of bottom water,
  - a poleward return flow at mid-depths,
  - with an equatorward flow of Antarctic Intermediate Water above,
  - and a convergence between the two latitudes of the surface waters.
- The zonally averaged transfer between isopycnals (referred to as  $w$  in WHG and as  $w^*$  here ) determined from the model residuals, was represented by a downwelling at all depths, implying that the large equatorward flow of Bottom Water is entraining the water from above.
- The net meridional fluxes of silica, phosphate, oxygen and fresh water were all found to be small and indistinguishable from zero.
- The net meridional heat flux was also found to be indistinguishable from zero;  $(-1.8 \pm 2.2) \times 10^{14}$  W at 28°S,  $(-0.3 \pm 3.5) \times 10^{14}$  W at 43°S.



- The large Indonesian Passage transports ( $\geq 10$  Sv) of Godfrey and Golding (1981) were not necessary to the solution. Limits were not determined since it was felt that it was not possible to distinguish the through flow transport from the wind-driven flux due to the uncertainty in the latter.

As previously mentioned, the purpose behind using the Scorpio data set in this research was first, to reproduce and so confirm the 1983 results. Second, we wish to examine the effects of the weighting schemes which will be used throughout the thesis and third, we will see if it is possible to extend the results to include an estimate of the flux through the Indonesian Passage into the Indian Ocean.

## 1.2 Comparison with 1983 Study

We began the current study with the Scorpio data before any interpolations or extrapolations had been applied. Temperature, salinity, oxygen, phosphate and silica data were taken at a variety of depths at each station, usually down to within 5 to 10 m of the bottom. These values were then interpolated (extrapolated where necessary) onto a set of 37 standard depths. In performing this process, the decision had to be made as to whether an extrapolation or interpolation should be done in the vertical or the horizontal directions. Our choice was to perform such manipulations in the following order (performing the next choice only if the previous choice did not succeed in producing a reasonable solution):

- perform vertical 3 point Aitken-Lagrange interpolation to obtain the majority of the values at the standard depths; use a vertical extrapolation below the lowest good data point
- perform horizontal interpolations, then extrapolations to fill in the remaining gaps,

- compare all results in the vertical and horizontal, checking for unreasonable solutions,
- perform the most appropriate interpolation or extrapolation on the remaining individual bad data points.

The Aitken-Lagrange interpolation was used in the 1983 study, however, the choice of exactly what interpolation or extrapolation to use in the case that the Aitken-Lagrange scheme did not work could not be reproduced since in many cases it was a subjective decision. However, there was no intention to reproduce either the exact data or the exact analysis procedure, so from the beginning it was expected that we would be unable to perfectly reproduce the 1983 results. This was acceptable as we were only looking for an agreement between the integrated solutions, not individual station values.

All the models in WHG were re-created with extremely similar results. Only those from S4, the model with the most constraints, are discussed here. We begin with a comparison to familiarize the reader with the data set and the prior results so as to lay a groundwork for the evaluation of the effects of the changes which will be made to the 1983 models. In the following discussion we will use the term S4-83 to indicate the model as it was defined in the 1983 study and S4-91 to indicate the model as is re-created here.

### **Models S4-83 and S4-91**

For the purpose of the comparison it was our intention to keep the 1991 model as close to the 1983 model as possible; however, certain decisions were made about how all the data in this research would be processed, so differences invariably arose. The major differences between the 1983 calculation and ours are the following:

- All depths (m) used in S4-83, were converted to pressures (db) in the model S4-91.
- In the 1983 calculation, all potential temperatures were referenced to the surface, causing the amount of water in each of the layers to be somewhat different. The extrapolation routines for determining values below the lowest observed depth were different in the two studies. This difference also affected the amount of water in the lower layers.
- As was found in the 1983 study, the 1991 model inversion results are fairly insensitive to the chosen initial level of no motion. Our model S4-91 results are based on an initial reference level of ( $\sigma_2 = 37.04$ ), which is essentially equivalent to the 1983 use of depth of 3500 m. Both S4-83 and S4-91 are consistent with a level of zero meridional velocity at about 3100 m at the Tonga-Kermadec Trench, descending to about 3600 m in the west (Warren 1981a).
- In the S4-83 the conserved quantity PO was defined in the ratio P:O, 1:135. The S4-91 model uses the classical ratio of 1:138 (Redfield 1963). According to the analysis of Minster and Boulhadid (1987) this difference should not be significant.
- The nutrients have been converted from  $\mu\text{moles/l}$  to  $\mu\text{moles/kg}$ . This change represents only a 2% to 3% difference.

A set of 14 layers were chosen for the 1983 study, which allowed the major water masses of South Pacific to be recognized. We use the same potential density interfaces. Table 1.4 describes the layers as they appeared in 1983 (model S4-83) as compared to those used in this research (model S4-91). The potential temperature referencing inconsistency, mentioned above, is responsible for most of the differences in the lower layers, including the complete lack of water in the lowest two layers at

Layer #	Upper Boundary	Lower Boundary	43S 1983 Lay. Dep. (km)	43S 1991 Lay. Dep. (km)	Difference (km)	28S 1983 Lay. Dep. (km)	28S 1991 Lay. Dep. (km)	Difference (km)
1	surface	$\sigma_0 = 26.80$	0.19	0.21	+0.02	0.45	0.48	+0.03
2	$\sigma_0 = 26.80$	$\sigma_0 = 27.00$	0.30	0.34	+0.04	0.16	0.18	+0.02
3	$\sigma_0 = 27.00$	$\sigma_0 = 27.20$	0.40	0.35	-0.05	0.29	0.28	-0.01
4	$\sigma_0 = 27.20$	$\sigma_2 = 36.60$	0.32	0.38	+0.06	0.32	0.36	+0.04
5	$\sigma_2 = 36.30$	$\sigma_2 = 36.80$	0.32	0.38	+0.06	0.32	0.40	+0.08
6	$\sigma_2 = 36.80$	$\sigma_2 = 36.98$	0.63	0.86	+0.23	0.76	1.28	+0.52
7	$\sigma_2 = 36.98$	$\sigma_2 = 37.01$	0.21	0.21	0.00	0.36	0.26	-0.10
8	$\sigma_2 = 37.01$	$\sigma_2 = 37.04$	0.26	0.27	+0.01	0.41	0.24	-0.17
9	$\sigma_2 = 37.04$	$\sigma_4 = 45.90$	0.29	0.20	-0.09	0.30	0.12	-0.18
10	$\sigma_4 = 45.90$	$\sigma_4 = 45.93$	0.16	0.18	+0.02	0.12	0.08	-0.04
11	$\sigma_4 = 45.93$	$\sigma_4 = 45.96$	0.16	0.32	+0.16	0.08	0.08	0.00
12	$\sigma_4 = 45.96$	$\sigma_4 = 46.00$	0.33	0.23	-0.10	0.10	0.18	+0.08
13	$\sigma_4 = 46.00$	$\sigma_4 = 46.02$	0.23	0.01	-0.22	0.10	0.00	-0.10
14	$\sigma_4 = 46.02$	bottom	0.08	0.0002	-0.08	0.09	0.00	-0.09
total			3.88	3.94	+0.06	3.86	3.94	+0.08

Table 1.4: Comparison of the Model S4-83 layers to the Model S4-91 layers.

28°S for our model S4-91. Some of the variations are due, in all likelihood to the different methods employed for calculating the zonal averages. Most of the layers match fairly well, except for layer 6. Since this layer is the thickest, we might expect it to display larger differences than the others. As will be seen, these slight differences in the layer definitions do not particularly affect the results. The major water masses are still recognizable.

Fig. 1.1 shows the zonally averaged profiles of potential temperature, salinity, oxygen, phosphate and silicate in the potential density layers. These profiles can be compared with those shown in Fig 2. of WHG. A number of the features discussed in section 1.1.1 are apparent in these profiles:

- the salinity minimum of the Antarctic Intermediate Water (AAIW) in the third layer,
- the oxygen minimum centered on about 1500 db in layer 5, which may represent water coming from the North Pacific,

---

Mass	Conservation in all layers Zero geostrophic + Ekman Flux across 28°S Zero geostrophic + Ekman Flux across 43°S Zero Net Flux in layers 11-14 of Tasman Sea at 43°S
Salt	Conservation in all layers Zero geostrophic + Ekman Flux across 28°S Zero geostrophic + Ekman Flux across 43°S
Oxygen	Conservation in layers 3-14
Silicate	Conservation in layers 3-8
Phosphate	No statements
PO38	Conservation in layers 3-14
Reference level	$\sigma_2 = 37.04$

---

Table 1.5: Constraints which define the Scorpio Model S4-91

- the very slight secondary oxygen minimum, perhaps due to the underlying AAIW in layer 2 at 28°S,
- the lack of phosphate and silicate at the surface
- the slight decrease of phosphate in the lowest layers (11-14 at 43°S, 11-12 at 28°S) which represent the Antarctic Bottom Waters (AABW)
- the residual of North Atlantic Deep Water (NADW), recognized by the small salinity maximum and silica minimum which appears in layer 10.
- The decrease of silicate in the AABW is barely seen in the 1983 study and is not visible here, except in the very lowest layers of 43°S.

The constraints of model S4-91 are described in Table 1.5. We used the same balance equations as those used in the 1983 study, that is, for conservation in layer  $i$ :

$$\sum_{j=1}^{43S} \rho_{ij} \mathbf{a}_{ij} (\mathbf{v}_{ijR} + \mathbf{b}_j) \mathbf{C}_{ij} - \sum_{j=1}^{28S} \rho_{ij} \mathbf{a}_{ij} (\mathbf{v}_{ijR} + \mathbf{b}_j) \mathbf{C}_{ij} \approx 0. \quad (1.1)$$

where,

$i, j$  are the layer and station pair indices, respectively

$v_R$  is the relative geostrophic velocity,

$\mathbf{b}$  is the reference level velocity,

$\mathbf{a}$  is the vertical interface area

$\mathbf{C}$  is the property concentration

The flux equations for the 43°S section were written for mass and salt as:

$$\sum_{i=1}^{\#layers} \sum_{j=1}^{43S} \mathbf{a}_{ij} \rho_{ij} (\mathbf{v}_{ijR} + \mathbf{b}_j) \mathbf{C}_{ij} \approx -Ek^{43S} \bar{C}^{surf}, \quad (1.2)$$

where  $Ek$  is the *a priori* estimate of the Ekman flux and  $\bar{C}^{surf}$  is the mean concentration in the surface layer. A similar equation is written for the 28°S section.

The equations 1.1 and 1.2 are then written:

$$\mathbf{A} \mathbf{b} + \mathbf{n} = -\mathbf{\Gamma}, \quad (1.3)$$

where, the elements of the  $\mathbf{A}$  matrix are  $\int_B^T \rho_{ij} \mathbf{a}_{ij} \mathbf{C}_{ij} dp$ ,  $\mathbf{n}$  represents the noise associated with each of the equations,  $\mathbf{b}$  is the vector of unknown reference level velocities.  $\mathbf{\Gamma}$  is the vector of known relative velocity transports plus other optional right hand side elements, such as Ekman flux or a known net transport through the box.

In both S4-83 and S4-91 the terms which represent cross-isopycnal transfer,  $\mathbf{w}^*$  are calculated from the residuals. The method is described by WHG. In all further models the cross-isopycnal transfer terms will be calculated within the inverse as is described in Appendix A.

Both S4 models use the Han and Lee (1981) annually averaged windstress values which result in an Ekman convergence between the two sections. All Ekman values used in this thesis are given in Table 1.6. For model S4-91, using the annual averages we have  $6.7 \pm 2.2 \times 10^9$  kg/sec equatorward at 43°S and  $4.3 \pm 1.0 \times 10^9$  kg/sec poleward at 28°S, giving an Ekman convergence of  $11.0 \pm 2.4 \times 10^9$  kg/sec .

The rows of the A matrix (*i.e.* the individual equations) are weighted by the mean value of the layer concentrations. The columns are weighted by the vertical area associated with the station pair as in the 1983 model.

Using criteria which are specified in Appendix A, we have chosen a rank of 17 for model S4-91. This means there are 17 independent equations so that we are able to determine 17 weighted averages of the 175 unknowns. WHG used rank 18. Nearby ranks do not give significantly different solutions. The rms value of the reference level velocities is small, only 0.39 cm/sec, with an error due to observational noise of  $< 0.07$  cm/sec for all  $b_j$ . However, none of the  $b_j$  are very well resolved. The diagonal elements of the resolution matrix are for the most part  $< 0.1$  and the resolution is not compact. The definition of a compact resolution is given in section Appendix A. The reference level velocities give the appearance of following the topography, a feature which was pointed out by Luyten and Stommel (1982), noted by WHG, and is discussed further in the next section.

The great similarity in the size and character of the resulting reference level velocities, compared to the 1983 solutions, gives rise to very similar absolute geostrophic velocities and zonally integrated transports. The absolute velocity field for our best estimate model (described later) is shown in Fig. 1.4. The most obvious features of the circulation are the poleward flows of the East Australia current in the west and the Peru-Chile Current off the coast of Chile, the equatorward Peru Current closer to the eastern boundary, and the deep western boundary current seen flowing along the effective western boundary in the central basin.

---

			10 <sup>9</sup> kg/s
Pacific Ocean	43°S	March	5.7 ± 2.9
		April	7.7 ± 3.5
		April-March avg.	6.7 ± 3.3
		Annual avg.	6.7 ± 2.2
Pacific Ocean	28°S	June	1.1 ± 3.0
		July	1.0 ± 2.8
		June-July avg.	1.0 ± 2.9
		Annual avg.	-4.3 ± 1.0
Indian Ocean	31°S	November	2.4 ± 2.3
		December	0.5 ± 1.6
		Nov.-Dec. avg.	1.5 ± 2.2
		Annual avg.	2.8 ± 2.6
		(Synoptic)	1.0
Indian Ocean	18°S	July	-15.7 ± 2.3
		August	-16.5 ± 10.3
		July-Aug. avg.	-16.1 ± 9.9
		Annual avg.	-10.8 ± 7.6
Atlantic Ocean	15°S	January	-7.1 ± 3.8
		Annual avg.	-7.5 ± 3.4
Atlantic Ocean	30°S	Jan-Feb	-2.0 ± 0.8
		Annual avg.	-1.4 ± 0.8

---

Table 1.6: Ekman flux values used in this study. A positive value implies a northward flux. Unless otherwise indicated all fluxes are computed from the wind stress tables of Han and Lee (1981). The Ekman flux value is derived from the mean value of the wind stress across the section from 5° squares, for the months indicated. The error is the standard deviation of the wind stress in the 5° squares across the section, for the months indicated. The 31°S synoptic value was provided by J. Toole.



43°S	Mass		Salt		Oxygen		Phosphate		Silica		PO38	
Model S4	91	83	91	83	91	83	91	83	91	83	91	83
Geostrophic	-2.2	-2.0	-75	-67	21	35	-11	-17	-244	-500	-589	-712
Ekman	2.2	2.0	74	361	12	12	2	9	4	4	802	703
Net	0.0	0.0	-1	294	33	47	-9	-8	-240	-496	213	31
Std. Err.	-	-	378	260	55	110	28	16	1366	640	5530	3700
Null Sp. Err.	0.1	-	3	181	3	24	2	8	167	357	184	2419

28°S	Mass		Salt		Oxygen		Phosphate		Silica		PO38	
Model S4	91	83	91	83	91	83	91	83	91	83	91	83
Geostrophic	0.07	-0.01	-5	-4	52	65	-10	-16	56	-84	898	755
Ekman	-0.07	0.01	-3	1	0	0	0	0	0	0	-21	-4
Net	0.0	0.0	-8	-4	52	65	-10	-16	-56	-84	876	751
Std. Err.	-	-	376	76	65	10	35	6	1517	270	5743	1110
Null Sp. Err.	0.1	-	3	1	3	5	2	3	163	168	282	284

Table 1.7: Vertically integrated fluxes across the two Scorpio sections for Models S4-83 and S4-91. The definitions of the standard error and nullspace error are given in Appendix B.

The zonally integrated flux densities (per km of depth) are depicted in Fig. 1.5. They are basically the same as those shown by WHG in their figures 5–9. A comparison of the 1983 fluxes and those we have produced are tabulated in Table 1.7. The Ekman flux estimates are obtained by assuming that the net geostrophic divergence across a section is equal and opposite to the Ekman flux. As found by WHG, the model does not find the Ekman values calculated from the annually averaged winds, to be consistent with the other model constraints.

Model S4-91 Ekman flux estimates of  $2.2 \times 10^9$  kg/sec equatorward at 43°S and  $-0.1 \times 10^9$  kg/sec poleward at 28°S are more consistent with the seasonal averages, which computed from Han and Lee (1981) for the months of the cruises are  $6.7 \pm 3.3$  at 43°S and  $1.0 \pm 2.9$  at 28°S.

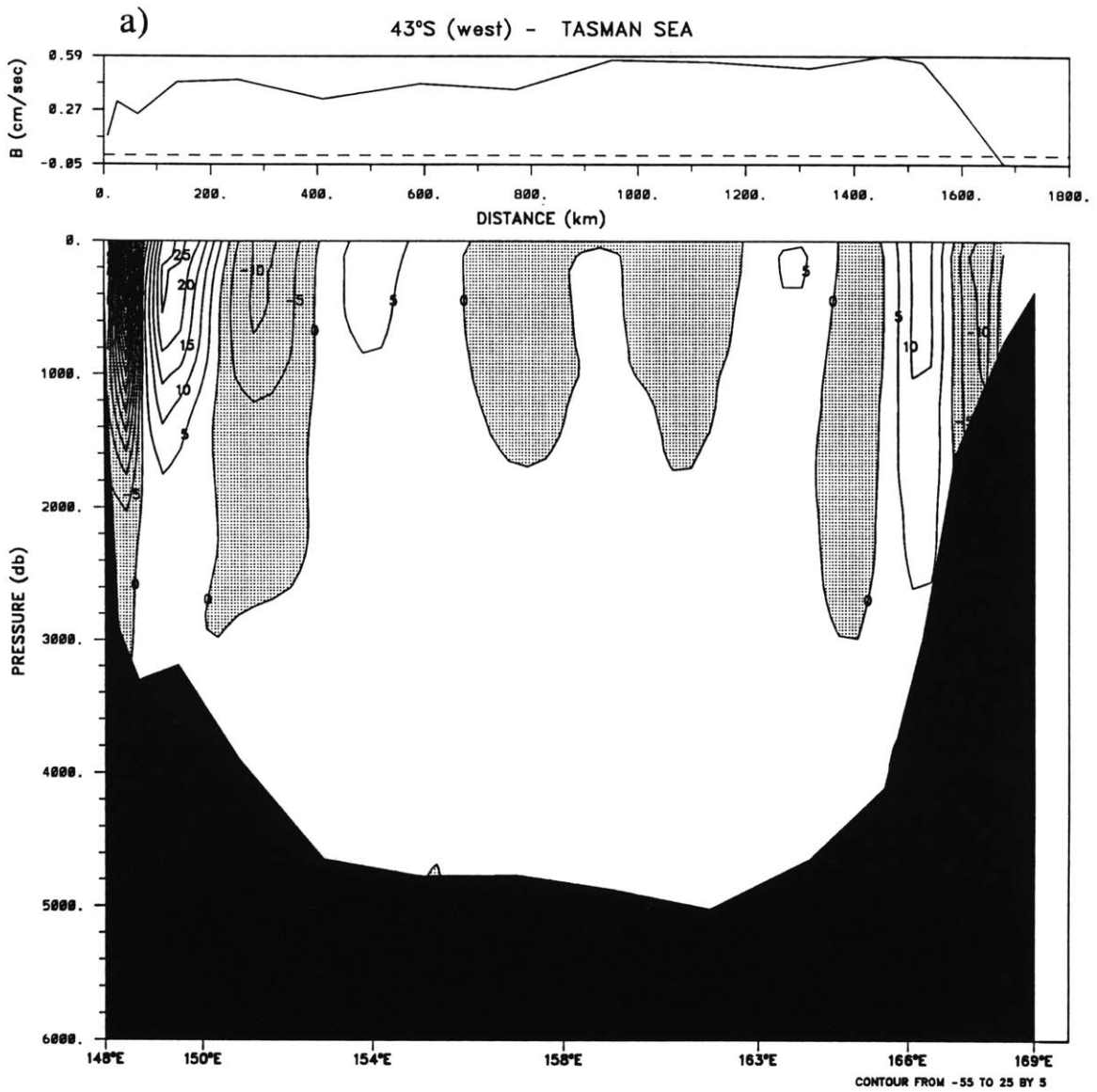
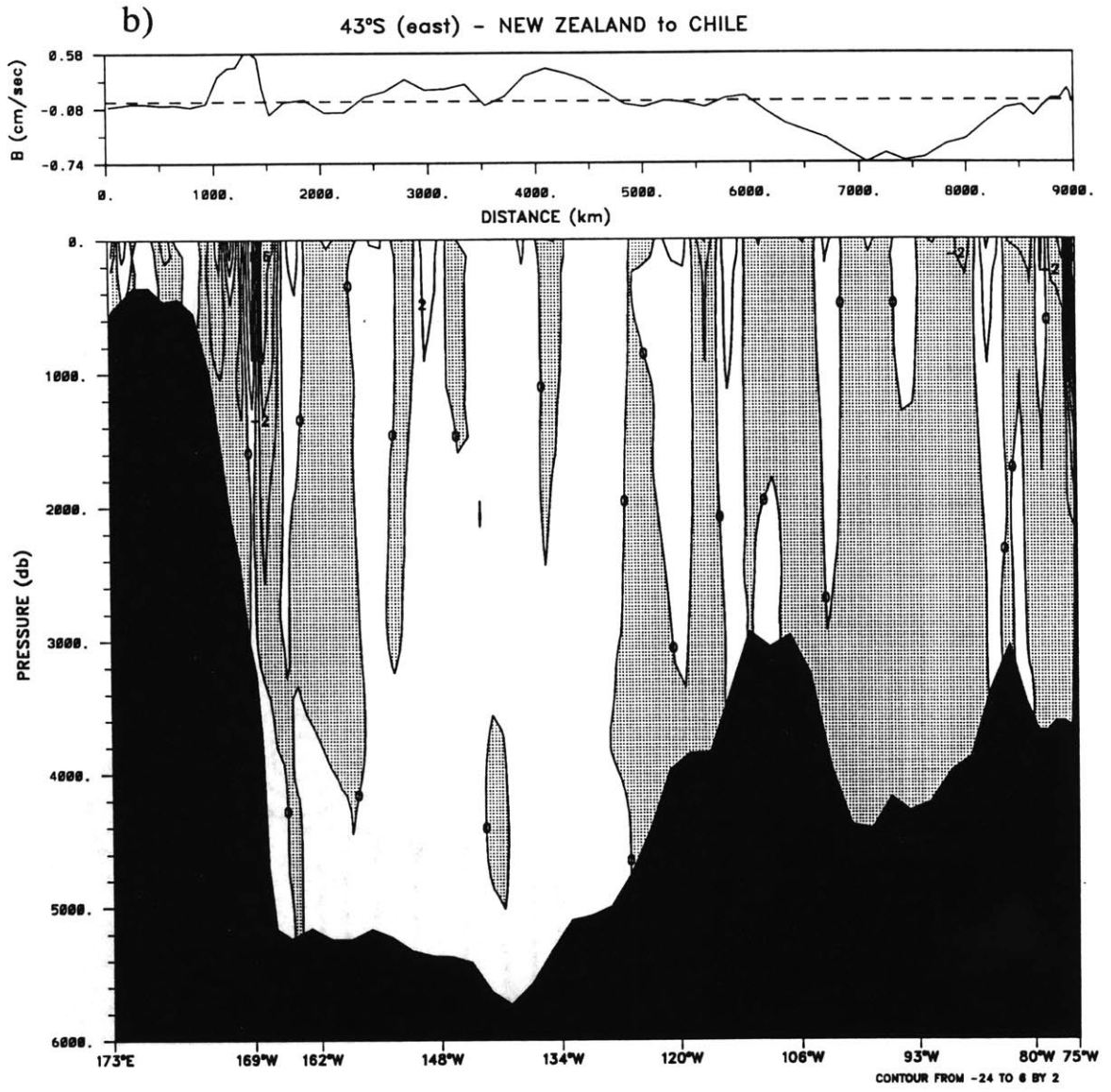
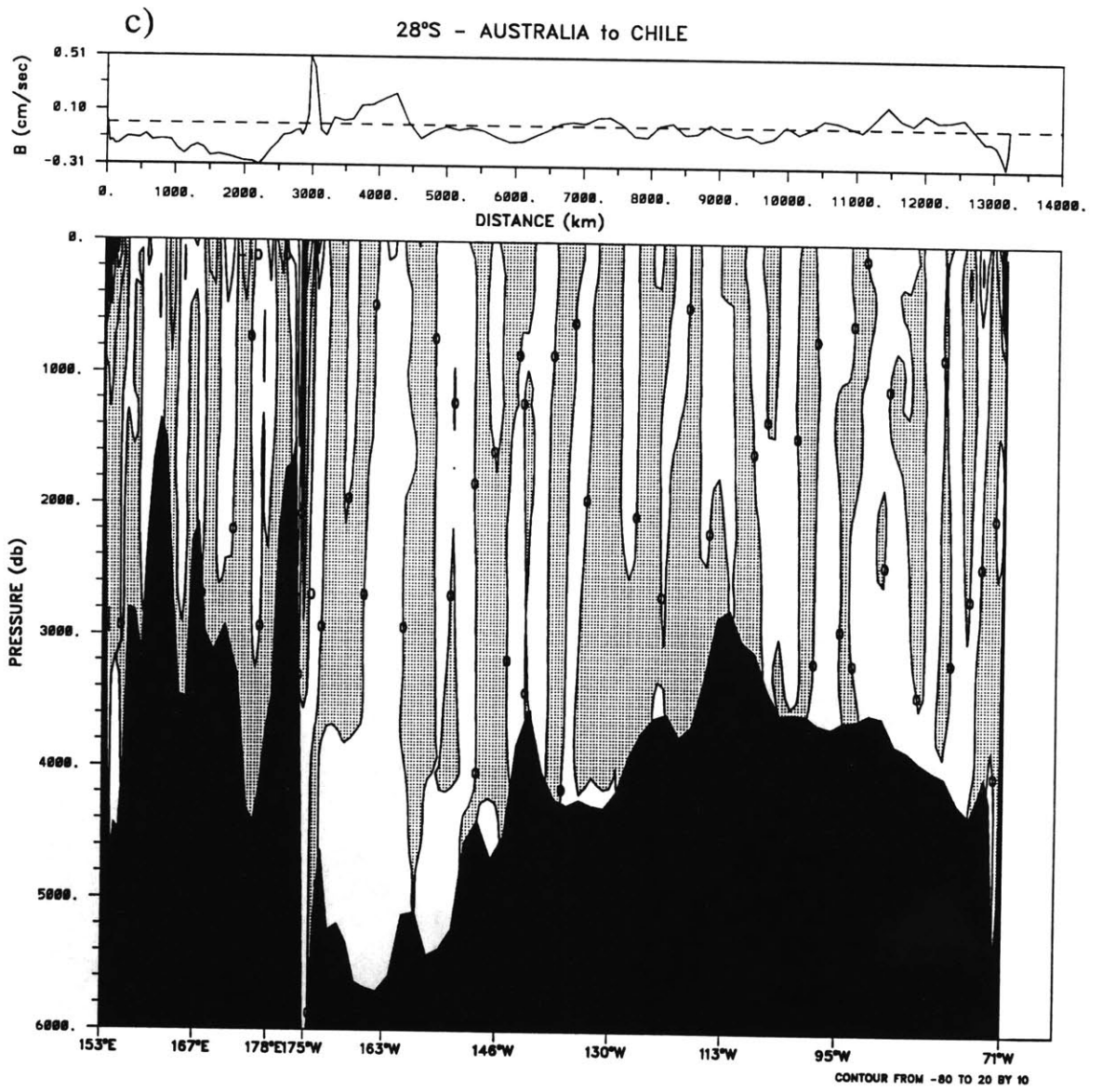


Figure 1.4: The absolute velocity field for our best estimate Pacific Ocean model, P3: (a) at 43°S, between Australia and New Zealand, (b) at 43°S, between New Zealand and Chile, (c) at 28°S, between Australia and Chile. The value of the reference level velocity at  $\sigma_3 = 41.54$  is displayed at the top.





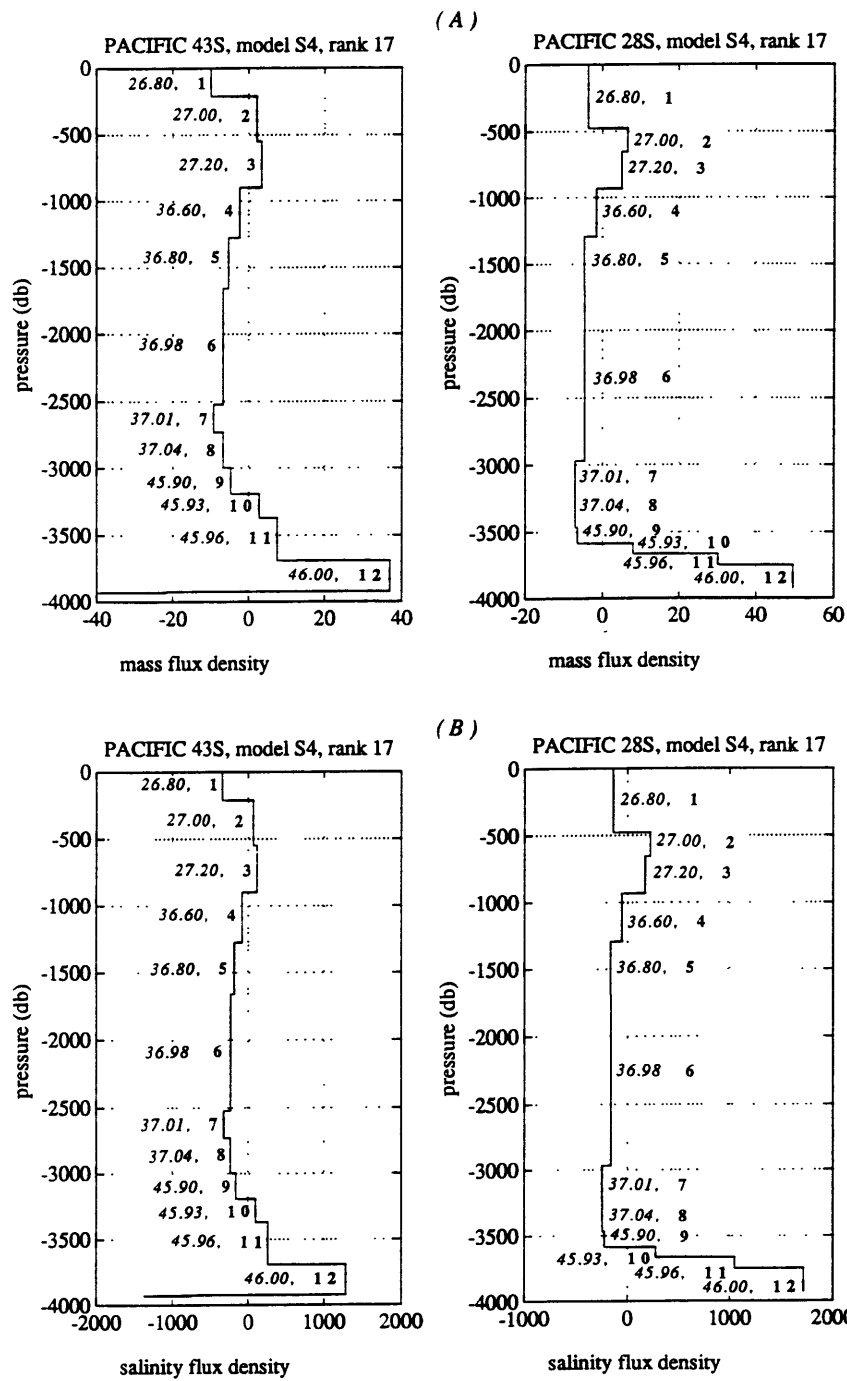
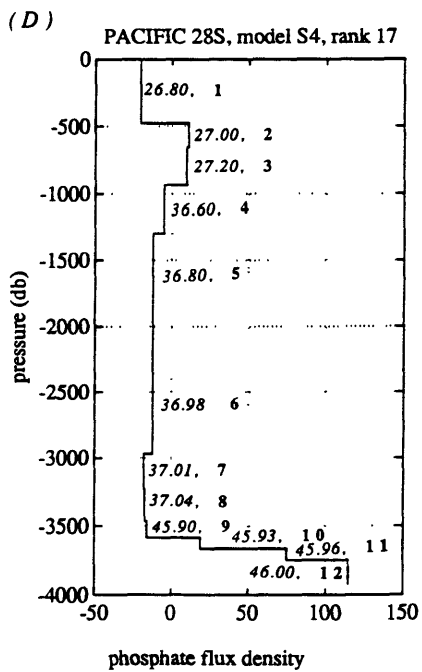
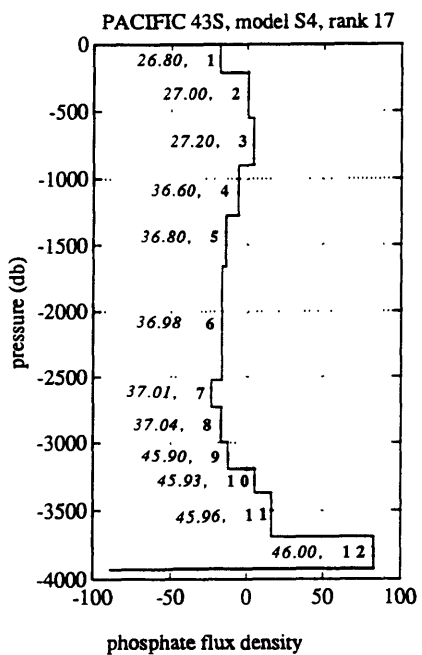
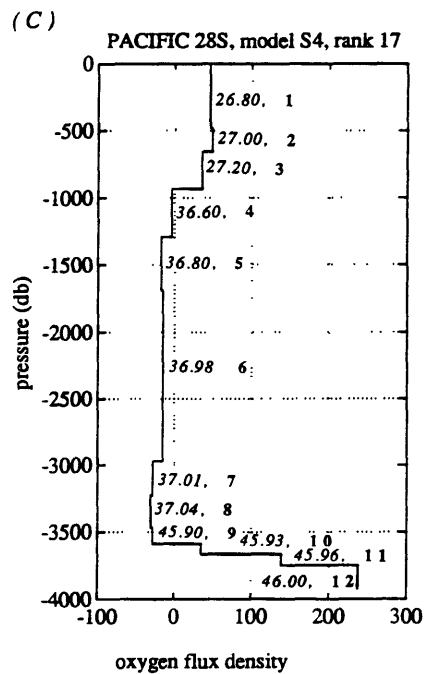
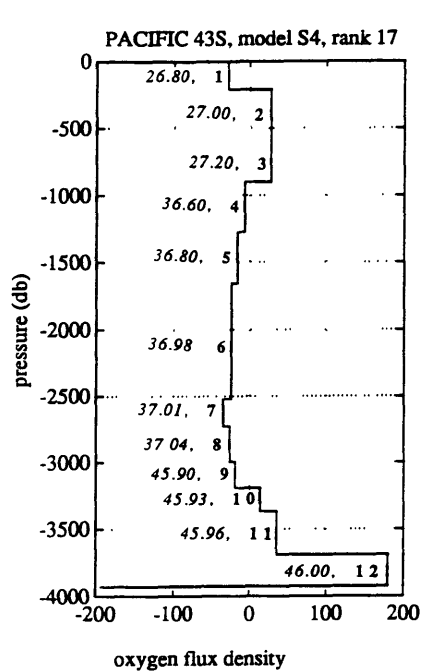
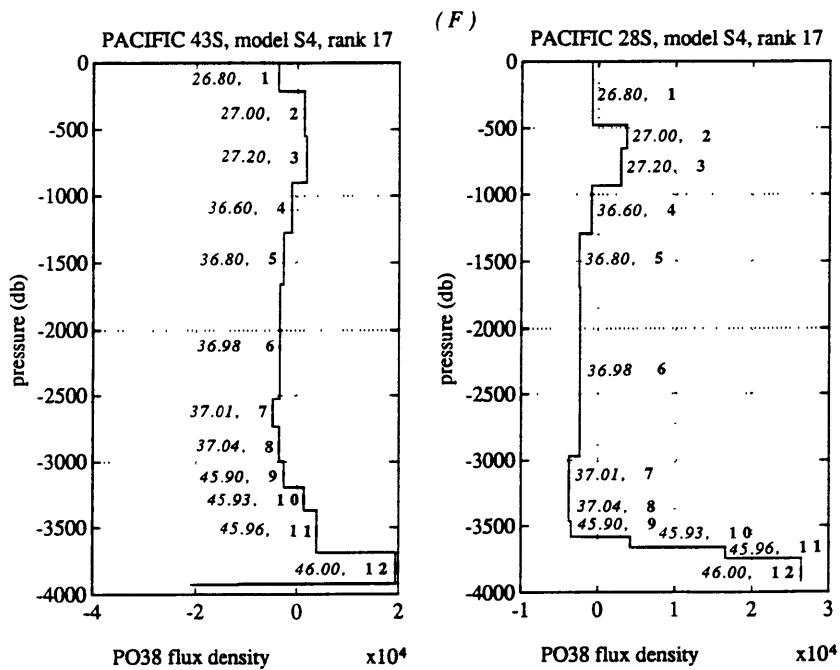
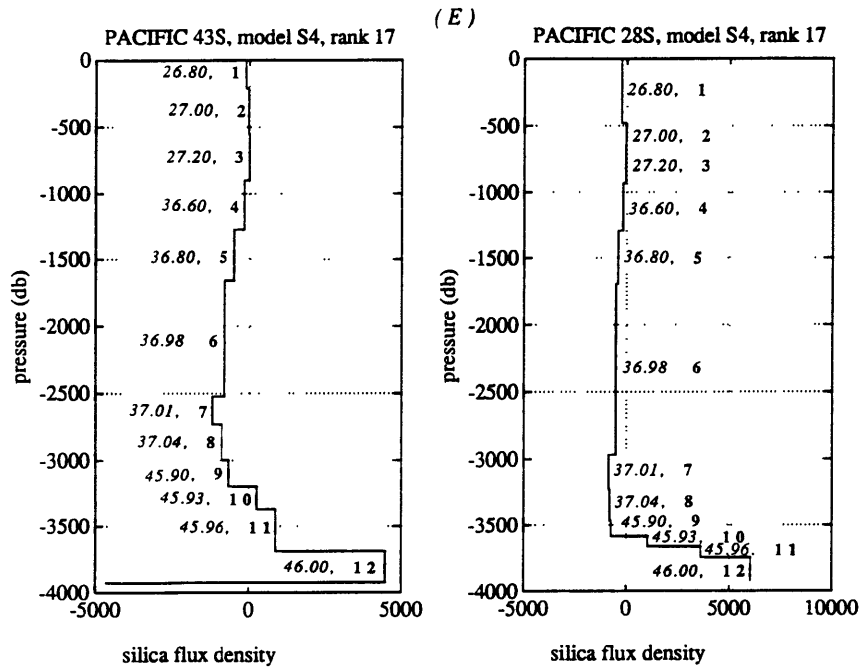


Figure 1.5: The zonally integrated flux densities per kilometer depth for model S4-91. These plots can be compared to figures 5–9 of WHG.





At the surface, there is a poleward geostrophic flux at both latitudes. Assigning the Ekman flow to the uppermost layer, the surface flux remains poleward at 28°S ( $-1.8_{geos} + -0.1_{ekman} = -1.9 \times 10^9$  kg/sec), but becomes ever so slightly equatorward at 43°S ( $-2.1_{geos} + 2.2_{ekman} = 0.1 \times 10^9$  kg/sec). Below the surface layer, is the equatorward flow of AAIW down to about 950 m, at which point the flow reverses to becomes strongly poleward down to  $\sim 3250$  db at 43°S and  $\sim 3600$  db at 28°S. This mid-depth flow is substantial, about  $13 \times 10^9$  kg/sec. Both sections display strong equatorward flows of bottom water (NADW and AABW) in the lowest layers,  $\sim 12 \times 10^9$  kg/sec. At 43°S there is a very small amount of water flowing poleward in the lowest layers. The amount is so small ( $0.1 \times 10^9$  kg/sec) as to be insignificant, but may be topographically induced as all the flux is concentrated on either side of a large peak at  $\sim 98^\circ$ W longitude which rises to within 600 meters of the surface.

Calculating the cross-isopycnal transfer terms,  $w^*$  from the residuals as described by WHG, we obtain a similar overall downwelling (Fig. 1.6), which can be interpreted as the bottom water flux entraining water from above as it flows equatorward, thus explaining the slight increase in magnitude from south to north (WHG). The 1983 paper gives a discussion of how such a downwelling can be rationalized in the face of the Stommel & Arons (1960) expected upwelling of warm water through Ekman pumping. The subject will be brought up again in the discussion of the inverse computed cross-isopycnal transfer.

As done by WHG<sup>3</sup>, the secondary residuals from the salt balance were used to obtain an estimate of the system noise. This method gave us an rms value of  $\sigma = 0.05 \times 10^9$  kg/sec. This value is somewhat larger than the value found by

---

<sup>3</sup>This method determines the cross-isopycnal transfer terms from the mass residuals and subtracts the resulting cross-isopycnal salt flux from the salt residuals to obtain a set of secondary salt residuals. The rms value of the secondary salt residuals is then divided by the mean salinity to obtain an rms error,  $\sigma$ .



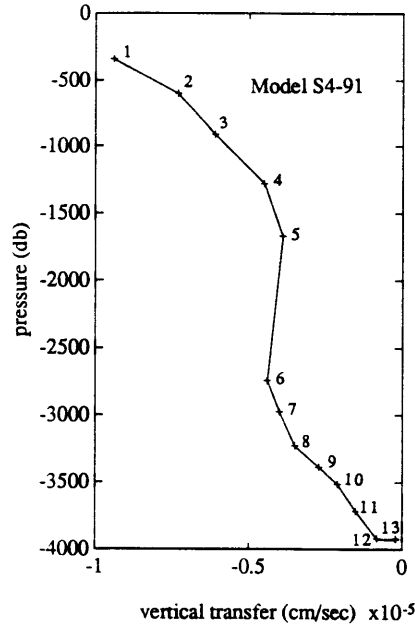


Figure 1.6: Cross-isopycnal transfer terms calculated from the mass residuals for model S4-91. Upward is indicated by positive values.

WHG ( $\sigma = 0.01 \times 10^9$  kg/sec ), which accounts for the larger standard errors associated with our flux estimates (Table 1.7).

The basic conclusion is the same as found by WHG, that none of the meridional fluxes estimated by this model is significantly different from zero. Since our flux estimates for the model so closely parallel those of WHG, a detailed discussion of their character will be left until the end of the chapter, after certain changes have been introduced to the model S4-91. The next section presents a discussion of the effects on the S4-91 model resulting from the inclusion of the cross-isopycnal transfer terms within the inverse calculation, changes to the weighting scheme and extensions to include leakage through the Indonesian Passage.

### 1.3 Extension of Model S4-91

#### Model S4a - Scaling by Column Length

The first change made to the S4-91 model weighting is to remove the column scaling which is based on the area of the vertical interface associated with the station pair and to replace it with a scaling by the length of the column. Before discussing the effect of this change the reasoning behind the use of the original scaling is presented.

The argument for station spacing weight given by Roemmich (1980) went as follows. For two station pairs whose associated distances differ by a factor of  $\alpha$ , the resulting  $\mathbf{A}$  matrix columns will also differ by the same factor  $\alpha$ .

$$\mathbf{A} = \begin{bmatrix} a_{1j} & \alpha a_{1j} \\ a_{2j} & \alpha a_{2j} \end{bmatrix} \quad (1.4)$$

The eigenvectors  $\mathbf{V}$  resulting from the SVD of  $\mathbf{A}$  and which span the rows of  $\mathbf{A}$  will also differ by the factor  $\alpha$ .

$$\mathbf{V}^T = \begin{bmatrix} v_{j1} & \alpha v_{j1} \\ v_{j2} & \alpha v_{j2} \end{bmatrix} \quad (1.5)$$

As a result the columns of the resolution matrix  $\mathbf{V}\mathbf{V}^T$  will also differ by this same factor  $\alpha$ .

$$(\mathbf{V}\mathbf{V}^T)_{i,j+1} = \sum_{l=1}^k v_{i,l}v_{j+1,l} \sum_{l=1}^k \alpha v_{i,l}v_{j,l}$$

$$\mathbf{V}\mathbf{V}^T = \begin{bmatrix} r_{1j} & \alpha r_{1j} \\ r_{2j} & \alpha r_{2j} \end{bmatrix} \quad (1.6)$$

Since the columns with the bigger values are better resolved, the solution will tend to be large where the column norms are large. This tendency is further discussed in Appendix A.

For the depth weighting, the argument as above may be applied to station pairs with the same station spacing and the same ratios of layer thicknesses to the total depth, but with total depths which differ by a factor of  $\alpha$ . It is then argued that without a depth normalization the result would be higher velocities at the deeper stations, an effect which does not seem to have a physical origin. For this reason Roemmich (1980) and WHG used the station pair's vertical interface area as the column weighting.

However, this effect of higher velocities at the deeper stations due to differing total depths, is not what appears to occur in our data. Roemmich (1980) notes, that the more usual situation (which is true for our data) is for the shallower stations not to contain all the density layers (*i.e.* different pairs do not contain the same ratios of layer thickness to total depth). The result is that the imbalances in the problem tend not to be resolved by placing larger values of  $\mathbf{b}_j$  at the deeper stations, but rather by placing the larger  $\mathbf{b}_j$  in those regions where some layers can be adjusted without adjusting others. Thus, the opposite effect occurs. The shallow regions tend to be those over topographic features and the resulting reference level velocities tend to be larger in shallow regions. This tendency is, at least partially, what gives rise to the effect of the velocities appearing to follow the topography.

Later on we will include the requirement that the Ekman convergence be balanced in the upper layer. It was found that this added constraint, with an area weighting, increased the effect of the topography on reference level velocities to the point where the solution in the interior remained very small while that near the coasts rose to 4–5 cm/sec. The first question is whether or not one believes

such high reference level velocities when found near the boundaries. They might be accepted in the western boundary regions, but we do not believe the general effect. For this reason, instead of using the area weighting as done in the 1983 study, we have used the column norm weighting. This weighting still acts to remove the effects of differing station spacing and the less obvious effect of differing layer thicknesses.

A rank of 17 was again chosen for the *best estimate*. The size of the residuals,  $(\mathbf{A}\mathbf{b} + \mathbf{\Gamma})^T(\mathbf{A}\mathbf{b} + \mathbf{\Gamma})$ , was very slightly reduced. The size of the solution,  $\mathbf{b}^T\mathbf{b}$  decreased dramatically. The resulting reference level velocities and flux estimates did not change appreciably<sup>4</sup>. The Ekman flux estimate changed by less than  $0.1 \times 10^9$  kg/sec . The only noticeable affect was on the estimate of  $\sigma$  from the secondary residuals, which was reduced to 0.03 from 0.05. This caused the standard error on the flux estimates to be somewhat less than before, but not enough to change the conclusion that the fluxes are not significantly different from zero.

The fact that the solution changed so little is encouraging. It indicates that the depth weighting was not removing any significant structure from the  $\mathbf{A}$  matrix. Therefore, we have not lost anything by not including this depth weighting.

### Model S4b - Calculating the Cross-Isopycnal Transfer Terms, $\mathbf{w}^*$

The second change made to the 1983 S4 model was to explicitly compute the values of the horizontally averaged cross-isopycnal transfer terms,  $\mathbf{w}^*$  using the inverse machinery. From this point, on the  $\mathbf{A}$  matrix contains rows of the form:

$$\sum_{j=1}^{43S} \rho_{ij} \mathbf{a}_{ij} (\mathbf{v}_{ijR} + \mathbf{b}_j) \mathbf{C}_{ij} - \sum_{j=1}^{28S} \rho_{ij} \mathbf{a}_{ij} (\mathbf{v}_{ijR} + \mathbf{b}_j) \mathbf{C}_{ij} - \quad (1.7)$$

$$\mathbf{a}_i^{Htop} \mathbf{w}_i^{*top} \mathbf{C}_i^{Htop} + \mathbf{a}_i^{Hbot} \mathbf{w}_i^{*bot} \mathbf{C}_i^{Hbot} \approx 0, \quad (1.8)$$

---

<sup>4</sup>The solution size,  $\mathbf{b}^T\mathbf{b}$  is always computed from the normalized (*i.e.* weighted) version of the vector  $\mathbf{b}$  (see equation A.11). The reference level velocities,  $\mathbf{b}_j$  are represented by the unnormalized version of the  $\mathbf{b}$  vector.

where,  $H_{top}$  and  $H_{bot}$  represent the horizontal interfaces above and below the layer.

Since the horizontal interface areas through which the cross-isopycnal transfer occurs are so much greater than the vertical areas through which the reference level velocities flow, it proved necessary to explicitly downweight these columns of the matrix before computing the column lengths. Without such downweighting all the information available in the system would go into calculating the  $\mathbf{w}^*$  values, leaving the  $\mathbf{b}_j$ 's almost completely unresolved. The downweighting factor was chosen such that the resolution ( the diagonal values of  $\mathbf{V}\mathbf{V}^T$  ) were approximately the same for the  $\mathbf{b}_j$  and  $\mathbf{w}^*$  terms.

This model was determined to have rank 16-17. The resulting reference level velocities are extremely similar to those found by the previous model, though a perhaps a little smoother. This comes as no surprise since the  $\mathbf{b}_j$ 's are bound to be less well resolved now that some of the available information must be used to resolve the  $\mathbf{w}^*$ 's. This effect is obvious if the  $\mathbf{w}^*$  are downweighted less. Estimated Ekman fluxes have not changed significantly ( $2.1 \times 10^9$  kg/sec poleward at  $43^\circ\text{S}$ ,  $0.02 \times 10^9$  kg/sec poleward at  $28^\circ\text{S}$ ) since the maximum cross-isopycnal flux anywhere is only about  $0.2 \times 10^9$  kg/sec .

The most interesting feature of including the cross-isopycnal transfer computation within the inverse is that the resulting solutions  $\mathbf{w}^*$  are quite unlike those calculated from the residuals. Fig. 1.7 compares the  $\mathbf{w}^*$  values computed from the residuals for model S4a to the  $\mathbf{w}^*$  values computed by the inverse in this model, S4b. Although the inverse computed  $\mathbf{w}^*$ 's show decreasing magnitude with depth they are much smaller and show none of the downwelling character of those calculated from the residuals. They oscillate in sign from interface to interface giving the appearance of being quite random. This same random nature of the  $\mathbf{w}^*$ 's exists even at the lowest ranks so it is not the result of having resolved these terms early on

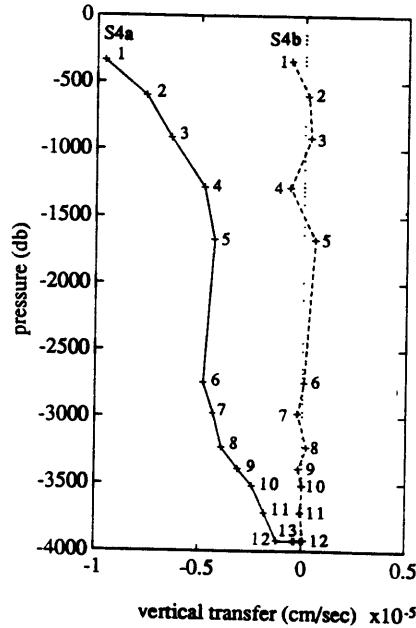


Figure 1.7: Cross-isopycnal transfer terms calculated from the mass residuals for model S4a compared to those computed within the inverse for model S4b. Positive values imply upward movement.

(at low ranks) and then creating the random character by including noise through the higher ranks ( smaller eigenvalues ).

The effect that these cross-isopycnal transfer terms appear so random in character leads us to conclude that either the information is not available in the data to resolve them or that the true nature of such zonally averaged values is different from what was expected. It is certainly true that if there is an upwelling ocean interior with strong downwelling in limited regions outside the interior as found by Warren (1976) in the western boundary, then it quite likely that the zonally integrated values will appear random. There is no way within this model to separate the two regions. It was also pointed out by WHG that  $w^*$  is normal to the isopycnals, whereas,  $\bar{w}$  in the linear vorticity balance,

$$\beta \bar{v} = f \frac{\partial \bar{w}}{\partial z} \quad f < 0 \quad (1.9)$$

is normal to the geopotential surfaces and therefore, does not represent the same quantity.

The mass residuals <sup>5</sup> for this model do not exhibit random behavior. They show a divergence at all layers except layer 6 and a decrease in magnitude with depth. The resulting value of  $\sigma$  calculated from equation A.10 now since the secondary residuals can no longer be used, is larger, producing a proportionally larger estimate of the standard error for the fluxes.

The solutions in which the residuals are assigned wholly to the cross-isopycnal transfer is not the one found by the inverse. The structure which remains implies that there is still some physics missing from the problem. It is possible that by downweighting the  $w^*$  terms so that they are no better resolved than the  $b_j$  that we have inadvertently lost the physics they represent. In the last section, a model will be presented in which the the  $w^*$  terms are not constrained (not downweighted)<sup>6</sup> and so are allowed to grow by an order of magnitude. This allows large cross-isopycnal transfer terms to represent nearly all the missing physics, reducing the residuals and thereby reducing the standard error estimates.

### **Model S4c - Weighting the rows by the expected uncertainty**

Having included the cross-isopycnal flow in the calculation, the next change made to model S4-91 was to downweight the equations by their expected uncertainty. The source of these uncertainties is explained in Appendix A. We take the expected uncertainties in any individual layer to be  $2 \times 10^9$  kg/sec , while the uncertainty in top to bottom flow is taken to be  $1 \times 10^9$  kg/sec . The uncertainty given to the flux equations for the individual sections was taken to be the square

---

<sup>5</sup>There are two types of residuals discussed in the thesis. The problem residuals used to calculate  $\sigma$  in equation A.10, are the residuals computed from  $(\mathbf{A}\mathbf{b} + \mathbf{\Gamma})$  where  $\mathbf{A}$ ,  $\mathbf{b}$  and  $\mathbf{\Gamma}$  are the weighted versions of the variables. The mass transport figures contain plots of mass residuals. These residuals are computed from the unscaled  $(\mathbf{A}\mathbf{b} + \mathbf{\Gamma})$  for the mass conservation equations. They represent the difference between a solution in which the layer conservation constraints are met exactly and actual solution.

<sup>6</sup>Here, 'not constrained' or 'not downweighted' means that  $w^*$  terms are allowed to be as large as the  $b_j$  terms.

root of the sum of the squares of the uncertainties in the top to bottom flow and the Ekman transport.

The rank remains at 16. There is little change in most of the solution. The reference level velocities are slightly smaller,  $b_{rms} = 0.3$  cm/sec. The cross-isopycnal transfer terms are slightly larger. The main difference occurs in the estimated values of the Ekman flux. At 43°S, all the layers above layer 11 ( $\sim 3700$  db) are supporting a geostrophic transport which carries more water poleward than in the previous model. At 28°S, all the layers except layer 6, are carrying more water equatorward. This produces an estimate of the Ekman fluxes consistent with those computed from the annual average wind stress: at 43°S,  $4.7 \times 10^9$  kg/sec equatorward, at 28°S,  $3.9 \times 10^9$  kg/sec poleward.

#### **Model S4d - Depth Weighting**

The final weighting change which will be made to model S4-91 is an attempt to remove the effect of the reference level velocities appearing to follow to the topography. In this work it was decided not to allow the magnitude of the reference level velocities to be dependent upon what we see as an artificial effect of the least squares solution, rather than a direct result of the physics included in the problem. The logic used here is that since the velocities tend to be larger in the shallower regions where some layers can be manipulated without affecting others, the station pairs (columns) in these regions should be downweighted. The weighting used on all the columns is square root of the average depth of the station pair. This weighting is the inverse of the depth weighting included in the original area weight.

The rank was reduced to 14 with this weighting, indicating that some structure had been removed from the matrix. In this case, there was actually very little difference in the solutions between ranks 10 and 15. Rank 14 was chosen based on the size of the residuals. The integrated transports are almost exactly the same as



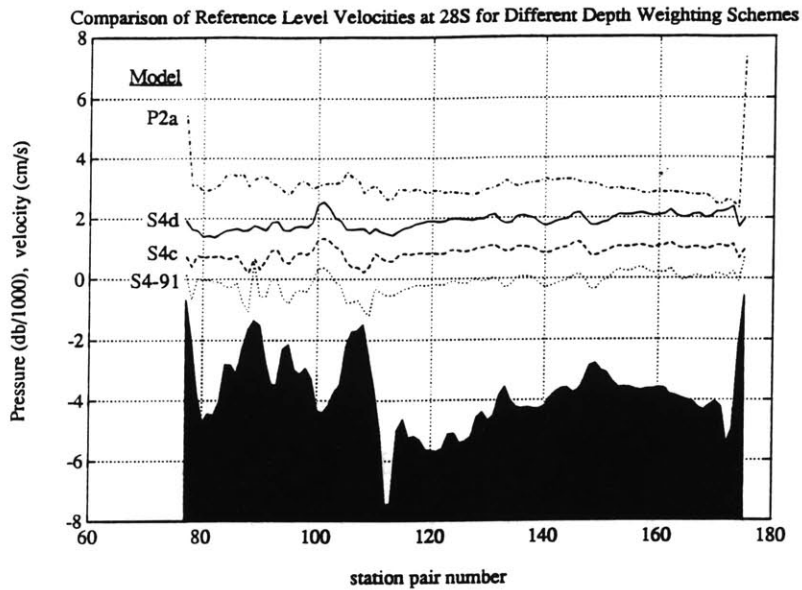


Figure 1.8: Comparison of the reference level velocities for the models S4-91 (original depth weighting), S4a (no depth weighting), S4d (new depth weighting) and P2 (original depth weighting with the requirement that the Ekman convergence be balanced in the top layer)

in the previous model. The effect on the reflection of the topography in the reference level velocities is in the right direction but not as great as might be expected (Fig 1.8). A much greater difference is seen in the section on model P2, where in an extension of the current model, a geostrophic divergence in the top layer is required to balance the Ekman convergence.

In summary, the original S4-91 model has been altered by removing the column weighting by station area and replacing it with a scaling by column length and station depth. The row scaling now includes the expected equation uncertainty which can be compared to the magnitude of the residuals when choosing the matrix rank. The cross-isopycnal transfer terms are now computed within the inverse. These changes result in somewhat larger mass residuals which retain a non-random character (a divergence at nearly all depths), and in estimate of the Ekman transports at the two latitudes that are low, but consistent with those calculated from

the annual average wind stress. Some changes have occurred in the estimates of the meridional property fluxes. They will be discussed later in the chapter.

These modifications are to be kept in place for all further models. The discussion will now turn to a set of models run on the southern basins of Pacific, Indian and Atlantic Oceans in turn.

In the Pacific Ocean, the models are presented in what could be construed as reverse order, since we have already begun with the complexities of model S4-91 in order to confirm the 1983 results and to illustrate the effects of weighting variations. In order not to perform an about face we shall continue along this line; first defining the new potential density interfaces to be used in the rest of the thesis, second introducing the constraint that the Ekman convergence be balanced in the surface layer, third using a set of models which introduce each data variable in turn to discuss the various transports and the importance of the individual constraints and finally, attempting to force a net flux through the South Pacific box to find a limit for the possible Indonesian Passage through flow.

### **Model P1 - 18 layers**

To create models which include water masses from oceans other than the South Pacific, it is necessary to refine the potential density interfaces to resolve a broader range of water characteristics. The next step in the extension of the model we have been working with is to allow for 18 layer interfaces + the top and bottom as opposed to the original 14. The interfaces are defined in Table 1.8 for all the oceans. Fig. 1.9 shows the layers for the Pacific. Comparing these to Fig. 1.1 one finds only two new details previously integrated out. Both appear in layer 2 ( $\sigma_\theta = 26.6 - 26.8$ ). These are the appearance of the salinity maximum believed to be due to the excess evaporation over precipitation in the central Pacific

Upper Boundary	Lower Boundary	Pacific 43°S	Pacific 28°S	Indian 31°S	Indian 18°S	Atlantic 30°S	Atlantic 15°S
Surface	$\sigma_\theta = 26.60$	12.13 34.42	16.30 35.24	15.37 35.46	19.20 35.19	16.97 35.61	19.32 36.13
$\sigma_\theta = 26.60$	$\sigma_\theta = 26.80$	9.63 34.64	10.15 34.73	11.22 34.96	11.57 35.07	11.17 34.95	11.67 35.08
$\sigma_\theta = 26.80$	$\sigma_\theta = 27.00$	7.63 34.48	7.92 34.52	8.86 34.66	9.20 34.76	8.76 34.68	9.57 34.86
$\sigma_\theta = 27.00$	$\sigma_\theta = 27.02$	5.62 34.33	5.76 34.36	6.42 34.48	6.93 34.58	5.79 34.42	6.78 34.60
$\sigma_\theta = 27.02$	$\sigma_1 = 32.00$	3.97 34.37	4.21 34.41	4.31 34.42	5.39 34.62	3.84 34.36	4.53 34.48
$\sigma_1 = 32.00$	$\sigma_1 = 32.16$	3.06 34.47	3.25 34.50	3.34 34.51	4.29 34.67	3.14 34.48	3.81 34.59
$\sigma_1 = 32.16$	$\sigma_2 = 36.73$	2.72 34.54	2.80 34.55	2.95 34.57	3.61 34.69	2.97 34.60	3.77 34.72
$\sigma_2 = 36.73$	$\sigma_2 = 36.80$	2.52 34.58	2.54 34.58	2.73 34.62	3.21 34.70	2.95 34.68	3.74 34.81
$\sigma_2 = 36.80$	$\sigma_2 = 36.92$	2.15 34.64	2.07 34.63	2.40 34.69	2.60 34.72	2.90 34.78	3.52 34.90
$\sigma_2 = 36.92$	$\sigma_2 = 36.97$	1.80 34.68	1.70 34.67	2.07 34.73	2.08 34.73	2.77 34.83	3.14 34.92
$\sigma_2 = 36.97$	$\sigma_2 = 37.00$	1.61 34.70	1.54 34.68	1.90 34.74	1.80 34.73	2.59 34.87	2.82 34.91
$\sigma_2 = 37.00$	$\sigma_2 = 37.04$	1.42 34.71	1.36 34.69	1.66 34.74	1.52 34.73	2.45 34.89	2.55 34.90
$\sigma_2 = 37.04$	$\sigma_3 = 41.54$	1.19 34.72	1.16 34.71	1.33 34.74	1.21 34.73	2.08 34.87	2.10 34.89
$\sigma_3 = 41.54$	$\sigma_4 = 45.93$	1.01 34.72	1.00 34.72	1.06 34.73	1.02 34.72	1.51 34.82	1.55 34.82
$\sigma_4 = 45.93$	$\sigma_4 = 45.96$	0.84 34.72	0.85 34.72	0.86 34.72	0.84 34.72	1.17 34.79	1.20 34.75
$\sigma_4 = 45.96$	$\sigma_4 = 46.00$	0.68 34.71	0.66 34.71	0.62 34.71	0.72 34.72	0.83 34.76	0.86 34.76
$\sigma_4 = 46.00$	$\sigma_4 = 46.02$	0.60 34.73	* *	0.40 34.70	* *	0.57 34.72	0.58 34.74
$\sigma_4 = 46.02$	bottom	0.56 34.74	* *	0.20 34.69	* *	0.31 34.67	0.29 34.71

Table 1.8: Layer boundaries and the associated layer average potential temperature (upper value, °C) and salinity (lower value, psu) for each of the six sections. An asterisk indicates that no water is contained in the layer for the particular section.

(Reid 1973) and stronger expression of the oxygen minimum perhaps due to the underlying AAIW.

Model P1 is the 18 layer version of model S4d. The results are extremely similar, as would be expected. The integrated mass transports for model P1 are plotted in Fig. 1.10. The 14 layer (S4d) model produced a *smoother* version of the same results found by the 18 layer model. The one noticeable difference is the loss of geostrophic transport in the upper 500 db of the 28°S section. The residuals retain their divergent character and the cross-isopycnal flow still shows a reduction of magnitude with depth as its only consistent feature.

### **Model P2 - Geostrophic-Ekman Balance Required in Surface Layer**

The greatest effects of the windstress occur in the upper layers of the water column. It therefore, seemed reasonable to perform a further experiment with our model in which an explicit constraint was included which would determine if the Ekman transport could be balanced in the surface layer. The balance we sought to achieve was between the Ekman convergence/divergence and the geostrophic convergence/divergence in layer 1.

This balance was first encouraged by removing the conservation constraints in the upper two layers. The removal of these equations had little effect, however. The SVD did not solve the problem by placing the Ekman flow in the upper layers, but instead produced a solution very similar to that found previously in model P1. The two noticeable differences were the appearance of the equatorward flow in the warmest layer of 28°S and the reinforcement of the residual structure, with greater values near the surface and diminished values towards the bottom. So the model was changed to require explicitly a balance between the Ekman convergence and the geostrophic divergence in the top layer.

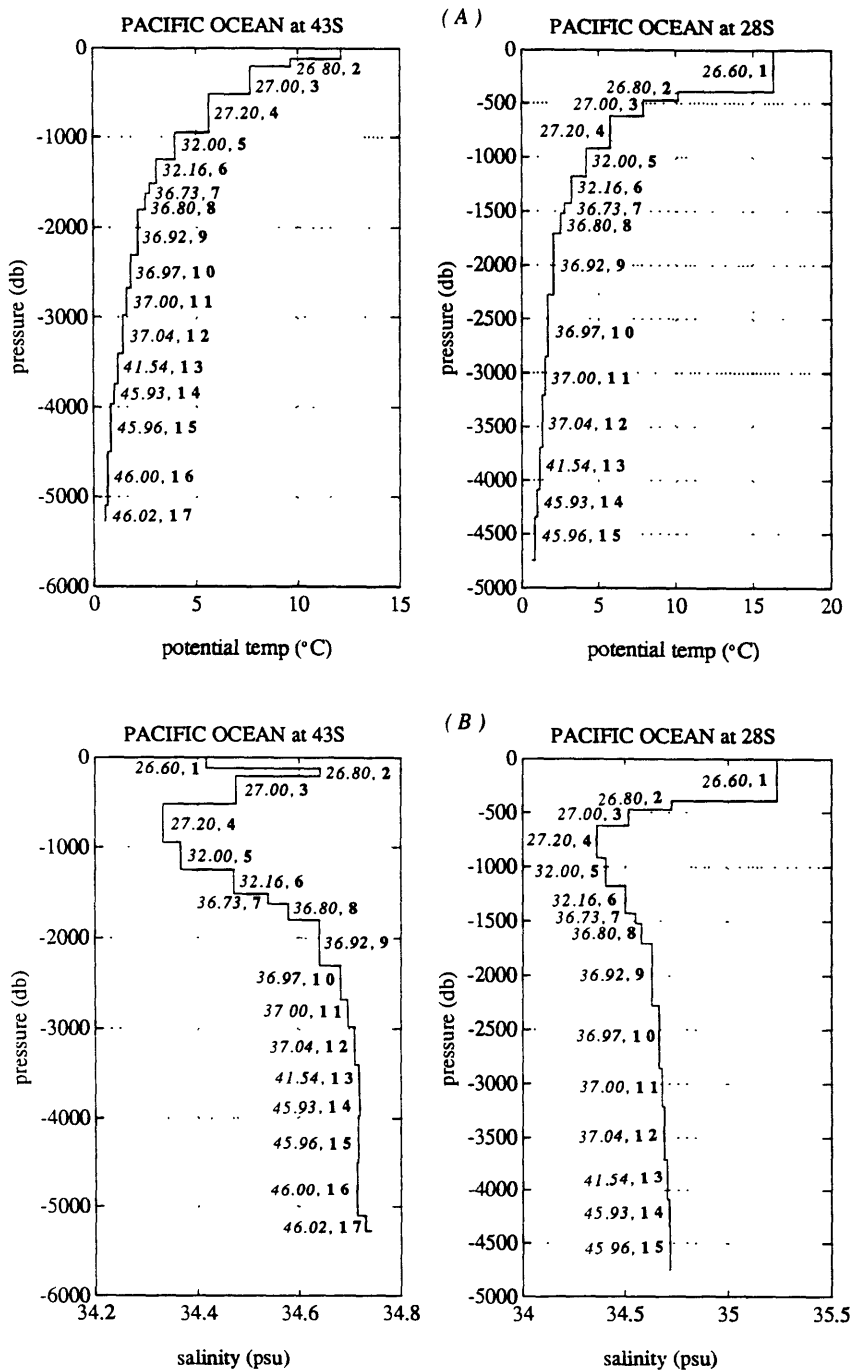
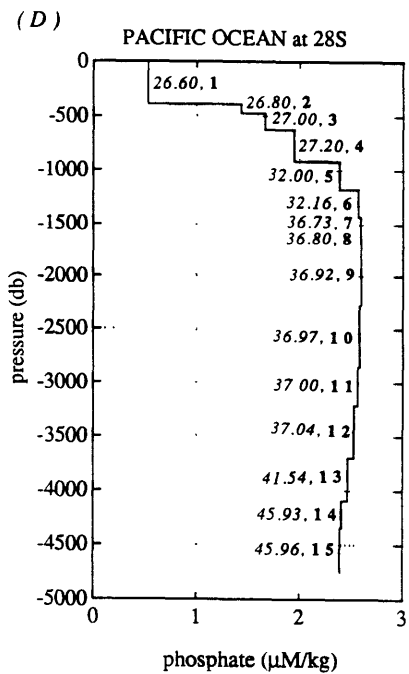
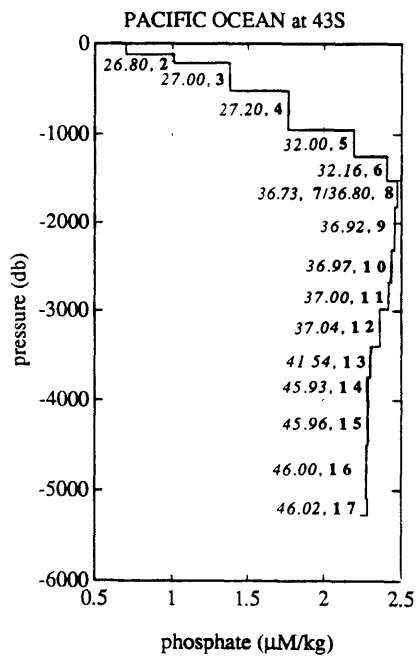
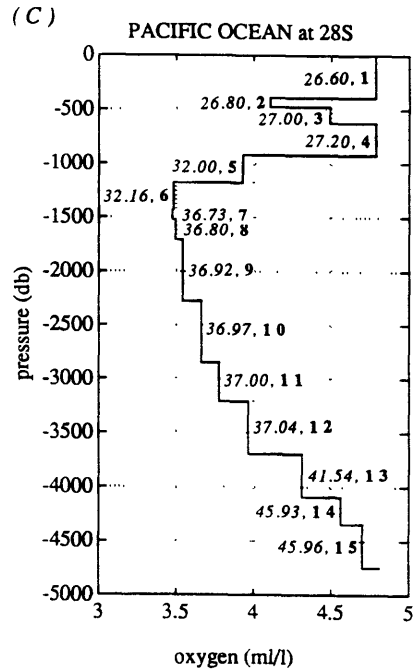
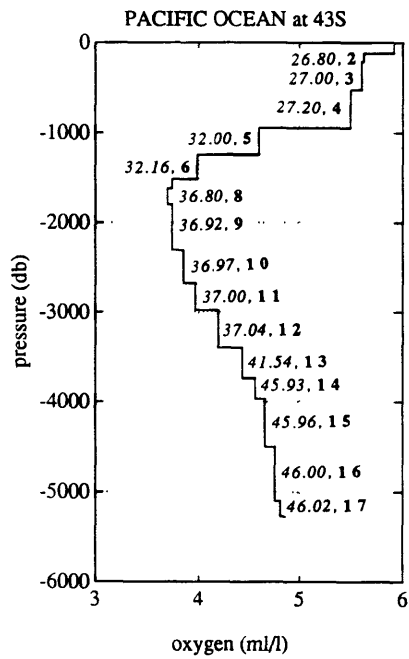
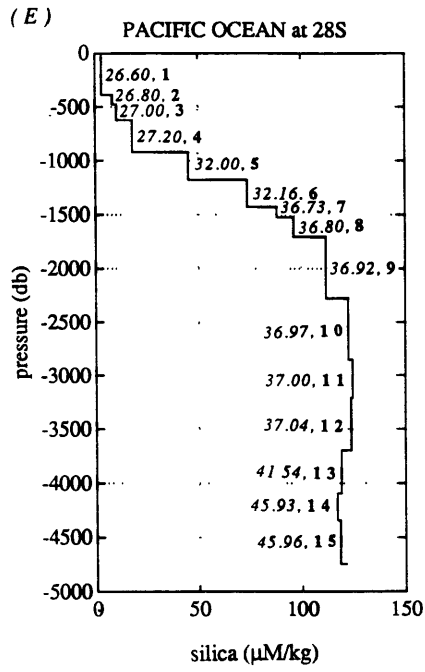
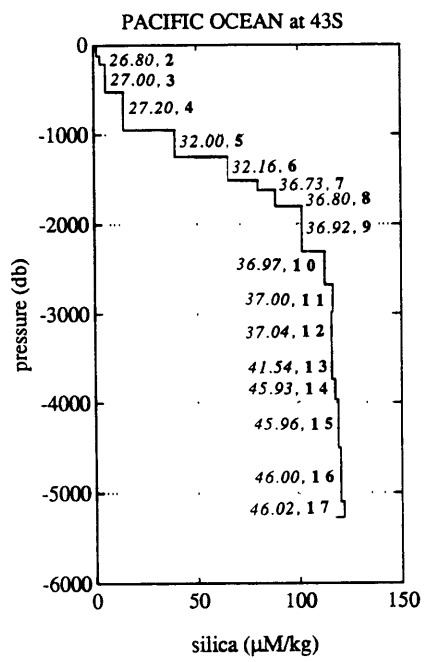


Figure 1.9: Zonally averaged profiles of temperature (a), salinity (b), oxygen (c), phosphate (d) and silica (e) for the Scorpio sections using the 18 layer model.





In this model the choice of rank comes down to a choice between a solution in which the surface mass residuals are large ( $\sim 6 \times 10^9$  kg/sec) (Fig 1.11) and the next higher rank in which the residuals have been reduced by the stricter application of the upper layer constraint (Fig. 1.12). The constraint which was added required that the convergence due to the wind stress be balanced by a net divergence of the geostrophic flow in the top layer. The solutions at the two ranks are quite different. We shall look at the higher rank solution compared to the model P1 solution as it represents an extreme (*ie.* the lower rank solution retains characteristics of both the higher rank solution and the P1 solution).

The higher rank solution finds the new requirement to be consistent with the other model constraints, but does not solve the problem by simply placing flows in the upper layers of the two sections equal and opposite to the associated Ekman flows at the two latitudes. At this rank the *a priori* estimate of the Ekman convergence is equal in magnitude to net the geostrophic divergence as computed from the mass residuals. The reference level velocities are larger  $b_{rms} = 0.8$  cm/sec compared to  $b_{rms} = 0.4$  cm/sec, a maximum value of 2.8 cm/sec compared to 1.2 cm/sec. They retain their overall character. The cross-isopycnal fluxes are also different. As seen in Fig. 1.12c there is now a downwelling feature in the upper interface, with the oscillating character reappearing below this.

At 43°S, the net (geostrophic + Ekman) transport in the surface layer has increased by  $\sim 2 \times 10^9$  kg/sec. The geostrophic poleward flow is completely confined to the surface layer. At 28°S, instead of a weak geostrophic poleward movement in the upper layer resulting in a net poleward transport, there is a strong  $7 \times 10^9$  kg/sec equatorward flux, leading to a net transport which is also northward. Below the surface layer, both sections display similar changes. The equatorward flow of AAIW is stronger and goes deeper than in the other models. The reversed flow



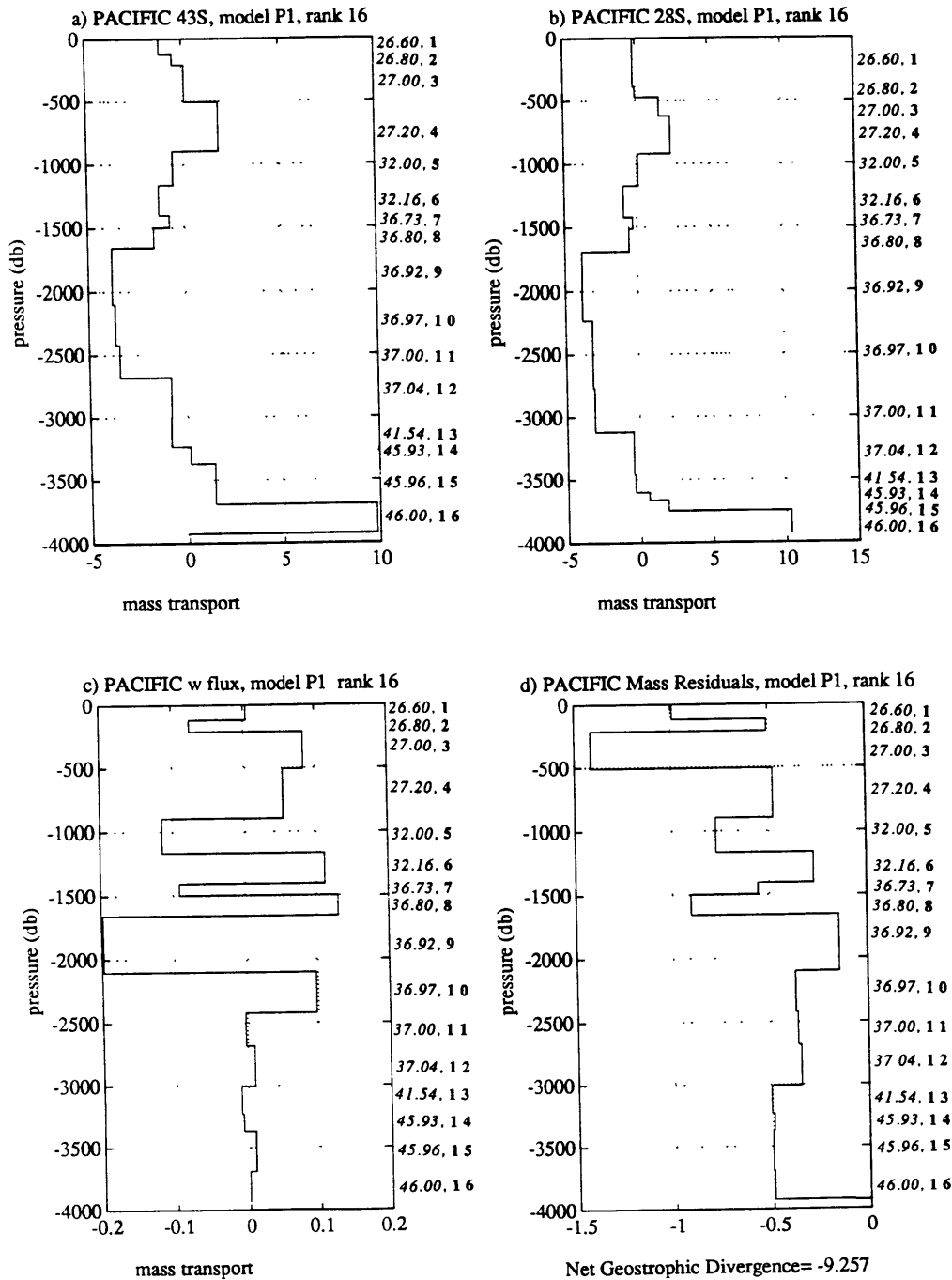


Figure 1.10: The zonally averaged mass transports from model P1 for the two Scorpio sections: (a) at 43°S, (b) at 28°S. (c) Mass transport across isopycnals due to the vertical transfer terms. (d) Mass residuals within each layer after the transports due to (a), (b) and (c) have been summed. The units are  $10^9$  kg/sec.

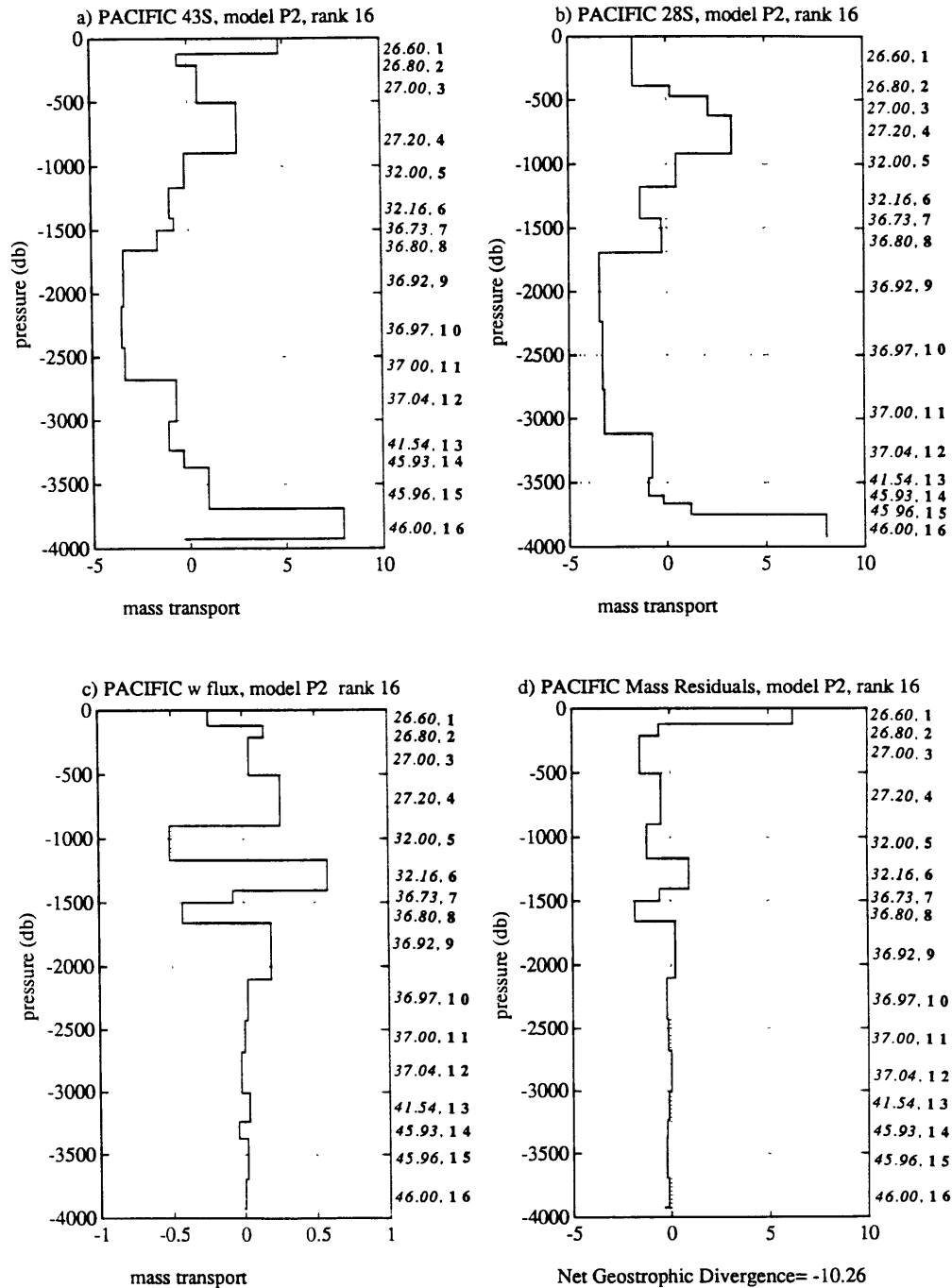


Figure 1.11: The zonally averaged mass transports from model P2 at the lower rank for the two Scorpio sections: (a) at 43°S, (b) at 28°S. (c) Mass transport across isopycnals due to the vertical transfer terms. (d) Mass residuals within each layer after the transports due to (a), (b) and (c) have been summed. The Ekman component has been included in the surface layer. The units are  $10^9$  kg/sec.

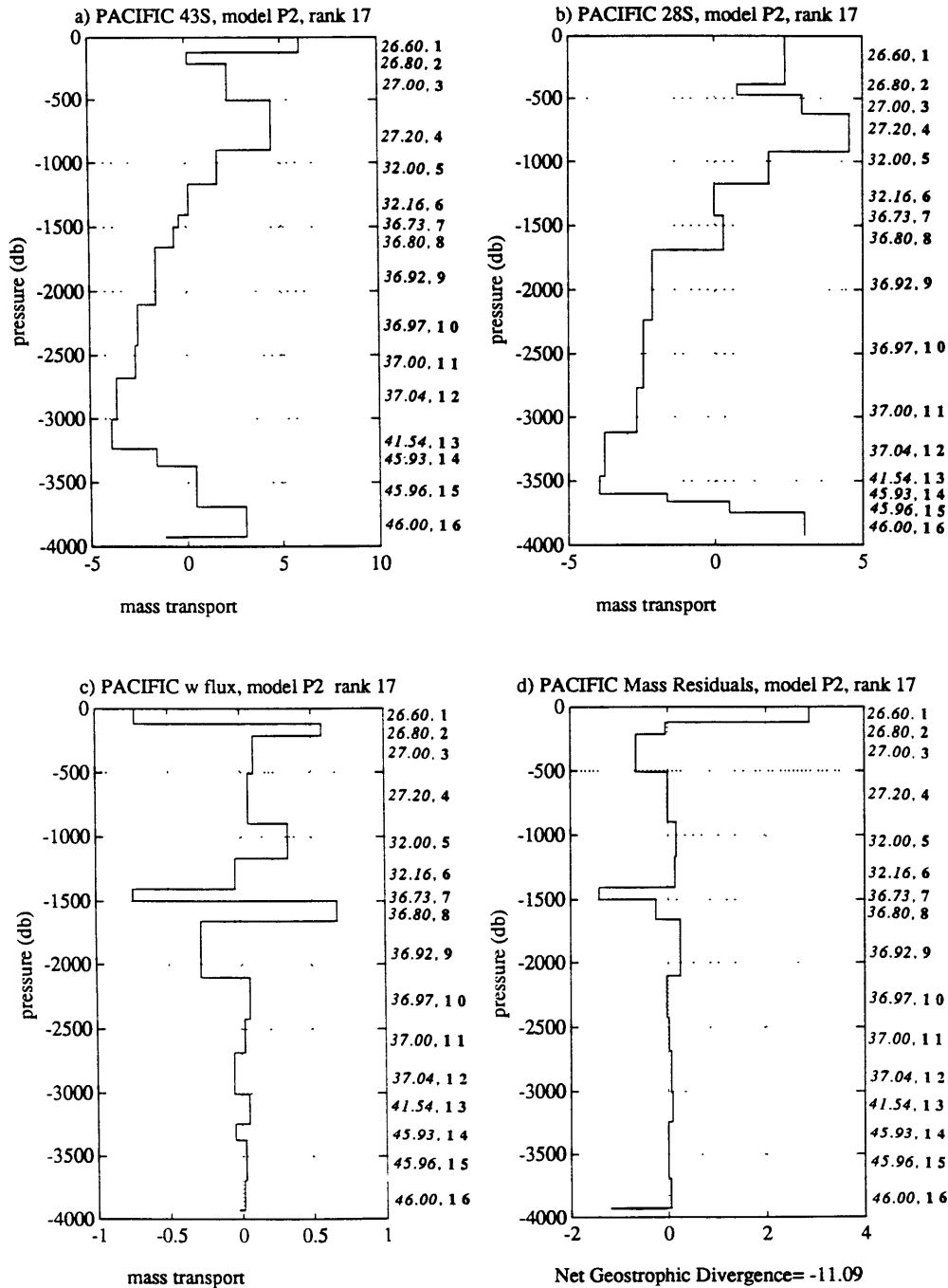


Figure 1.12: The zonally averaged mass transports from model P2 at the higher rank for the two Scorpio sections: (a) at 43°S, (b) at 28°S. (c) Mass transport across isopycnals due to the vertical transfer terms. (d) Mass residuals within each layer after the transports due to (a), (b) and (c) have been summed. The Ekman component has been included in the surface layer. The units are  $10^9$  kg/sec.

beneath this is also stronger, whereas in the lowest layers the equatorward flow of bottom water has weakened, now representing only  $2-3 \times 10^9$  kg/sec .

Figs. 1.13a and 1.13b illustrate the difference in the circulation produced by models P1 and P2. Although the  $w^*$ 's are not resolved, the P1 mass flux residuals imply that there is a strong ( $> 8 \times 10^9$  kg/sec ) downwelling from the surface layer to the AAIW waters beneath, between the two latitudes. The AAIW absorbs a couple of Sverdrups of this flux, but the rest must be entrained by the poleward mid-depth flow. Similarly, below the bottom waters entrains about  $1.5 \times 10^9$  kg/sec from above as they journey equatorward between  $43^\circ\text{S}$  and  $28^\circ\text{S}$ .

The solution for P2 differs from the P1 solution in the strength of the downwelling. The convergence in the top layer is only about  $4 \times 10^9$  kg/sec and significant portion of this is entrained in the AAIW. The mid-depth poleward flow gains only about  $1 \times 10^9$  kg/sec from above. In the previous model the mass source for this flow (assuming no large inputs north of  $28^\circ\text{S}$ ) would appear to be mainly upwelling bottom water in the north. In the current model most of the total mass flux of mid-depth poleward flow would come from the downwelling of surface and AAIW water. Downwelling from above occurs in both models. The difference is whether the downwelling occurs between these two latitudes or further north.

Turning to the lower rank P2 solution (Figs. 1.11 and 1.13c ) we find that the reference level velocities are little changed ( $b_{rms} = 0.4$  cm/sec) from the P1 solution. The net geostrophic divergence nearly matches the *a priori* estimate of the Ekman convergence. The equatorward bottom flux is  $\sim 9 \times 10^9$  kg/sec and does not appear to entrain any water from above. As in the other models, the mid-depth poleward flow is strong. It appears to entrain some water from above and below. In this model about  $2/3$  of the water in the mid-depth flow comes from upwelling of bottom water to the north.

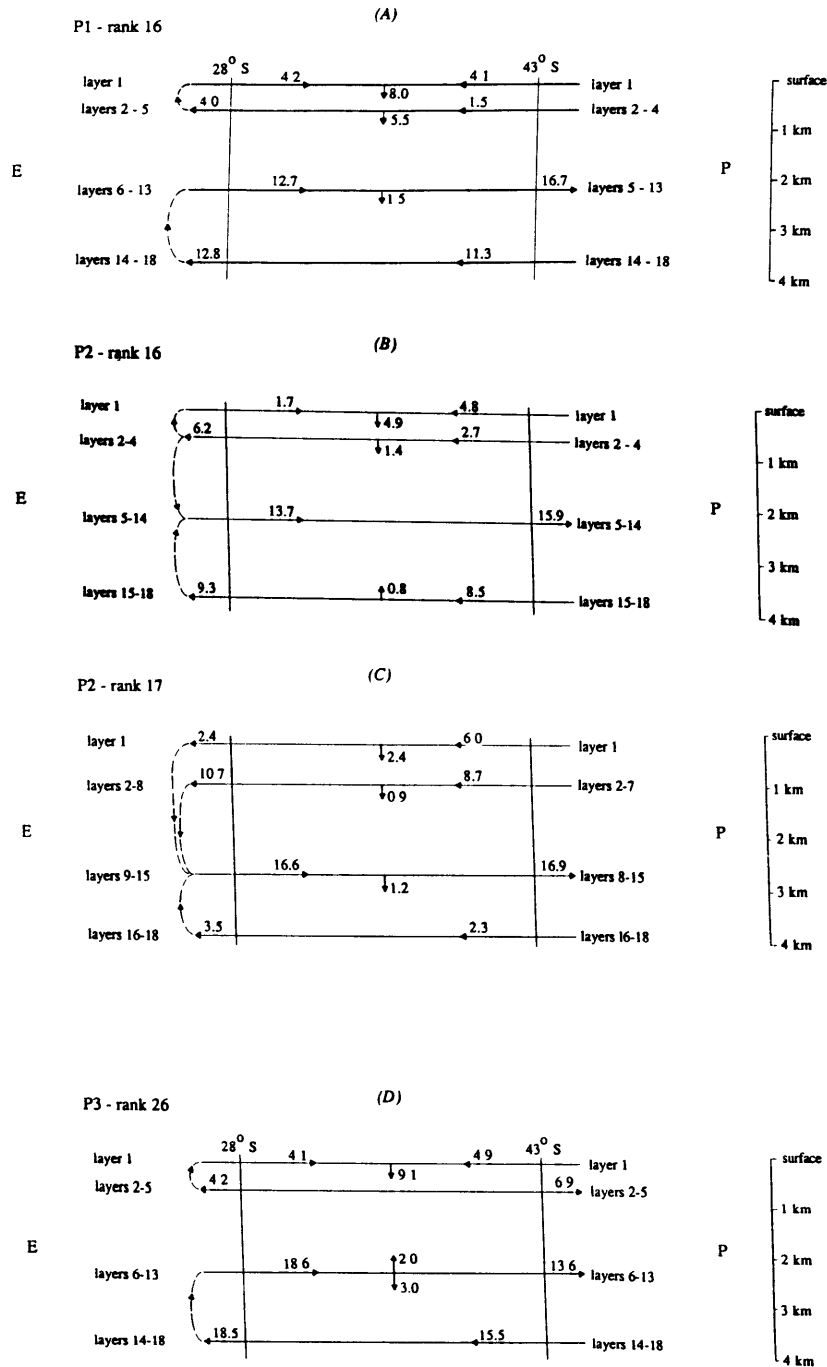


Figure 1.13: Schematic interpretation of the zonally averaged circulation based on the Scorpio sections: (a) Model P1 at rank 16, (b) Model P2 at rank 16, (c) Model P2 at rank 17 and (d) Model P3 at rank 26. Each line is at the mean depth of the layer or set of layers it represents. The vertical transports are computed by balancing mass from the bottom up. Transports are in units of  $10^9$  kg/sec

As mentioned earlier in the section on model S4d, the model P2 was also run, without the depth weighting. The solution for the reference level velocities was shown in comparison to a model including the depth weighting in Fig 1.8. It displays quite a different character from the previous solution;  $b_{rms} = 0.9$  cm/sec,  $b_{max} = 4.3$  cm/sec. The Ekman constraints still appear to be consistent with the other model constraints, but instead of solving the problem by spreading out the extra divergence of the entire reference level field, it instead increases the velocities sharply in the coastal regions. Since these are regions which contain boundary currents, it would appear that this solution could also be deemed physically sensible. It is personal preference, but we shall discard this solution for the reason explained previously: that is, the existence of the higher velocities in the shallow regions are believed to be more an artificial effect of the least squares solution, than one required by the physics of the system.

The choice between the two solutions, which were arrived at by either requiring or not requiring the Ekman convergence to be balanced in the top layer is also a matter of personal preference. We choose to use the one which *does* force the balance, but at a lower rank. We choose the lower rank solution for two reasons, one physical, the other technical. First, although it cannot be completely ruled out there is no observational evidence to support large amounts of downwelling in the northern Pacific (the freshness of the water in the upper layers of the Pacific makes it very difficult for sinking to occur). Secondly, we require from our models that the *a priori* estimates of the residuals be similar to those found *a posteriori*, therefore the lower rank is a more appropriate choice.

### *Property Fluxes*

As was found in the 1983 study, none of the calculated fluxes are distinguishable from zero. As explained in the previous section the standard errors are larger than found in the S4-91 and S4a models because the observation noise,  $\sigma$ , is now

being calculated from the residuals (equation A.10) rather than from the residuals left after the  $w^*$ 's have been manually subtracted. Since our choice of weights and constraints has affected the vertical structure of the mass transports it is useful to discuss the pattern of convergences and divergences in light of previous results.

However, before doing this we shall introduce a further refinement to the model which was first mentioned back in the section on model S4b. To reduce the standard error, the residuals need to be reduced. In model P3, we remove the downweighting applied to the  $w^*$  columns of the  $A$  matrix. Although the column normalization is still included, the removal of the explicit downweighting factor allows the cross-isopycnal transfer terms to become almost fully resolved (The diagonal elements of  $VV^T$  associated with these terms are approximately unity). The size of the  $w^*$  's increases by an order of magnitude to  $O(10^{-5}$  cm/sec) and the mass residuals are reduced to about  $0.2 \times 10^9$  kg/sec in each layer (Fig. 1.14). A schematic illustration of the resulting circulation is shown in Fig. 1.13d where it can be seen that the importance of vertical transfer in the circulation between the two sections has increased, especially near the surface. The deep circulation cell is stronger and to the north the circulation is similar to that produced by model P1.

The integrated property flux values are given in Table 1.9. We have estimates of the meridional heat flux in the South Pacific of  $0.1 \pm 0.6$  PW equatorward at  $43^\circ\text{S}$  and  $-0.4 \pm 0.9$  PW at  $28^\circ\text{S}$ . In spite of the many changes and the large error, these values are quite similar to those found by WHG. At the southern latitude, all our models have produced an equatorward heat flux as did almost all the models of WHG. In all cases these heat flux results have not been significantly different from zero.

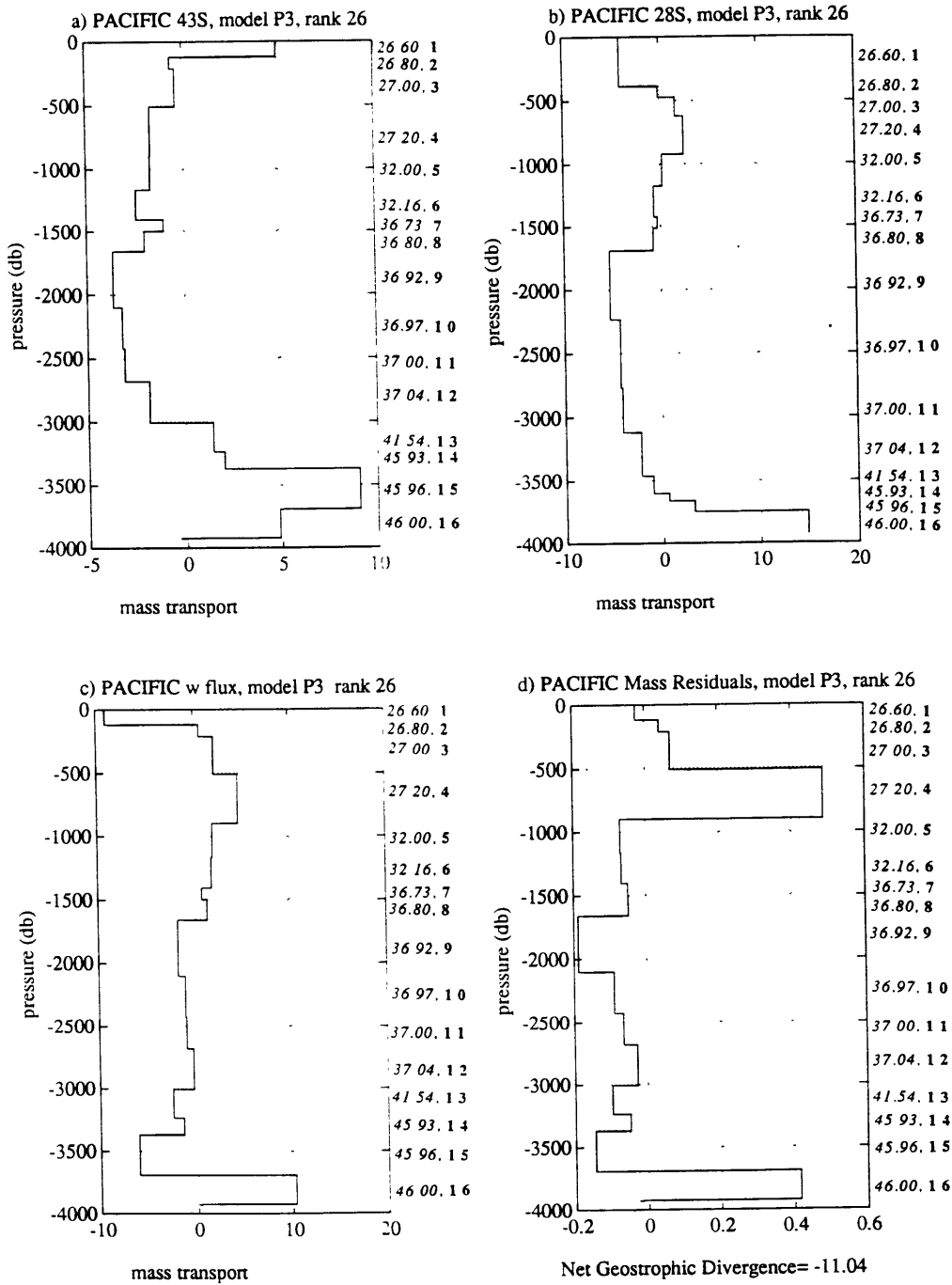


Figure 1.14: The zonally averaged mass transports from model P3 for the two Scorpio sections: (a) at 43°S, (b) at 28°S. (c) Mass transport across isopycnals due to the vertical transfer terms. (d) Mass residuals within each layer after the transports due to (a), (b) and (c) have been summed. The Ekman component has been included in the surface layer. The units are  $10^9$  kg/sec.



Model	P3	P4	Std. Error	Nullspace Error	Units
Net Transport	0	20			10 <sup>9</sup> kg/sec
43°S Heat	0.1	-	0.6	0.2	PW
28°S Heat	-0.4	-	0.9	0.2	
net conv.	0.5				
43°S Oxygen	39	126	73	15	10 <sup>9</sup> mL/sec
28°S Oxygen	64	148	162	14	
net conv.	-25	-22			
43°S Phosphate	-15	29	50	8	kmol/sec
28°S Phosphate	-10	34	51	9	
net conv.	5	5			
43°S Silica	-142	1578	2316	688	kmol/sec
28°S Silica	-135	1585	1919	671	
net conv.	-7	-7			
43°S PO38	-321	9571	7198	820	kmol/sec
28°S PO38	1521	11290	4567	1139	
net conv.	-1842	-1719			
Ekman 28°S	-4.4	-4.3			10 <sup>9</sup> kg/sec
Ekman 43°S	6.7	6.7			

Table 1.9: Property fluxes for the Pacific Ocean Models P3 and P4. Positive flux values are northward. Positive convergence values imply that more of a tracer enters the region between the two sections than leaves. The standard and nullspace errors are defined in Appendix B.

At 28°S, the heat flux doubled in size from -0.2 to -0.4 PW back in model S4c, when the row weighting by equation uncertainty was included. The increase in heat flux was due to the an associated increase in the Ekman flux estimate at this latitude which rose from approximately zero in model S4b to  $-4 \times 10^9$  kg/sec in model S4c. In model P3, very little change has occurred in the surface flow and as a result the heat flux estimate is similar.

Comparing these heat flux values with the other estimates given in Table 1.2, it is seen that our values are within the range of the previous estimates. Keep in mind that the standard error indicates that our 43°S value could easily have the opposite sign. Our estimates are small, as other direct heat flux estimates have been in comparison to the indirect estimates.

The similarity between the heat flux values at the two latitudes suggests that there is virtually no transfer to or from the atmosphere within this region. This

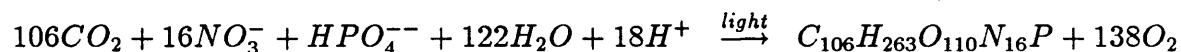
result is consistent with the findings of others (Hastenrath 1982, Weare *et al.* 1981 and Talley 1984).

### *Nutrient and Oxygen Fluxes*

Silicate, phosphate and oxygen are all minor dissolved components of seawater. Unlike major components, such as sodium, magnesium and sulfate, they are nonconservative in that they vary in their concentration ratios to chloride, in different locations because they are involved in the biological cycles within the ocean.

There is biological consumption and so, depletion in the surface waters. Reintroduction occurs at depth through death, decomposition and dissolution. These processes occur quickly compared to the rate of vertical mixing and so produce strong vertical gradients in concentration.

Most organic matter in the ocean is formed through photosynthesis in the euphotic zone ( *i.e.* to the depths where light can penetrate). The photosynthesis reaction which occurs can be written (Berner and Berner 1987): <sup>7</sup>



In the surface waters there is an abundance of all the components except nitrate and phosphate. When these two are present, photosynthesis and production of oxygen can occur. Then as the plentiful supply of phytoplankton are consumed by higher life forms, respiration takes place. Oxygen is consumed. Dead matter sinks and bacteria which also consume oxygen, liberate carbon dioxide, nitrates and phosphates, creating greater concentrations at depth.

Opaline silica is not part of the photosynthetic process, but is a hard part secreted by both benthos (bottom dwelling plants and animals) and plankton. The

---

<sup>7</sup>The ratios 106:16:1, C:N:P and 276:1, O:P, are commonly called the Redfield ratios (Redfield 1963). The quantity called PO38 which is used in our models as a conservative quantity is the ratio of 1 mole of phosphate to 138 of oxygen.

major source of opaline silica is however, those benthos and plankton which live in the euphotic zone (Berner and Berner 1987), resulting in a greater benthic source in shallow regions and a greater planktonic source in the deep ocean, and contributing to the overall variation in concentration. Opaline silica is quite soluble and therefore dissolution occurs throughout the water column in the open ocean producing an increasing concentration with depth. Broecker and Peng (1982) describe this cycle between the surface and bottom waters using box modelling combined with oceanic circulation and residence time estimates to produce estimates of nutrient concentrations.

In the Pacific, very little has been done in terms of estimating nutrient fluxes. We, therefore, present our results as a comparison of those of WHG. The integrated property flux results of WHG were given in Table 1.7. These values can be compared with those of our model P3 which are given in Table 1.9.

Based upon a GEOSECS meridional section through the Western Pacific (Broecker and Peng 1982), there is an increase in the silica content of the deep water to the north of 40°S. In agreement with this picture we find poleward fluxes of silica at both 43°S and 28°S and a net production<sup>8</sup> within the box, as did WHG. However, our production rate is lower due to a smaller flux at the southern latitude. As expected from the low surface concentrations, the silica flux is largely due to flow in the deep layers. The greatest overall difference between the WHG model and our own is in the relative strength of the deep circulation cell at the two latitudes. WHG found a bottom water flux of  $12 \times 10^9$  kg/sec at both latitudes. In model P3, we have a bottom water flux of  $19 \times 10^9$  kg/sec at 28°S but only  $16 \times 10^9$  kg/sec at 43°S. At 43°S, the highest concentrations are contained in the bottom water, whereas at 28°S the highest concentrations occur between about 2300 db

---

<sup>8</sup>Throughout this thesis the term production is used synonymously with divergence, while consumption implies convergence.

and 3600 db. The rearrangement of transport between the mid-depth and bottom water fluxes and relative silica concentrations at the different depths and latitudes accounts for the decrease in the estimate of net production in the region. WHG estimate the net silica production between 1200 and 3500 m at  $-0.3 \pm 0.2 \mu\text{M}/\text{kg yr}$ . We obtain consumption between 1200 and 3000 m and a production below 3000 m of about  $-0.2 \pm 0.6 \mu\text{M}/\text{kg yr}$ . WHG compare this to Fiadeiro's (1975) model estimate of  $-0.36$  to  $-0.11 \mu\text{M}/\text{kg yr}$ . In accordance with the net production of silica at depth, we find a net consumption in the surface layers (down to 500 m) of  $0.1 \pm 0.3 \mu\text{M}/\text{kg yr}$ . WHG found a similar value of  $0.2 \pm 0.1 \mu\text{M}/\text{kg yr}$ . As far as silica is concerned the pattern of divergences and convergences is consistent with the theory (consumption near the surface and production at depth) and has not varied a great deal in throughout the various changes made to the model. The fluxes themselves however, are sensitive to the chosen model constraints.

Our oxygen fluxes are similar to those found by WHG ( $43^\circ\text{S}_{WHG}$ :  $47 \pm 110$ ,  $43^\circ\text{S}_{P_3}$ :  $39 \pm 72$ ,  $28^\circ\text{S}_{WHG}$ :  $63 \pm 10$ ,  $28^\circ\text{S}_{P_3}$ :  $63 \pm 160$ , all units in  $10^3 \text{ mL}/\text{sec}$ ). There is a net production in the surface layers of  $5.6 \pm 3.8 \times 10^6 \mu\text{M}/\text{m}^2\text{yr}$  consistent with biological activity and the net consumption of silica near the surface. There is a total production within the box of  $6 \pm 12 \times 10^6 \mu\text{M}/\text{m}^2\text{yr}$ , which is greater the WHG's value of  $1 \pm 8 \times 10^6 \mu\text{M}/\text{m}^2 \text{ yr}$ .

As in WHG, we retain in the residuals some oxygen production down 1700 db. WHG discusses how an increase in rank and an associated increase in solution size will removed this anomaly, as will the inclusion of a nominal mixing coefficient. However, it is also true that these anomalies are not significant within the error, so the question as to which solution (lower or higher rank) is appropriate, may be moot. Unlike WHG, at depth our oxygen residuals tend to oscillate in sign as do the mass residuals since the increase in oxygen concentration with depth is similar at both latitudes. Overall, however, we still find a small net consumption of oxygen

at depth ( $1.6 \times 10^{-3} \mu \text{ M/kg yr}$ ) as would be expected in an environment where respiration rather than photosynthesis is taking place. WHG's value is somewhat larger,  $1.6 \times 10^{-2} \mu \text{ M/kg yr}$ , as is the estimate of Fiadiero and Craig (1978) of  $4\text{--}5 \times 10^{-2} \mu \text{ M/kg yr}$ . The difference in magnitude among the estimates is hardly significant as the error for both our model P3 and WHG's mode S4-83 is on the order of  $10 \mu \text{ M/kg yr}$ .

The phosphate fluxes are quite similar in character to the mass fluxes. Over the whole box there is a small production of  $0.3 \pm 2 \times 10^{-2} \mu \text{ M/kg yr}$ . Reflecting the oxygen production, there is some phosphate consumption at mid-depths. It is expected that as oxygen is consumed at depth through respiration, phosphate would be produced but in the deep water we find a net consumption of phosphate.

#### *Freshwater Flux*

The rate of addition of freshwater between either of the sections and the Bering Straits can be calculated in the following manner. Let the salt and freshwater fluxes be defined,

$$\bar{T}_T \bar{S}_T + \bar{T}_{Ek} \bar{S}_{Ek} + \bar{T}_L \bar{S}_L = 0 \quad (1.10)$$

$$\bar{T}_T + \bar{T}_{Ek} + T_L + T_F = 0 \quad (1.11)$$

where,

T refers to the absolute geostrophic flux across the section

Ek refers to the Ekman flux across the section

L refers to the leakage out of the area north of the section

F refers to the rate of addition of freshwater from excess evaporation over precipitation and river runoff north of the section.

– refers to the section average

Multiplying the equation 1.10 by the mean salinity for the section,  $S_o$  and subtracting it from equation 1.9 gives an expression for the freshwater input which satisfies both salt and mass conservation,

$$\bar{T}_T(\bar{S}_T - S_o) + \bar{T}_{Ek}(\bar{S}_{Ek} - S_o) + \bar{T}_L(\bar{S}_L - S_o) = FS_o \quad (1.12)$$

Using the results of model P3, allowing for a Bering Straits leakage of  $0.8 \times 10^9$  kg/sec at  $32.5^\circ/\text{oo}$  (Coachman and Aagaard 1988) leaves Ekman transports of  $7.4 \times 10^9$  kg/sec at  $43^\circ\text{S}$  and  $-3.6 \times 10^9$  kg/sec at  $28^\circ\text{S}$  when mass is balanced. Assuming  $\bar{S}_{Ek}$  is the mean salinity of the top layer for the section, gives values of F equal to  $0.1 \times 10^9$  kg/sec for  $43^\circ\text{S}$  and  $-0.2 \times 10^9$  kg/sec for  $28^\circ\text{S}$  (a net evaporation between the two sections of  $0.3 \times 10^9$  kg/sec ). WHG reported values of 0.08 and  $0.06 \times 10^9$  kg/sec ( a net freshwater input of  $.02 \times 10^9$  kg/sec between the sections). They all differ from the Baumgartner and Reichel (1975) estimates of  $0.49 \times 10^9$  kg/sec and  $0.52 \times 10^9$  kg/sec at the southern and northern latitudes, respectively ( a net evaporation of  $0.03 \times 10^9$  kg/sec ). Our estimates are sensitive to the salinity chosen for the Ekman flux and because the Bering Strait outflow was not included in the inverse the estimates are also sensitive these terms.

### *Independence of Model Constraints*

Two sets of models were run using different initial reference levels (deep and shallow) in which the various constraints on mass, salt, silica and phosphate were included one at a time in order to gain some insight into the importance of the various properties in constraining the system and into which of the particular

constraints gave the stability in the flux values with changing initial reference level. The conclusion from this set of runs was that:

- As found both others (Fu 1986, Rintoul 1988,1991) the salinity constraints do not supply much information independent of the mass constraints.
- Both silica and PO38 contain some additional independent information.
- The mass fluxes are fairly insensitive to the choice of reference level even when only mass conservation is used.

### Model P4 - Flow through the Indonesian Passage

Having discussed the importance of the various constraints as they affect transport estimates, we will now turn to the question of whether or not the data in the Scorpio hydrographic sections are consistent with any of the estimates of the through flow to the Indian Ocean through the Indonesian Archipelago as discussed in section 1.1.2.

In model P4, we included the possibility of a net flux through our box in the South Pacific, so that the flux equations which were previously written:

$$T_{geostrophic} + T_{Ekman} \approx 0, \quad (1.13)$$

are now written:

$$T_{geostrophic} + T_{Ekman} \approx T_{leakage}, \quad (1.14)$$

where, T is the transport through the section and leakage includes the flow out through both the Indonesian Archipelago and the Bering Straits.

Coachman and Aagaard (1988) give an estimated value for the flow through the Bering Straits of 0.8 Sv at a salinity of 32.5‰. As seen in Table 1.1, the estimates of flow through the Indonesian Passage range from 1.7 to 20 Sv. Most

estimates specify a flow of the upper 200 - 400 m of the water column. Piola and Gordon (1983) specify a salinity between  $33^{\circ}/_{\infty}$  and  $33.6^{\circ}/_{\infty}$ . We chose to force a net equatorward flux of  $20 \times 10^9$  kg/sec through our box, with  $0.8 \times 10^9$  kg/sec of it at  $32.5^{\circ}/_{\infty}$  and the rest at  $33.6^{\circ}/_{\infty}$ .

The mass transport results shown in Fig 1.15, appear to support the possibility of such a large net flux across the two latitudes. The rms reference level velocity has hardly changed ( $\mathbf{b}_{rms P4} = 0.34$  cm/sec,  $\mathbf{b}_{rms P3} = 0.33$  cm/sec). The differences required to support a net mass transport have been spread evenly across the breadth of each section.

At  $43^{\circ}$ S, the  $\sim 20$  Sv of through flow is spread out as more equatorward flow in every layer, with the maximum increase occurring in layers 9 and 15. The net surface flux is still equatorward. Layers 3 and 4 were poleward in model P3 and are now moving in the opposite direction. These layers were considered to be part of the salinity minimum of AAIW. The mid-depth poleward flow has been reduced to  $8.5 \times 10^9$  kg/sec from  $19 \times 10^9$  kg/sec. The equatorward flow of deep and bottom has strengthened by nearly  $5 \times 10^9$  kg/sec to  $22 \times 10^9$  kg/sec.

At  $28^{\circ}$ S the changes are similar. The greatest increase in equatorward flow occurs in layers 9, 10 and 16. The flux of bottom water has increased to  $22 \times 10^9$  kg/sec as layer 13 carries water towards the equator and the northward transport in layers 14–16 has increased by  $4 \times 10^9$  kg/sec.

The net geostrophic divergence is consistent with the estimate of the Ekman convergence calculated from the annual average wind stress. Subtracting these values from the net flux at each section and assuming there is a flux of  $0.8 \times 10^9$  kg/sec through the Bering Straits gives an upper limit estimate on the flux through the Indonesian Passage of  $18.9 \times 10^9$  kg/sec, consistent with the input estimate of  $19.2 \times 10^9$  kg/sec. Using the top layer salinity for the Ekman fluxes and the value of



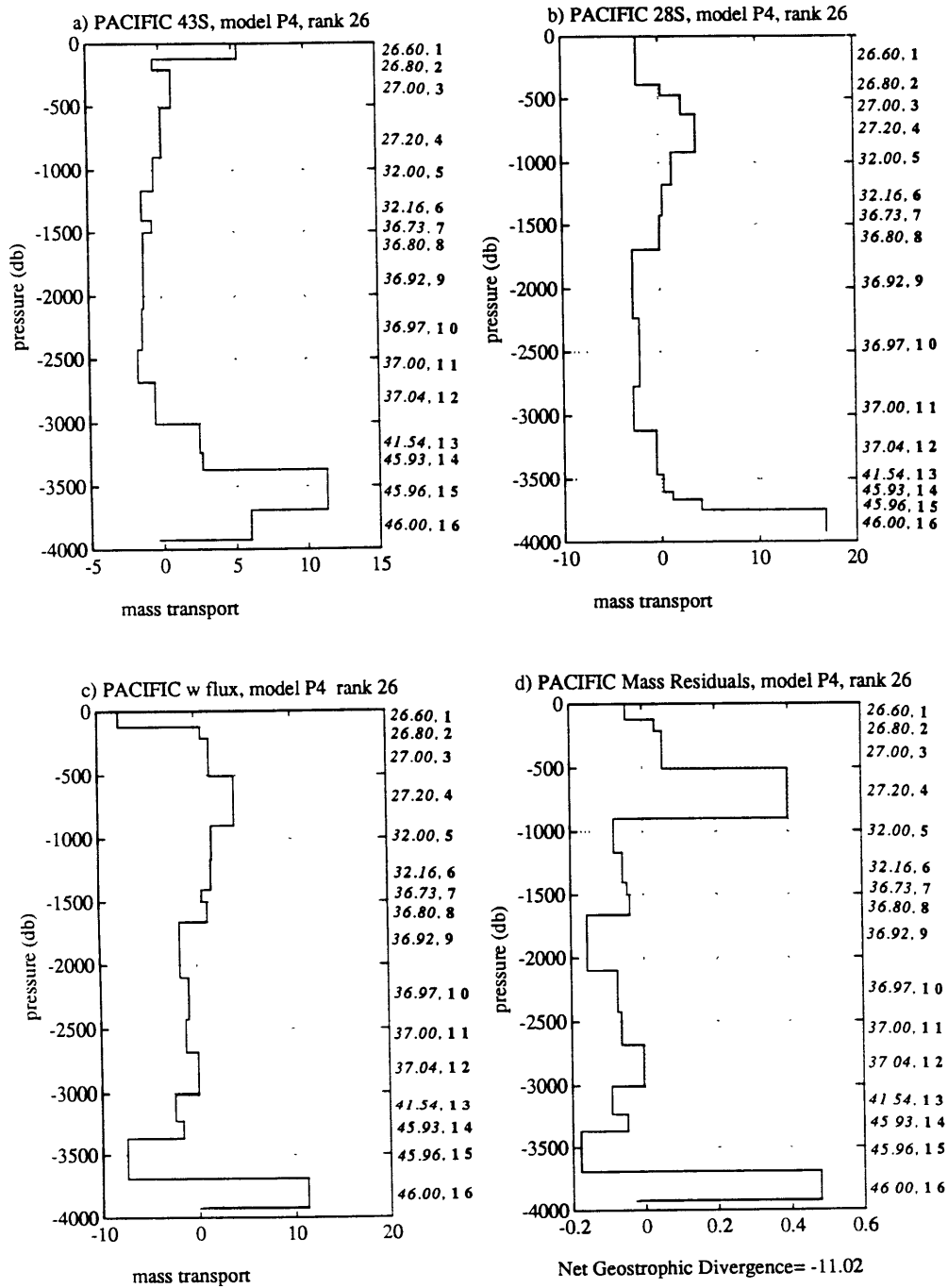


Figure 1.15: The zonally averaged mass transports from model P4 for the two Scorpio sections: (a) at 43°S, (b) at 28°S. (c) Mass transport across isopycnals due to the vertical transfer terms. (d) Mass residuals within each layer after the transports due to (a), (b) and (c) have been summed. The Ekman component has been included in the surface layer. The units are  $10^9$  kg/sec.

32.5‰ quoted by Coachman and Aargaard (1988) for the Bering Straits leakage implies a through flow salinity of 34.9‰ at 43°S and 34.5‰ at 28°S. These estimates are higher than the range given by Piola and Gordan (1983), 33.0‰ to 33.6‰. This would indicate that for the very high through flow estimates, either the water becomes considerably fresher as it travels northward or some reasonably large portion of the flux must be making its way through the deep channels of the archipelago.

To freshen this water to 33.6‰ requires an input of freshwater of about  $0.5 \times 10^9$  kg/sec at 28°S and  $0.7 \times 10^9$  kg/sec at 43°S. These values are similar to the estimate of freshwater input north of these latitudes given by Baumgartner and Reichel (1975) of about  $0.5 \times 10^9$  kg/sec. However, in support of a more saline through flow it can be seen in Wyrski's (1988) atlas that although the surface salinities near the Indonesian Archipelago display salinities  $<32$ ‰ in some seasons, the salinities between 300 and 600 m are on the order of 34.5‰ to 34.6‰. The expected salinity of the through flow is therefore difficult to pin down with this data set.

Since mass is no longer conserved when a net transport is included, the heat flux across these sections cannot be discussed. We can however discuss the flux of temperature based on a zero at 0°C. For model P3 the estimated temperature flux at 28°S is  $-87 \pm 225 \times 10^9$  °kg/sec. The temperature flux for model P4 which includes the  $20 \times 10^9$  kg/sec net mass transport is  $-12 \pm 240 \times 10^9$  °kg/sec. At 43°S the previous estimates was  $13 \pm 130 \times 10^9$  °kg/sec. It is now  $69 \pm 130 \times 10^9$  °kg/sec. Although these changes are tending towards an equatorward flux of temperature at both latitudes, they are not significant within the error and are still within the range of previous estimates. The oxygen flux has also increased as would be expected with the increased flow off oxygen rich bottom water. The net production of oxygen between the sections is about the same as in the previous model. The

nutrient fluxes have changed in accordance with the oxygen fluxes and the increased bottom water flow (Table 1.9).

The conclusion is that this model which estimates a possible transport through the Indonesian Passage of upto  $19 \times 10^9$  kg/sec is physically reasonable. The necessary freshwater input north of our sections to produce the relatively fresh through flow expected is similar to the estimates of freshwater input calculated from excess evaporation over precipitation and river runoff. The Scorpio sections can support a net mass flux as great as the largest estimates of through flow transport but they do not contain enough information to limit it. The effect of such a large through flow will be to increase the northward transport of temperature and oxygen.

Increasing the *a priori* estimate of through flow to  $30 \times 10^9$  kg/sec , produces more extensive, but similar changes to the model. How great a through flow is actually supported by the Scorpio data is dependent upon how much one is willing to see the circulation change. It is therefore, not possible to set an absolute upper limit on the through flow based on this data set alone. The fact that temperature flux becomes increasingly equatorward with increasing through flow leads us to conclude that although the largest through flow estimates are possible, they are likely to not to be long term means. The interannual and seasonal variations in the through flow discussed in section 1.1.2 would lend support to the idea that the Scorpio data set can be consistent with a periodically high through flow and a northward temperature flux in the South Pacific without being inconsistent with a through flow which in the long term carries less water and does not require the northward flux of temperature.

In the next chapter, using two sections in the southern Indian Ocean we shall first look at the effect of the various constraints on the zonally integrated transport at  $18^\circ\text{S}$  and  $31^\circ\text{S}$ . We will then combine the best estimate model from the Indian Ocean with our best estimate from the Pacific (model P2) and examine the effect of

the combined constraints on the transports and the possible limit to the Indonesian Passage through flow.

## Chapter 2

### The South Indian Ocean

#### 2.1 Introduction

In this chapter we consider the circulation in the southern Indian Ocean. Using a set of models in which property constraints are added one by one, we will produce a best estimate of the fluxes across  $18^{\circ}\text{S}$  and  $31^{\circ}\text{S}$  and discuss the relative importance of the constraints imposed. The solutions will be compared to previous results with emphasis on the role the Indian Ocean plays in balancing the global heat budget. As in the Pacific, we will also consider the affect of a large Pacific-Indian through flow upon our best estimate solution. In the final section, we will present a model which combines the constraints used in the South Pacific Ocean with those applied here in the South Indian Ocean. The motivation is twofold, first to investigate the effect of the various constraints on the meridional flux estimates and second, to determine the consistency of a high Indonesian Passage through flow in the presence of constraints from both the connecting oceans. A discussion of results in terms of global pathways of water masses will be left until Chapter 4.

As in Chapter 1, we will begin with a description of the region, the circulation and water masses as they have been described in the literature and discuss previous

estimates of heat transport in the southern Indian Ocean before describing the data and presenting the model results.

### 2.1.1 Water Masses and Circulation

The Indian Ocean basin, like the Atlantic and Pacific, is open to the Southern Ocean, whose boundary is described by the subtropical convergence located at about 40°S. The Indian Ocean is completely closed off to the north and west by the continents of Africa and Asia, but to the east, it is connected to the Pacific, between Australia and the island chain of Timor, Java and Sumatra.

The topography of the Indian Ocean basin is complex (Fig 2.1). In the southern region between 18°S and 31°S, the region of interest in this thesis, the ocean is divided into a number of separate basins, by a set of ridges running in the north-south direction. At 18°S, running from the west to the east coast, there is the Mozambique Basin, Mascarene Basin, Central Indian Basin and the Northwest Australian or Wharton Basin. The two eastern basins are completely separated by the island of Madagascar. At 31°S, the eastern ocean divides into the Mozambique and Madagascar basins. The Central Indian and Wharton basins are continuous between the two latitudes except for an east-west ridge between ~ 30°- 35°S, off the coast of Australia. The large number of basins provides an equally large number of western boundaries along which deep water entering the Indian Ocean can flow.

As in the Pacific, the surface circulation in Southern Indian Ocean is also in the form of an anti-cyclonic gyre. The northern limit of the gyre is at ~ 10°S (Tchernia 1980). The southern limit is the ACC. In February this southern boundary reaches to 38°S, but in August it reaches as far north as 30°S (Lutjeharms and Valentine 1984).

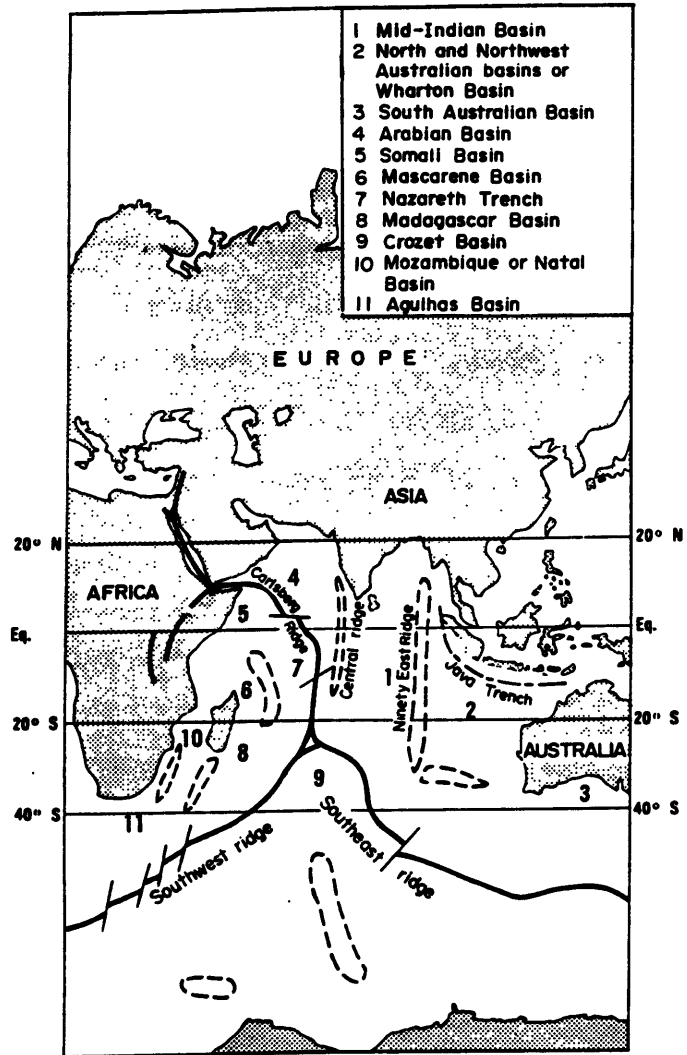


Figure 2.1: Topography of the Indian Ocean, from Tchernia (1980).

At 18°S there are two effective western boundaries for the surface flow in the Southern Indian Ocean. The westernmost is the coast of Africa. The island of Madagascar creates the second. The region between Madagascar and Africa has a sill depth of 2500 m. According to Warren (1981b) the northward transport at 18°S of upper layer waters of about 20 Sv is largely balanced by the southward flow along the east coast of Madagascar.

On the eastern side of the southern Indian Ocean the Leeuwin Current off the west coast of Australia complicates the simple picture of the basin wide surface anti-cyclonic gyre. The Leeuwin Current does not flow equatorward like the eastern boundary currents in the South Pacific and Atlantic, but rather flows towards the pole. It carries about 5 Sv of warm, fresh water, low in oxygen and high in nutrients to depths of about 250 m (Smith *et al.* 1991), southward against the prevailing winds. Weaver (1990) suggests that its poleward character relies upon the existence of the Pacific-Indian through flow, which carries equatorial Pacific waters around the northwest tip of Australia into the Indian Ocean. The Leeuwin Current is believed to be driven by an along shore density gradient which in turn drives an onshore geostrophic flow which bends southward upon meeting the coast of Australia. The current does express seasonal variations which appear to be due to variations in the windstress rather than variations in the along shore pressure gradient or the magnitude of through flow (Weaver 1990). Below the Leeuwin Current is an equatorward flow also of about 5 Sv (Thompson 1983) which carries the more saline, oxygen rich and nutrient poor South Indian Central water northward, closing the main anti-cyclonic gyre.

In the deep Indian Ocean, the Central Indian Ridge and Ninety-East Ridge divide the flow originating in the Antarctic into three distinct circulation systems. In the Mascarene and West Australian Basins, the equatorward flow of the western boundary currents appears to be associated with a weaker, poleward flow to the



east of the boundary. The Central Indian Basin is closed off below about 3500 m. Deep water which exists at depths greater than this finds its way into the Central Basin through passages in the Ninety-East Ridge from the West Australian Basin. The deep water from the Antarctic travels into the Indian Ocean not only from the west, but also from the east around southwest Australia.

The layering of the water properties in the subtropical region of the southern Indian Ocean is characterized by a number of different water types. Color plates of properties across the 18°S section are available in Warren (1981b). Numerous other sections are illustrated in Wyrтки's atlas (1988). The reader is referred to these two sources for examination of details in the temperature, salinity, oxygen and nutrient distributions.

### *Surface Water*

The surface water tends to have variable characteristics. Warren (1981b), in his description of the 18°S hydrographic section which we will be using, characterizes this water as being fresh compared to the pycnocline, warm, and nearly saturated with dissolved oxygen due to the rate of biological consumption. The surface salinity minimum is at about 10°S, increasing to the north, south and west. The suspected causes of this low salinity are the relatively fresh inflow from the Pacific and the excess precipitation over evaporation in the northeastern basin.

### *Salinity Maximum*

Below the surface water, centered at about 250 m is a water mass represented by a salinity maximum, due to the excess evaporation over precipitation between 25° and 35°S (Warren 1981b). This water has been given many names. We shall use the term subtropical surface water, coined by Wyrтки (1973) as it is a reminder of its origin.

### *Oxygen Maximum*

The Indian Ocean Central Water (ICW) centered at about 700m (Tchernia 1980) at 32°S and between 400-500 m (Warren 1981b) at 18°S corresponds to an oxygen maximum. It has been suggested that the origin of this water is sinking at the subtropical convergence (Svedrup *et al.* 1942). Another suggestion is that it is formed through deep vertical convection (Wyrski 1973, McCartney 1977) between the latitudes of 40°S and 50°S. This theory is supported by the low silica and phosphate content of the water from the surface all the way down to these depths.

### *Salinity Minimum*

The salinity minimum associated with the AAIW is found at a depth of about 900-1000 m at 18°S and about 1200 m at 31°S. This water mass has been recognized as far north as 10°S (Wyrski 1973) where it has upwelled to depths of 600-800 m. Beyond this it is lost as it meets in the high salinity Red Sea Water (Metzl *et al.* 1990 ) and the fresh inflow from the Pacific.

### *Intermediate Oxygen Minimum*

Below the AAIW, at about 1800 m at 40°S and rising to 600 m is the northern basins in an intermediate oxygen minimum and an associated phosphate maximum. Warren (1981b) suggests that this minimum is possibly due to *in situ* consumption of dissolved oxygen and a regeneration of phosphate. There is no associated maximum in the silica concentrations at these depths, but the maximum may simply be hidden by the overall increase in silica with depth.

### *Salinity Maximum*

The deep water centered at ~ 2500 - 3000 m displays the salinity maximum and phosphate minimum characteristic of the NADW (Metzl *et al.* 1990). This water arrives in the Indian Ocean after rounding the southern tip of Africa and is

Lat.	Date	Type	Reference	$10^{15}$ W
15°S	1985	i	Hsuing	-1.6
18°S	1986	d	Fu	-0.69
20°S	1989	i	Hsiung <i>et al.</i>	-0.23 to 0.0
28°S	1980	i	Hastenrath	-.49
30°S	1982	i	Bunker (from Georgi & Toole)	-0.98
30°S	1985	i	Hsuing	-1.42
32°S	1978	d	Bennett	-0.46 to 1.76
32°S	1985	d	Toole & Raymer	-0.6
32°S	1986	d	Fu	-0.25
40°S	1982	d,i	Georgi & Toole	+0.043 to -0.089
40°S	1982	i	Bunker (from Georgi & Toole)	-0.36

Table 2.1: Estimates of northward heat transport in the Indian Ocean. Type 'd' implies a direct estimate. Type 'i' implies an indirect estimate.

therefore, more apparent in the east than the west. Below 4000 m is the temperature minimum of the AABW which flows into the Indian Ocean along the numerous deep western boundaries which divide the individual basins at depth. It's northward flow is inhibited by the shallower sills it encounters.

In section 2.1.3, the appearance of these water masses (surface, subtropical surface, CIW, AAIW, NADW and AABW) as they are seen in our data will be described.

## 2.1.2 Review of Previous Results

Table 2.1 presents previous estimates of the heat transport in the southern Indian Ocean. Although the range of heat flux estimates here is not as great as was found in the South Pacific, it is still fairly large and the sign of the heat flux still appears to be in question. Unlike the South Pacific indirect estimates, those made for the southern Indian Ocean do not appear to be any larger than the direct estimates.

In the Indian Ocean there is no region to the north where large amounts of heat can be lost to the atmosphere in the formation of cold water. Thus it would appear that in this basin in particular, any heat gained in the northern regions must be transported by the ocean, southward, out of the Indian Ocean.

### 2.1.3 Description of the Data Used

In the Indian Ocean two data sets were used (Table 1.3). At 18°S, the hydrographic section of Warren (1981b) which was occupied between July 7th and August 19th 1976 was used as the northern boundary of the inverse box. This section does not quite span the entire basin, but runs from Madagascar to Australia. The southern boundary, at approximately 31°S was made by a CTD section kindly provided by J. Toole. It was occupied between the 12th of November and the 17th of December 1987 and ran from Durban South Africa to Perth Australia.

The station spacing at 18°S has a maximum of 208 km, but reduces to a minimum of 14 km on the east side of the Ninety East Ridge, with a mean spacing of about 125 km. The minimum station spacing at 31°S is 2 km. The maximum is 188, with an overall mean of 81 km.

A detailed description of the measurement methods and the data itself is available for the 18°S section in Warren (1981b). A similar description will be available for the 31°S section (Toole, in preparation).

Fig. 2.2 shows the zonally averaged vertical profiles of potential temperature, salinity, oxygen, phosphate and silica for both sections based on the 18 layer model described in Table 1.8.

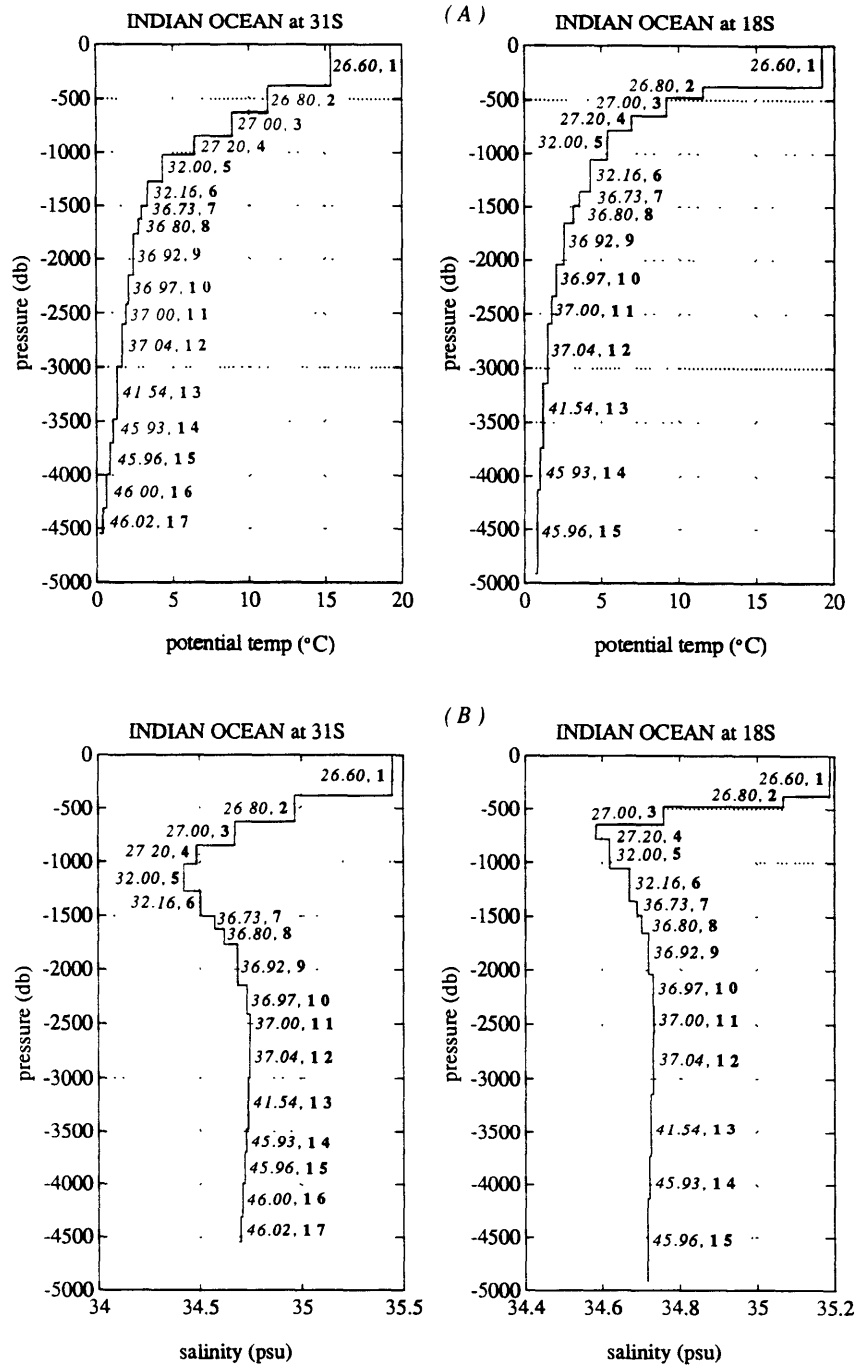
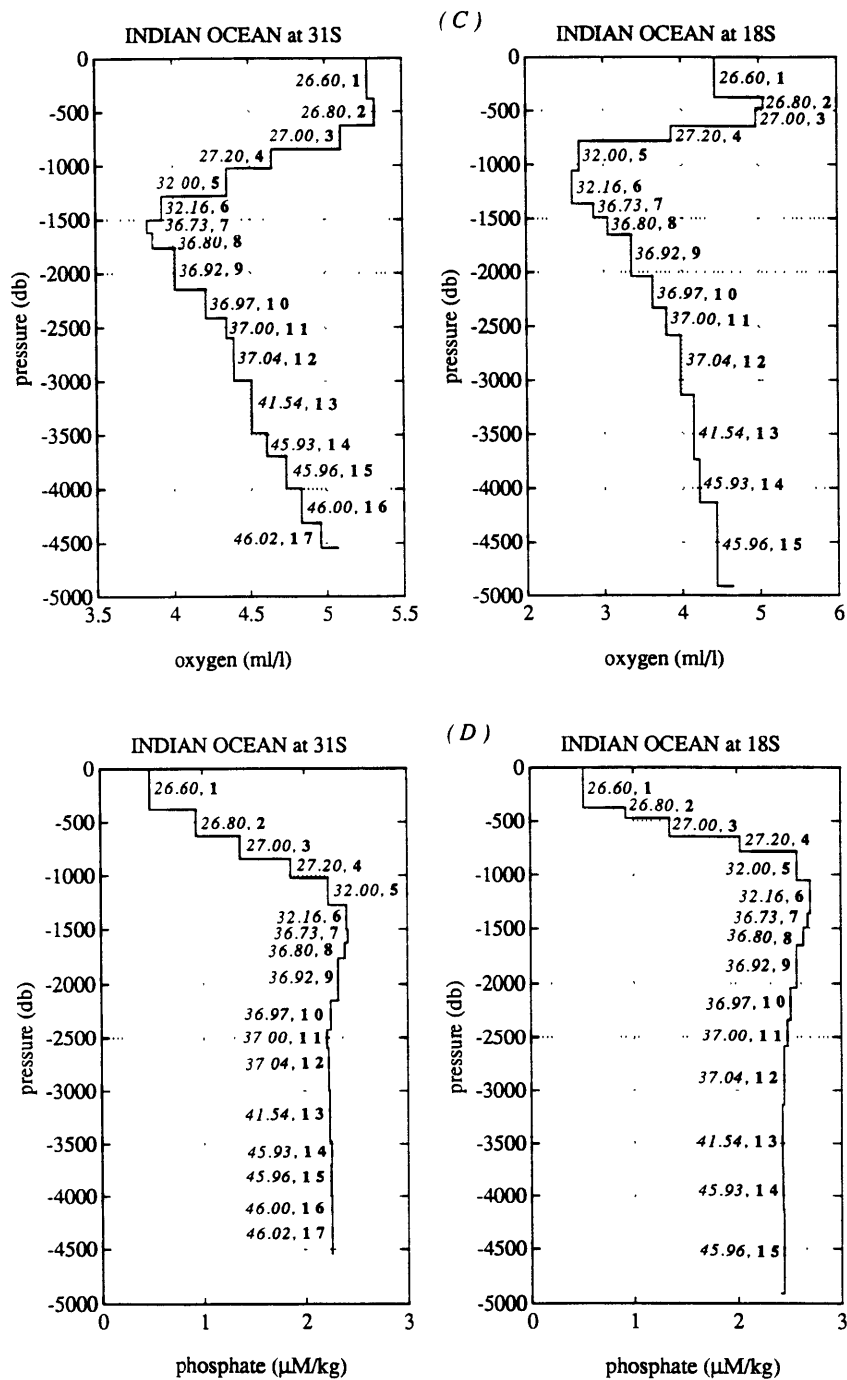
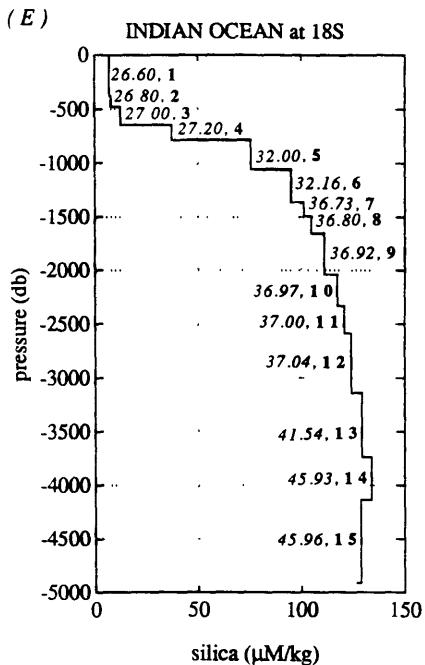
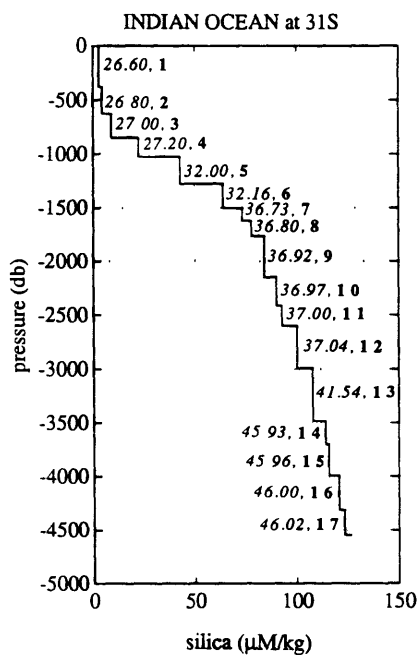


Figure 2.2: Zonally averaged profiles of temperature (a), salinity (b), oxygen (c), phosphate (d) and silica (e) for the Indian Ocean sections using the 18 layer model.





- The surface water (50-100 m) described in section 2.1.1 is not resolved with the given layers, but its characteristics of high temperature, high oxygen and low nutrients are readily apparent.
- The salinity maximum, centered on about 250 m and thought to be due to the excess evaporation between 25° and 35°S, is represented by the uppermost layer.
- The oxygen maximum of the Central Indian Water is seen in layer 2 at 31°S and layers 2-3 at 18°S.
- The minimum in salinity, whose origin is the AAIW is seen in layers 4 and 5 (possibly also layer 6 at 31°S).
- The intermediate oxygen minimum is centered on ~ 1500 db (layer 7) at 31°S and rises to about 1200 db (layer 6), with decreasing values ( ~ 2.75 ml/l compared to ~ 3.75 ml/l) at 18°S. The associated phosphate maximum is also visible. The lack of an associated silica maximum is apparent at both latitudes.
- The salinity maximum characteristic of the NADW at ~ 2250-3000 m is barely discernable in layers 11 and 12. The phosphate minimum is not apparent at 18°S, but just visible at 31°S. Due to the zonal averaging, distinctions between the deep western boundary flows in the various South Indian Ocean basins (discussed in detail by Warren 1981b) are not apparent. The one exception may be the silica maximum associated with the deep water of Central Indian Basin which is seen at 18°S at ~3750-4100 db (layer 14). The fact that the silica maximum is not visible at 31°S is consistent with the notion that this water is moving poleward from a region of very high silica concentrations in the North Central Indian Basin.



- The lowest temperatures, associated with the AABW are readily apparent below 4000 db, in both sections.

## 2.2 Indian Ocean Models

### *Models I1 and I1a - Conservation of Mass*

The simplest model used in the Indian Ocean requires the total geostrophic flow across the southern boundary of the box, at 31°S to balance the Ekman flow ( $T_{vg} + T_{ek} \approx 0$ ). Across the northern section, 18°S, the balance is among the geostrophic flux, the Ekman flux and the transport associated with the Mozambique Current ( $T_{vg} + T_{mz} + T_{ek} \approx 0$ ). There is a mass conservation constraint for each of the layers and a geostrophic divergence in the surface layer is required to balance the Ekman convergence between the sections. This model has a total of 21 equations, used to determine 176 unknowns (102  $b_j$ 's at 31°S, 57  $b_j$ 's at 18°S and 17  $w^*$ 's)

The flux attributable to the Mozambique Current is highly uncertain. Duncan (1970) gives an estimate of 26 Sv, whereas Sætre and De Silva (1984) conclude that there is no consistent flow at all between Madagascar and Africa. Intermediate values have been found by Fu (1986) and Harris (1972) of -6 Sv and -10 Sv, respectively. We use a mean value of  $-11 \times 10^9$  kg/sec with an uncertainty of  $14 \times 10^9$  kg/sec<sup>1</sup>.

The Ekman values were again calculated from the Han and Lee (1981) annual average wind stress values (Table 1.6); at 31°S,  $2.7 \pm 2.5 \times 10^9$  kg/sec, at 18°S,  $-10.8 \pm 7.6 \times 10^9$  kg/sec. At 31°S there was also a synoptic value available of 1

---

<sup>1</sup>This does not include the Harris (1972) estimate, as it was initially overlooked. Including this value produces a mean of  $-11 \pm 11 \times 10^9$  kg/sec, which means we are perhaps slightly overestimating the uncertainty.

Sv.<sup>2</sup> However, since this value was within the error of the annual average and since it is not obvious that the local synoptic winds drive the Ekman transport, it was decided to retain consistency among these estimates by using the annual average.

Appendix C details the affect of the disparity between the uncertainties at the two latitudes which eventually lead to an extra column weighting for the 18°S section.

### Models I1 and I1a - Conservation of Mass in Isopycnal Layers

We begin with model I1a which has an initial reference level at 18°S of  $\sigma_1 = 32.16$ , which is approximately 1300 db, the depth of the oxygen minimum. At 31°S, we used the station specific reference levels provided by J. Toole from his analysis of the water properties for this section. To determine the model sensitivity to the initial assumption about these *levels of no motion* we also ran the model using an initial reference level of  $\sim 3500$  db,  $\sigma_3 = 41.54$ . This corresponds to the split between the lower equatorward flow of deep and bottom waters and the overlying, silica rich flow poleward flow.

In both models the solution size required to reduce the residuals to an acceptable size was  $b_{rms} \approx 0.5$  cm/sec. The greatest values of  $\mathbf{b}_j$  occur in the western boundary regions of both sections. The cross-isopycnal transfer terms display the same oscillatory behavior as those found in the Pacific models. The deep initial reference level produces the character of decreased amplitude with depth. The shallower initial reference level does not appear to require the larger values of  $\mathbf{w}^*$ 's in the upper layers.

The absolute velocity field for our best estimate model (to be chosen later) is shown in Fig. 2.3. At 18°S, there are very high velocities (upto 1.5 m/s) near

---

<sup>2</sup>The synoptic Ekman value was supplied by John Toole resulted from wind stress estimates made during the cruise.

the east coast of Madagascar. Just to the east of this poleward current, there is a much smaller counter current. There are three deep western boundary currents flowing to the north. The one in the western basin appears to be offset from the east coast of Madagascar. Against the Central Indian Ridge, there is a broader, northward flow extending to the Ninety–East Ridge. In the eastern basin, the deep western boundary current flowing along the Ninety–East Ridge is seen with a counter current; a feature found by Fu (1986). There is a relatively weak southward flow with velocities upto 11 cm/sec representing the Leeuwin Current offset from the West Coast of Australia. At 31°S, the most obvious feature is the strong, poleward flow of the Agulhas Current against the east coast of South Africa. The Leeuwin Current, on the eastern side of the basin, is again offset from the coast, but at this latitude attains velocities upto 40 cm/sec. The northward flows of the deep western boundary currents are again apparent in all the basins. The broadest deep flow is in the Central Indian Basin.

The zonally integrated meridional transports (Fig. 2.4 and Fig. 2.5) are similar in structure for the two initial reference levels, but they differ somewhat in magnitude. In the following discussion the Ekman component has been assigned to the top layer. At 31°S:

- There is a large poleward flow of surface and subtropical surface water in the warmest layer ( $-11_{SIRL}, -13_{DIRL}, \pm 9$ )<sup>3</sup>.
- This overlies a small equatorward flow ( $1 \pm 8$  for both the SIRL and the DIRL).

---

3

SIRL refers to the shallow initial reference level

DIRL refers to the deep initial reference level

units are  $10^9$  kg/sec

- Below this, down to  $\sim 2000$  db for the DIRL and  $\sim 1750$  db for the SIRL, is a poleward flow ( $7_{SIRL}, 12_{DIRL}, \pm 18$ ) of water which we had associated with the salinity minimum of the AAIW and the intermediate oxygen minimum. It may be that there is, in fact a net equatorward flow of AAIW in the ocean interior but that this is offset by large poleward flow of water in the Agulhas Current, which though saltier and warmer than AAIW, has a similar potential density. (J. Toole personal communication).
- The combined flows of the NADW and the AABW provide a balancing northward flux ( $17_{SIRL}, 25_{DIRL}, \pm 21$ ). In layer 14, which contains the silica maximum of the Central Indian basin, the transport is much reduced in the SIRL model.

At  $18^\circ\text{S}$  the character of the zonally integrated meridional transports is similar:

- The upper poleward flux has a similar magnitude to the  $31^\circ\text{S}$  flux namely, ( $-11_{SIRL}, -13_{DIRL}, \pm 26$ ).
- The equatorward flow of CIW below this, is slightly larger at  $18^\circ\text{S}$  for the SIRL, but it is essentially non-existent in the DIRL model ( $1_{SIRL}, 0_{DIRL}, \pm 22$ ).
- The intermediate poleward flow is again confined to shallower depths in the SIRL model where it extends to only about 1400 db, as compared to the DIRL model where it still reaches to  $\sim 2250$  db. The amounts of water carried by the two models also differ ( $-5_{SIRL}, -9_{DIRL}, \pm 48$ ).
- The equatorward flux of deep and bottom water is again strong with the weaker flow being associated with the SIRL model ( $16_{SIRL}, 25_{DIRL}, \pm 70$ ).

The mass residuals, shown in Figs. 2.4d and 2.5d are similar for the two initial reference levels and contain no obvious structure.

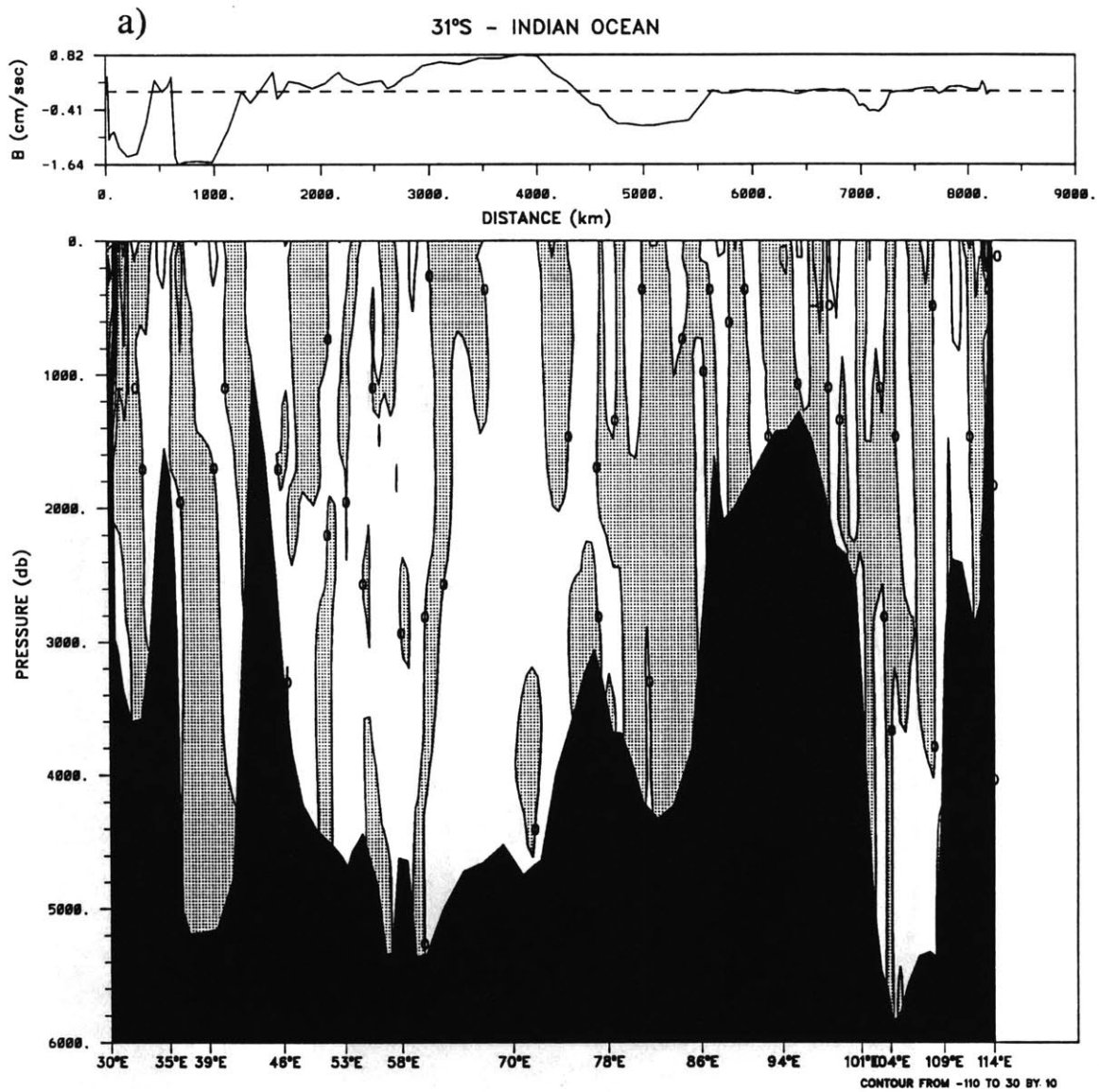
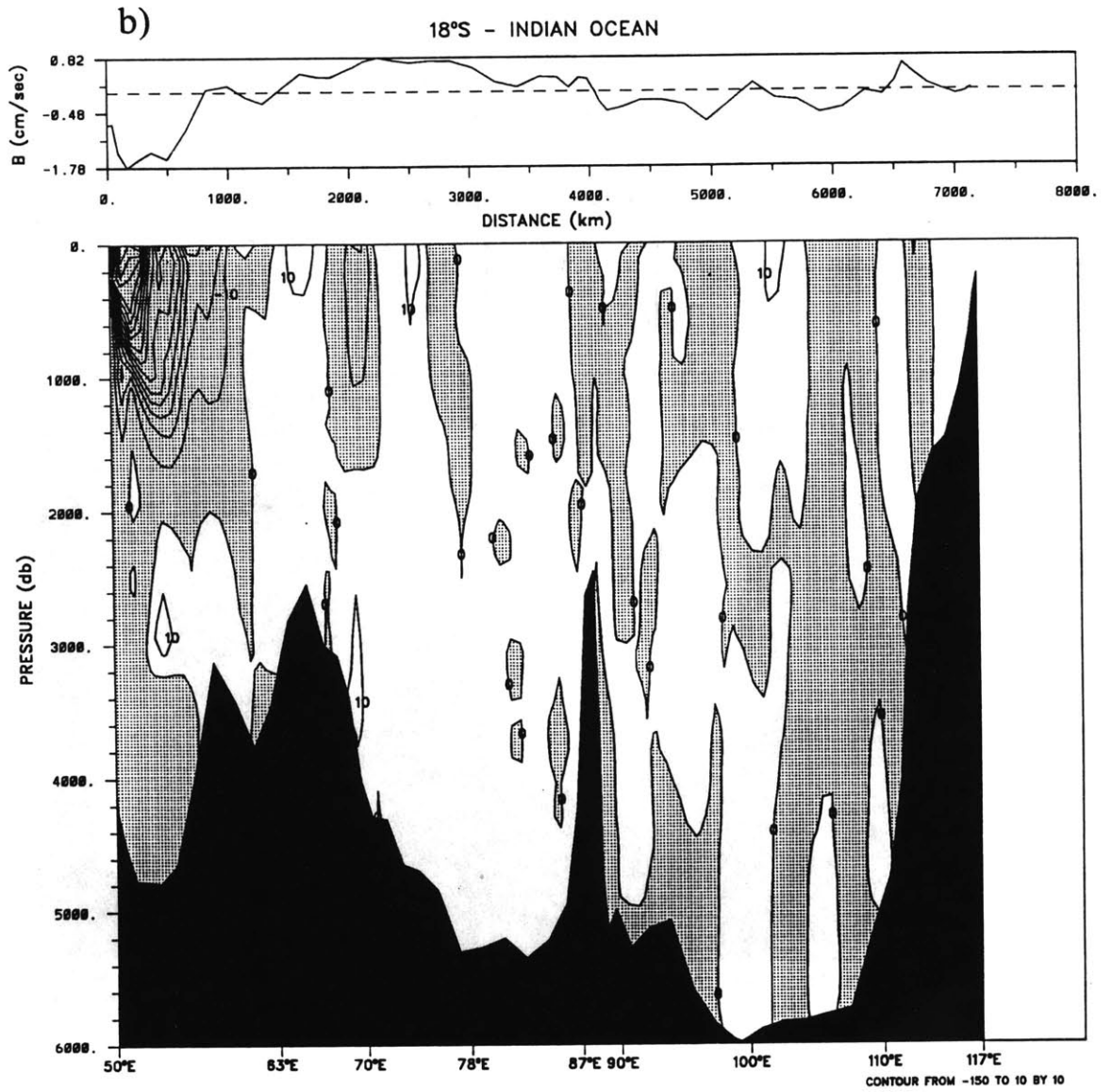


Figure 2.3: The absolute velocity field for our best estimate Indian Ocean model, I4b: (a) at 31°S, between South Africa and Australia and (b) at 18°S, between Madagascar and Australia. The reference level velocities at  $\sigma_1 = 32.16$  for 18°S and at the station specific reference levels provided by J. Toole at 31°S are displayed at the top.



As in the Pacific models, the model-estimated Ekman transport is assumed to balance the net geostrophic transport at 31°S. For both initial reference levels this results in an Ekman mass flux of  $\sim 2.5 \times 10^9$  kg/sec . This estimate is consistent with the value produced using the annual average wind stress. To find the Ekman flux at 18°S, it is assumed that the top layer geostrophic divergence exactly balances the Ekman convergence. Given the Ekman transport at 31°S, it is then possible to compute that at 18°S. Again the values estimated for the two models which use different initial reference levels are not significantly different and are consistent with the those computed from the annual average windstress ( $11_{SIRL}$ ,  $11_{DIRL}$ ).

The estimated flow through the Mozambique Channel at 18°S is taken to be the residual of the balance between the Ekman and net geostrophic flows at this latitude. The values obtained ( $-3.5_{SIRL}$ ,  $-2.7_{DIRL}$ ) are on the low end of the large range found in the literature.

The fact that the model has little difficulty in finding solutions consistent with the initial estimates is encouraging. It appears that it is possible to find consistent solutions using data sets which were obtained ten years apart and in different seasons. The fairly large flexibility built into the model constraints due to some of the uncertainties involved may be responsible in part, at least, for our ability to merge these two data sets. This does not rule out the possibility of seasonal or even interannual variability, but does indicate that we cannot determine them and allows us to continue the experiment of combining these varied sets of data.

### *Property Fluxes*

We have shown that there are some variations in the mass transports of the two models using the different initial reference levels. We now turn to the effects produced by these differences on the property fluxes across the two sections (see Table 2.2). The net heat flux which is on the order of  $1 \pm 3$  PW to the south, is not

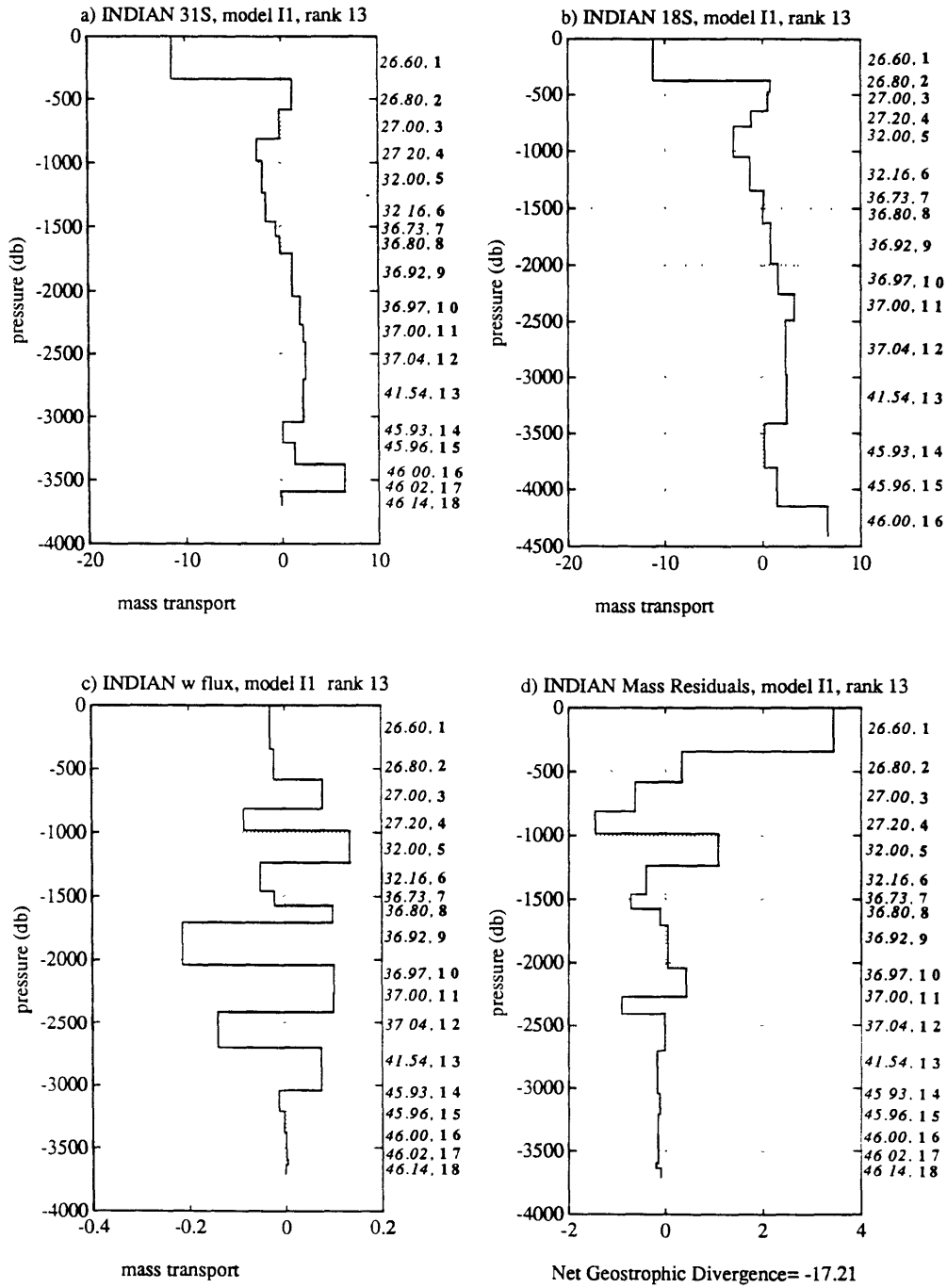


Figure 2.4: The zonally averaged mass transports from model I1 (uses a shallow reference level) for the two Indian Ocean sections: (a) at 31°S, (b) at 18°S. (c) Mass transport across isopycnals due to the vertical transfer terms. (d) Mass residuals within each layer after the transports due to (a), (b) and (c) have been summed. The Ekman component is included in the surface layer. The units are  $10^9$  kg/sec.



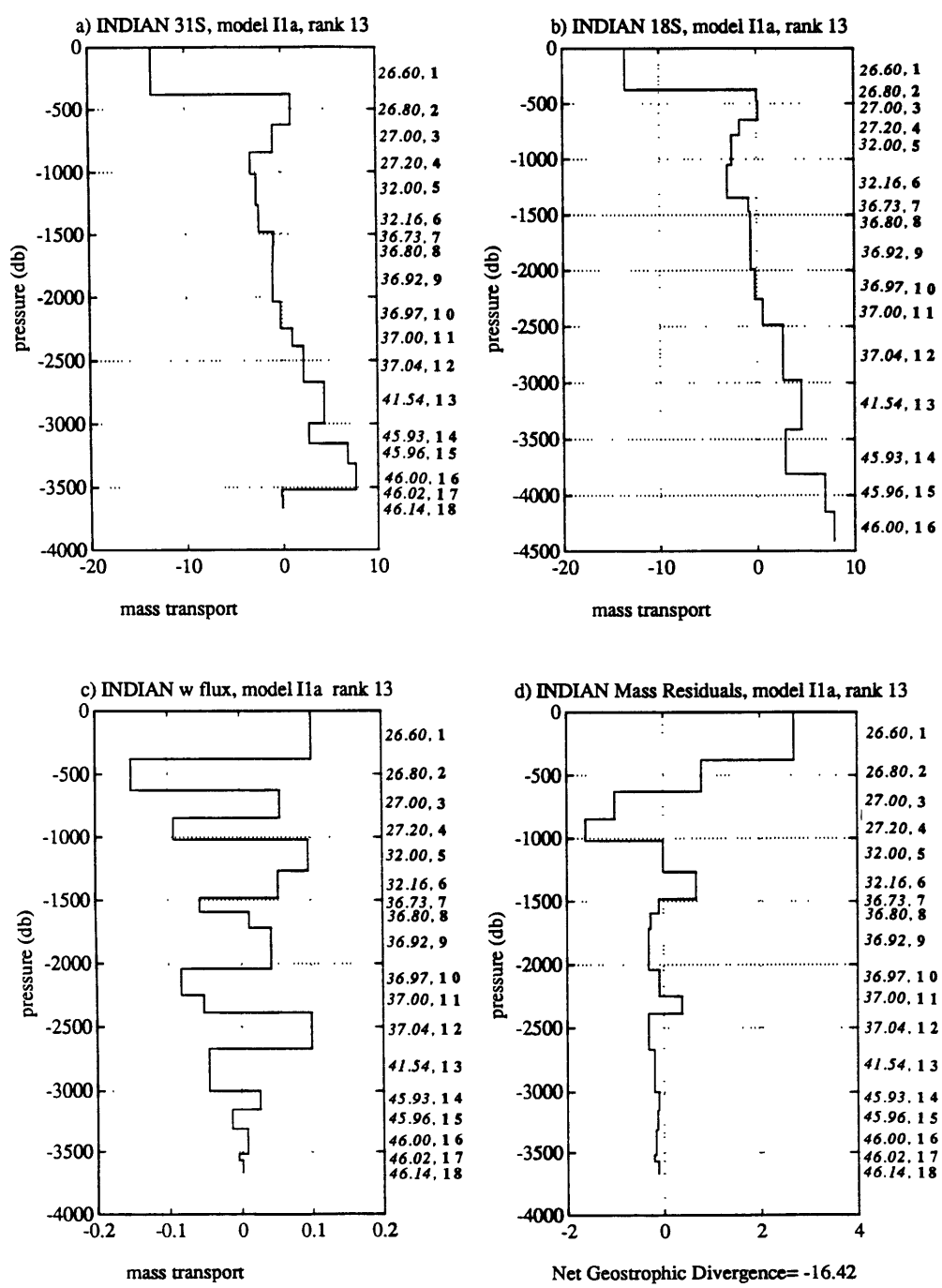


Figure 2.5: The zonally averaged mass transports from model I1a (uses a deep reference level) for the two Indian Ocean sections: (a) at 31°S, (b) at 18°S. (c) Mass transport across isopycnals due to the vertical transfer terms. (d) Mass residuals within each layer after the transports due to (a), (b) and (c) have been summed. The Ekman component is included in the surface layer. The units are  $10^9$  kg/sec.

	Model I1 SIRL	Model I1a DIRL	Std. Error	Nullspace Error	Units
31°S Heat	-0.9	-1.2	2.4	0.2	PW
18°S Heat	-0.9	-1.2	2.3	0.3	
net conv.	0.0	0.0			
31°S Oxygen	44	42	152	12	10 <sup>9</sup> mL/sec
18°S Oxygen	36	23	366	16	
net conv.	8	19			
31°S Phosphate	17	25	95	9	kmol/sec
18°S Phosphate	15	20	214	11	
net conv.	2	5			
31°S Silica	610	1693	7457	974	kmol/sec
18°S Silica	1248	2224	10350	674	
net conv.	-638	-531			
31°S PO38	4347	5329	16800	1061	kmol/sec
18°S PO38	3716	3748	45400	1584	
net conv.	631	1581			
Mozambique	-3.5	-2.7			10 <sup>9</sup> kg/sec
Ekman 18°S	-11.1	-11.4			
Ekman 31°S	2.6	2.5			

Table 2.2: Property fluxes for the Indian Ocean Models I1 and I1a which conserve mass in isopycnal layers. Positive flux values are northward. Positive convergence values imply that more of a tracer enters the region between the two sections than leaves. The standard and nullspace errors are defined in Appendix B. The standard error is the average for the two models

greatly affected by the difference in initial reference level. This is so because most of the transport variation occurs at the deeper levels where the temperatures are lower and vary less with depth.

At 18°S, in particular, the oxygen flux is somewhat more affected by the change in initial reference level, as there is much more variation in oxygen concentration with depth compared to temperature, and there is a steady increase in the oxygen values below about 1000 db. In both models, besides the surface layers, the largest fluxes of oxygen are in the deep equatorward moving layers (except for layer 14), indicating that the Indian Ocean is being ventilated through the influx of NADW and AABW along the western boundaries.

The transports of phosphate are also a little sensitive to the choice of initial reference level. When combined with oxygen in the PO38 quantity there is a fairly

large sensitivity. The net convergence of PO38 within the box is twice as large for the deep reference level model, due to a large increase in the flux at 31°S.

The silica fluxes are extremely sensitive to the initial reference level assumptions, especially at 31°S. The fluxes nearly tripled in DURL model. On the other hand the net production of silica within the box does not appear to be particularly sensitive to the initial assumptions.

### *Conclusions*

These results have shown that using only mass conservation constraints it is possible to find solutions consistent with the initial estimates of the Ekman and Mozambique Current transports.

The solutions found for the two models using different initial reference levels are similar in character, but vary somewhat in the magnitude of the fluxes in the various layers. The zonally integrated meridional transports were found to be:

- a net poleward flow of the surface waters,
- a small return flow at about 500 db,
- a net poleward flow below extending to about 1700 db,
- and a strong influx of oxygen rich NADW and AABW which balances the surface and intermediate flows out of the basin, and is consistent with Warren's (1981b) estimate of 20 Sv northward in the deep layers.

### **Models I2 and I2a - Mass and Salt Conservation in Isopycnal Layers**

It was found that including conservation of salinity did not provide much in the way of new, independent information to the system. The zonally integrated transports for the model including salt equations are shown in Table 2.3 to be similar

	Model I2 SIRL	Model I2a DIRL	Std. Error	Nullspace Error	Units
31°S Heat	-0.9	-1.2	2.4	0.2	PW
18°S Heat	-0.9	-1.1	2.2	0.2	
net conv.	0.0	-0.1			
31°S Oxygen	46	43	154	13	10 <sup>9</sup> mL/sec
18°S Oxygen	33	25	328	13	
net conv.	13	18			
31°S Phosphate	15	23	100	7	kmol/sec
18°S Phosphate	16	17	215	9	
net conv.	-1	7			
31°S Silica	425	1613	7773	793	kmol/sec
18°S Silica	1271	2065	10450	557	
net conv.	-846	-452			
31°S PO38	4084	5094	17520	937	kmol/sec
18°S PO38	3625	3400	45410	1346	
net conv.	459	1694			
Mozambique	-3.4	-3.0			10 <sup>9</sup> kg/sec
Ekman 18°S	-10.2	-9.9			
Ekman 31°S	3.3	4.0			

Table 2.3: Property fluxes for the Indian Ocean Models I2 and I2a which conserve mass and salt in isopycnal layers.

to those found using only mass conservation. Both Fu (1986) and Rintoul (1988) reached the same conclusion concerning the inclusion of salinity conservation in their inverse models. We have chosen to retain these equations to maintain consistency with the calculations done in the Pacific.

It was found by both Wunsch (1983) and Rintoul (1988) that the information available in the nutrient data appears to be independent of the contained in the mass and salinity data. The next set of models include nutrient conservation equations in an effort to better resolve the circulation and to determine the extent to which this data in the Indian Ocean contains independent information. The next three sections illustrate the order in which the various constraints were added.

### Models I3 and I3a - Addition of Silica Conservation in Isopycnal Layers

The first set of constraints added to our model required that silica be conserved in isopycnal layers between the two sections, well below the euphotic zone and well above the bottom (layers 4 - 12). The inclusion of such constraints implies

	Model I3 SIRL	Model I3a DIRL	Std. Error	Nullspace Error	Units
31°S Heat	-0.9	-1.1	3.5	0.2	PW
18°S Heat	-0.9	-1.1	2.7	0.2	
net conv.	0.0	0.0			
31°S Oxygen	46	46	270	550	10 <sup>9</sup> mL/sec
18°S Oxygen	31	27	550	12	
net conv.	15	19			
31°S Phosphate	15	21	141	6	kmol/sec
18°S Phosphate	14	15	296	9	
net conv.	1	6			
31°S Silica	442	1374	11420	695	kmol/sec
18°S Silica	1202	1869	14720	550	
net conv.	-760	-495			
31°S PO38	4094	4929	25890	881	kmol/sec
18°S PO38	3260	3263	64000	1404	
net conv.	834	1666			
Mozambique	-1.1	-2.5			10 <sup>9</sup> kg/sec
Ekman 18°S	-10.4	-9.8			
Ekman 31°S	3.4	3.6			

Table 2.4: Property fluxes for the Indian Ocean Models I3 and I3a which conserve mass, salt and silica in isopycnal layers.

that there is little reason to expect the large silica production (  $> 500$  km/sec ) expressed by our first two models, in the region between the two sections.

What is found is that although the matrix rank has increased by 2, indicating that the new, independent information was added, the magnitude of the silica production has not changed significantly (Table 2.4). The reason is that most of the silica production occurs in the layers in which conservation was not required.

The rms reference level velocities are essentially unchanged by the addition of the new constraints. As a result, the character of the meridional circulation is extremely similar to that found for conservation of mass alone (Fig. 2.4 and 2.5). The only obvious difference seen, is that the oxygen flux at 18°S now appears to be somewhat less sensitive to the change in initial reference level due to the substantial increase in mass flux of AABW in the lowest two layers for the SIRL model. This difference can be traced to changes in the reference level velocity in the Wharton

Basin where a large proportion of the bottom water resides (see the plates provided by Warren 1981b).

### **Models I4 and I4a - Addition of PO38 Conservation in Isopycnal Layers**

In this next model the phosphate and oxygen are conserved in layers 4 to 18, below the euphotic zone, in their combination form of PO38, derived from the Redfield ratios (Redfield 1963). The rank of the matrix increased by 1 with the addition of these constraints, again indicating the presence of independent information in the nutrient data.

The resulting reference level velocities are again, little changed. The cross-isopycnal transfer terms show for the first time the characteristic behavior found in the Pacific, of larger  $w^*$ 's values in the upper layers as well as, the distinct decrease in magnitude with depth. Unlike the Pacific, however, upper level downwelling is not apparent and there is little or no transport between the first and second layers. This would indicate that the Ekman convergence is being balanced solely by horizontal advection.

The pattern of convergences and divergences for oxygen, phosphate and PO38 has changed of very little, though the nutrient fluxes themselves, have increased with the inclusion of the PO38 constraints (Table 2.5). The estimated production of silica has increased for both initial reference levels. This is mainly caused by an increase in the silica flux across 31°S, apparently due to an increase in the transport of silica rich deep and bottom water across this latitude.

The other notable and related difference in this model, at least for the SIRL is that layer 14, containing the silica maximum associated with the Central Indian Basin is now moving to the south.

## Models I5 and I5a - Addition of Total Silica Conservation

It was found by Rintoul (1988) that the inclusion of the requirement that total silica be conserved with his North Atlantic box brought about a greater consistency between the deep and shallow initial reference level velocity solutions. According to Broecker and Peng (1982), there is a trough in the silica concentration to the south of our region with increasing values to the north which would indicate some production. Therefore, it may not be appropriate to place such a constraint on our box. However, since our silica production appears to be quite large, > 300 to 500  $\mu\text{M}/\text{sec}$  we decided to try the experiment anyway, to see whether we could also create greater consistency between the solutions using the two different initial reference levels.

The inclusion of the requirement that total silica be conserved within the box raised the matrix rank by 1. To meet the new constraint, the reference level velocities at  $18^\circ\text{S}$  were somewhat reduced, while those at  $31^\circ\text{S}$  were increased. The affect on the mass flux was similar to the change that occurred between models I3 and I4, except that along with the increase in the silica flux at  $31^\circ\text{S}$ , there is an associated decrease in the silica flux at  $18^\circ\text{S}$  (Table 2.6). The consumption of oxygen has decreased, especially in the SIRL model, while the consumption of phosphate has increased. Total conservation of silica is not, as expected, completely consistent with the data as production within the box is still apparent.

We choose not to keep the total silica conservation constraint because it appears to not be consistent with the other model constraints and because it did not have the desired affect of narrowing the difference between the solutions using the two different initial reference levels.

Instead, we shall choose the shallow initial reference velocity version of the model without total silica conservation as our best estimate solution, keeping in

	Model I4 SIRL	Model I4a DIRL	Std. Error	Nullspace Error	Units
31°S Heat	-1.0	-1.2	3.2	0.2	PW
18°S Heat	-0.9	-1.1	2.4	0.2	
net conv.	-0.1	-0.1			
31°S Oxygen	42	42	229	11	10 <sup>9</sup> mL/sec
18°S Oxygen	31	26	432	11	
net conv.	11	16			
31°S Phosphate	19	25	128	6	kmol/sec
18°S Phosphate	17	19	230	7	
net conv.	2	6			
31°S Silica	877	1780	10770	645	kmol/sec
18°S Silica	1359	2048	11550	508	
net conv.	-482	-268			
31°S PO38	4485	5293	22310	839	kmol/sec
18°S PO38	3723	3740	49860	1128	
net conv.	762	1553			
Mozambique	-0.3	-1.6			10 <sup>9</sup> kg/sec
Ekman 18°S	-10.5	-10.2			
Ekman 31°S	3.5	3.7			

Table 2.5: Property fluxes for the Indian Ocean Models I4 and I4a which conserve mass, salt, silica and PO38 in isopycnal layers.

	Model I5 SIRL	Model I5a DIRL	Std. Error	Nullspace Error	Units
31°S Heat	-1.	-1.2	2.9	0.1	PW
18°S Heat	-0.9	-1.1	2.0	0.1	
net conv.	-0.1	-0.1			
31°S Oxygen	36	38	257	7	10 <sup>9</sup> mL/sec
18°S Oxygen	35	24	416	10	
net conv.	1	14			
31°S Phosphate	23	27	127	4	kmol/sec
18°S Phosphate	16	17	220	6	
net conv.	7	10			
31°S Silica	1452	2040	11250	398	kmol/sec
18°S Silica	1294	1965	11060	396	
net conv.	-158	-75			
31°S PO38	4748	5407	22490	689	kmol/sec
18°S PO38	3789	3472	48320	1043	
net conv.	959	1935			
Mozambique	-1.1	-0.2			10 <sup>9</sup> kg/sec
Ekman 18°S	-10.0	-10.3			
Ekman 31°S	3.8	3.8			

Table 2.6: Property fluxes for the Indian Ocean Models I5 and I5a which conserve mass, salt, silica and PO38 in isopycnal layers, and conserve total silica.



mind that the nutrient and oxygen fluxes are sensitive to this choice. Before continuing a few refinements were made to the model. The first was to see if decreasing the initial reference level in the region of the Agulhas Current could reverse the net flow of AAIW, that is, send it equatorward as we expected it to be. The attempt was unsuccessful however. As we raised it from 2000 db up to 1500 db (the depth of the oxygen minimum) and then to 1200 db (the depth of the salinity minimum) we only succeeded in some rearrangement of the NADW and AABW the flows. These two sections do not give us a true time average of the ocean circulation and it is only over the long term that one can expect to find the AAIW to be flowing towards the equator. We therefore, decided to accept the net poleward flow of AAIW in our best estimate solution. The next refinements included downweighting the surface layer based on the uncertainty in the Ekman Flux estimates and corrections to the distances assigned to a couple of the station pairs at 31°S. Neither of these changes had any significant effect upon the solution and shall be kept in the model.

So far all discussion of the flux estimates has disregarded the errors involved in their computation. As in the Pacific models, the *error of omission*, due to our lack of knowledge about the problem null-space, are small, indicating that unless the assumptions concerning the model are fairly drastically changed, the solution will not change significantly. For example, it would take a 10 cm/sec change in the rms reference level velocities here, to change the heat flux by the 1 PW needed to reverse the sign of the heat flux.

The *standard error*, stemming from the uncertainty in the flux due to the reference level velocities remains large. Again this is because, we did not assign the remaining structure in the residuals to a simple cross-isopycnal velocity as done in Wunsch *et al.* (1983). The size of the standard error is dependent upon the value of  $\sigma$  chosen (see Appendix B). If it is calculated from equation A.10, as we have done, it will remain of fairly constant size as long as our choice of solution

Through Flow	Model I4b	Model I6	Standard Error	Null Error	Units
31°S Heat	-1.3		2.1	0.2	PW
18°S Heat	-1.2		2.4	0.3	
net conv.	-0.1				
31°S Oxygen	35	-51	176	13	10 <sup>9</sup> mL/sec
18°S Oxygen	19	-58	294	13	
net conv.	16	7			
31°S Phosphate	31	-10	96	7	kmol/sec
18°S Phosphate	24	-19	162	10	
net conv.	7	9			
31°S Silica	1962	148	9388	663	kmol/sec
18°S Silica	2168	343	5970	761	
net conv.	-206	-195			
31°S PO38	5878	3610	12805	895	kmol/sec
18°S PO38	4185	-5180	35155	1370	
net conv.	1693	1570			
Mozambique	-1.6	-1.7			10 <sup>9</sup> kg/sec
Ekman 18°S	-13.2	-13.4			
Ekman 31°S	2.4	2.1			

Table 2.7: Property fluxes for the Indian Ocean Models I4b and I6 which conserve mass, salt, silica and PO38 in isopycnal layers. These models both allow the vertical transfer terms to grow to the size of the reference level velocities, if necessary.

remains dependent upon the size of the residuals. Therefore, as in the models, P3 and P4 the  $w^*$  terms were allowed to grow, unrestrained by specific column weights (although the columns are still weighted by their length), and so take up some of the residuals. The results for this model I4b are given in Table 2.7.

When this change was made to the Pacific models, we were able to find a solution with an extremely similar circulation to the model without unrestrained growth of the  $w^*$  terms, but with reduced standard error. In the Indian Ocean model I4b a much stronger circulation cell is produced. At 31°S the net poleward flow from the surface extending down to  $\sim 1700$  m is balanced by an equatorward flow of NADW and AABW of  $27 \times 10^9$  kg/sec . At 18°S the poleward flow extends down to 3000 m and is balanced by a  $30 \times 10^9$  kg/sec of bottom water. There is a large transport between layers 12 and 13 ( $12 \times 10^9$  kg/sec ) and also between layers 14 and 15 ( $9 \times 10^9$  kg/sec ). The reduction in the standard error is not as impressive as it was in the Pacific Ocean as the decrease in residuals at higher ranks was offset

by an even greater reduction in the eigenvalues. Even at ranks 10 greater than the one chosen the mass residuals in the surface layer remained large ( $O(2 \times 10^9 \text{ kg/sec})$ ) due to the uncertainty in the Ekman estimates.

The Ekman fluxes are still consistent with the input estimates of  $-11 \pm 8$  at  $18^\circ\text{S}$  and  $3 \pm 3$  at  $31^\circ\text{S}$ , and are now -13 and 2 at the northern and southern latitudes respectively. The Mozambique transport estimate is smaller, only  $2 \times 10^9 \text{ kg/sec}$ , as it has been since nutrient conservation was included. (Compare Tables 2.3 and 2.4.)

The heat flux estimates for all the various models have been fairly consistent, with the DIRL models producing values which are generally greater than the SIRL estimates by about 0.2 PW. Our heat flux estimate for the SIRL model I4b of  $-1.3 \pm 2 \text{ PW}$  at  $31^\circ\text{S}$  and  $-1.2 \pm 2 \text{ PW}$  at  $18^\circ\text{S}$  are of the same sign but somewhat larger than most of the estimates shown in Table 2.1. They indicate that there is little heat lost to the atmosphere in this region. They are consistent with the viewpoint that heat gained in the north Indian Ocean is being transported to the south within the ocean rather than being transferred to the atmosphere in the process of forming deep water.

### **Model I6 - Requiring an Indonesian Passage Through Flow**

In the final Indian Ocean model, we again attempt to force a net flux through the our box, whose characteristics are based upon the Indonesian Archipelago through flow. Model I6 is equivalent to our best estimate, SIRL model, I4b but includes the same large net mass and salinity fluxes used in the Pacific experiment,  $19 \times 10^9 \text{ kg/sec}$ .

- At  $31^\circ\text{S}$  we have:  $T_g + T_{EK} \approx T_{thruflow}$ .
- At  $18^\circ\text{S}$  we have:  $T_g + T_{MZ} + T_{EK} \approx T_{thruflow}$ .

Allowing the model to run and then assuming that the requirement for the net flux is met at both latitudes produces the integrated results shown in column 3 of Table 2.7, with Ekman and Mozambique estimates similar to the previous model results.

The rms reference level velocity has increased slightly. The character of the  $\mathbf{b}_j$ 's is extremely similar, indicating that the net flow has been produced by changing the reference level velocity slightly across the entire breadth of the sections rather than at any particular location. The character and magnitude of the cross-isopycnal transfers have experienced little change. There are still substantial exchanges between layers 12 and 13 (downwelling) and layers 14 and 15 (upwelling).

The mass transports across the sections have changed to accommodate the net mass flux. As in the Pacific, at 31°S most of the major changes have taken place in the deep water, here below layer 8 (1700 m). Only the water in layer 14, between about 3000 and 3200 db, has reversed direction to flow poleward. At 18°S the mass flux in layer 11 flows poleward, as does the water in layers 2 and 3. At both latitudes the poleward flow of surface and intermediate water has increased, while the equatorward flow of deep and bottom waters has decreased. Running this model with the unconstrained cross-isopycnal transfer terms produced a solution in which the major portion of the NADW mass was apparently moving to the south. This type of circulation does not occur in the current solution.

The property fluxes have, of course, also been affected by the presence of the net poleward mass flux. Referring to Tables 2.7, column 3 for the present model and column 2 for model I4b, we see that the major difference is the reversal of direction rather than a large change in the magnitude of the oxygen and phosphate fluxes. The fluxes of silica are, however, much smaller. There is little change in the pattern of convergences and divergences. As in the Pacific, the temperature flux

(zero at 0°C), although it has increased a little, appears to be fairly insensitive to the addition of a large Pacific-Indian through flow.

There is nothing about the character of the circulation produced by this model which would lead us to believe that the largest through flow estimates are not consistent with this data set.

### **Model PI - Indian and Pacific Models**

Using conservation of mass and salinity between the 28°S section in the Pacific Ocean and the 18°S section in the Indian Ocean, and taking into account the freshwater input between the sections, the best estimate Pacific and Indian Ocean Models (P4 and I6 respectively) are combined. As illustrated in Fig. 1.3, using sections in both the Indian and Pacific oceans allows us to connect the two basins and to create an area which encloses the Indonesian Archipelago. The motivation is to examine the effect upon the circulation and in particular, the Pacific-Indian through flow, when the constraints provided by these two basins are viewed as belonging to a single ocean system.

The combined model required an Indonesian Passage through flow of  $19.2 \times 10^9$  kg/sec and an outflow through the Bering Straits of  $0.8 \times 10^9$  kg/sec . The rank of the resulting matrix was chosen to be 50, which is equal to the combined ranks of the two models, P4 and I6 run separately plus two. The solutions at ranks 49 through 54 were all similar.

To determine estimates for the Ekman flux at each latitude and the transport through the Mozambique channel, the following assumptions were made concerning the constraint equations.

- The net mass flux through each section is due to the *a priori* estimate of the Indonesian Passage through flow + the loss/gain of freshwater from the

northern most latitude of the basin to the section + in the Pacific only, the *a priori* estimate of outflow through the Bering Strait + at 18°S in the Indian Ocean, the transport through the Mozambique Channel.

- The Ekman flux at each latitude is equal and opposite to the net top to bottom geostrophic mass flux.
- In the Indian Ocean the constraint that the Ekman convergence be balanced by a geostrophic divergence in the surface layer is perfect. This allows us to produce an estimate of the Mozambique Current transport. The other possibility would have been to assume that the *a priori* estimate of the Mozambique Current transport was correct and that any residual would be taken up by the upper layer across the section. Since both the Mozambique flux and the Ekman flux are both associated with fairly large errors, it is a matter of personal preference as to which assumption should be made.

These assumptions are the same as those made for the individual models except that in the previous Pacific Ocean models we assumed the Ekman flux estimates had been met perfectly since their sum exactly matched the *a priori* estimate of their convergence. The through flow was then estimated. The difference is very small (*i.e.*  $19.2 \times 10^9$  kg/sec for the combined models compared to  $18.9 \times 10^9$  kg/sec for the Pacific model alone).

The reference level velocities were found to be similar in character and magnitude to those determined using the separate models. Table 2.8 compares the layer transports for the various models which support Indonesian Passage through flow. In model P4, most of the required net equatorward transport was produced by an increased equatorward flow below layer 13. In the combined model it is spread more evenly through the water column with an increased equatorward transport above layer 13 of  $13 \times 10^9$  kg/sec , compared to  $5 \times 10^9$  kg/sec for model P4. There is a

31°S Layers	I4b	I6	PI
Net Transport	0.0	19.2	19.2
Ekman Flux	2.4	2.1	2.7
Net Surface	-13.8	-14.6	-14.2
2-8	-12.9	-17.4	-18.7
9-12	11.3	6.9	7.1
13-18	15.4	5.8	7.1

18°S Layers	I4b	I6	PI
Net Transport	0.0	19.2	19.2
Ekman Flux	-13.2	-13.4	-14.1
Net Surface	-14.4	-16.3	-16.7
2-8	-5.2	-10.6	-9.8
9-12	-8.5	-14.6	-13.7
13-18	29.8	24.3	24.2
Mozambique	-1.6	-1.7	-3.2

43°S Layers	P3	P4	PI
Net Transport	0.0	19.2	19.2
Ekman Flux	6.7	6.6	6.7
Net Surface	4.9	5.4	5.9
2-4	-2.7	0.5	1.2
5-12	-19.1	-8.5	-1.3
13-18	16.9	22.0	13.5

18°S Layers	P3	P4	PI
Net Transport	0.0	19.2	19.2
Ekman Flux	-4.4	-4.3	-4.3
Net Surface	-4.1	-2.4	-1.5
2-6	3.5	8.0	9.9
7-12	-18.0	-8.2	-3.2
13-18	18.5	22.3	14.3

Table 2.8: Mass Transport in the core layers of the South Indian and South Pacific, comparing the combined model (PI) results with the individual basin model results. All units are in  $10^9$  kg/sec.

net gain of fresh water over the north Pacific Ocean according to Baumgartner and Reichel (1975), requiring the net flux at our latitudes to be less saline than the net flux through the Indonesian Passage. This might account for the increased flux in the upper layers. The  $\sim 19.2 \times 10^9$  kg/sec of Indonesian Passage through flow has a salinity of about  $33.6\text{‰}$ , consistent with the *a priori* estimate. Consistent with increased compensation for the net flux occurring in shallower and therefore, warmer layers the estimated temperature flux has increased from 0.1 PW to 0.3 PW at  $43^\circ\text{S}$  and from -0.1 to 0.0 at  $28^\circ\text{S}$ . The standard errors on the temperature flux estimates have increased (1.7 PW at  $43^\circ\text{S}$  and 1.1 PW at  $28^\circ\text{S}$ ). This is most likely due to the influence of the larger uncertainties in the Indian Ocean input estimates.

In the combined model, the solution is quite similar to that found in the separate models. As in the separate model, I6 (Indian Ocean) the greatest compensation for the large amount of required net poleward flow occurs below layer 8. The difference between this model and the I6 model is that here a smaller portion of the compensation for the net flux has taken place in the bottom water while more has occurred in the intermediate layers. There is also a larger estimate for the Mozambique transport ( $-3.2 \times 10^9$  kg/sec ). The temperature flux estimate of  $-1.5 \pm 1.3$  PW poleward at both latitudes is similar to the values found model I6 but with a lower standard error.

The effect of combining the constraints from the two oceans is that in the Pacific a greater portion of the compensation for the net flux occurs in the layers above 3200 m (as was true in the I6 model) while in the Indian Ocean little change has occurred. The increased estimates of the Mozambique Current transport is due to the decreased net, top to bottom mass flux through the  $18^\circ\text{S}$  section in the PI model, compared to model I6. This stems from the reorganization of the transport among the various layers which itself is due to the inclusion of the fresh water flux in the model as well as the constraints requiring mass and salinity conservation



between the basins. The conclusions have not changed. There seems to be no particular reason to rule out the large through flow value based on the resulting circulation within the two ocean basins, unless the tendency towards an equatorward temperature flux in the Pacific is considered to be unrealistic. We do not consider the Pacific temperature flux to be different from zero. The heat flux at  $\sim 30^{\circ}\text{S}$  from these two oceans with a through flow on the order of 20 Sv is  $-1.5 \pm 2$  PW. Decreasing the estimate of the through flow will change the temperature flux within each of the two basins but will not have much effect the net heat flux. Since both the circulation in the two basins and heat flux estimate of this model (PI) are reasonable we will chose this to be our *best estimate* solution for the South Pacific and South Indian Oceans.

In the next chapter we will examine the South Atlantic circulation in much the same manner as we have examined the South Indian circulation here using two sections, and incremental approach to building the models.

## Chapter 3

### The South Atlantic Ocean

#### 3.1 Introduction

In this chapter we turn to the South Atlantic Ocean. Using the same method as was applied in Indian Ocean, we determine meridional fluxes of mass, heat and nutrients across two sections. The southern section spans the South Atlantic between  $23^{\circ}\text{S}$  and  $30^{\circ}\text{S}$ . It will henceforth be called the ' $30^{\circ}\text{S}$ ' section. The northern section crosses between  $18^{\circ}\text{S}$  and  $10^{\circ}\text{S}$ . This will be called the ' $15^{\circ}\text{S}$ ' section.

The analysis procedure will be much the same as that used in Chapter 2 which described the South Indian Ocean. As in the other two oceans we will present a discussion of how the various constraints affect the solution and our best estimate flux solutions will be compared with previous results.

Continuing as we have, we begin with a description of the region, the circulation and the water masses as they are described in the literature. In the second section we present previous estimates of the heat flux in the South Atlantic and follow with a brief description of the data used in the analysis before presenting the model results.

### 3.1.1 Water Masses and Circulation

The South Atlantic Basin is bordered by the coasts of South America and Africa. It is divided in the north-south direction along its center by the Mid-Atlantic Ridge which rises to depths of 1750 m. Between 20°S and 40°S, the deep South Atlantic is divided zonally by the Rio Grande Rise in the west, which does allow passage of deeper waters through the Vema Channel (Hogg *et al.* 1982) and in the west by the Walvis Ridge, which is continuous at 3000 m.

Between about 15°S and 40°S the surface circulation, as in the other southern oceans is best described by an anticyclonic gyre. The northern zonal boundary of the gyre is the South Equatorial Current (SEC) which is seen anywhere from 20°S to 3°N (Tchernia 1980). The results of Fu (1981) and Tsuchiya (1986) suggest that the main portion this westward flow which bounds the southern gyre tends to lie to the south of 10°S. North of this, the water flows toward the east. At the coast of South America, the SEC splits. Most of the water appears to turn equatorward but there is a southern branch which transports warm water poleward along the western boundary in the Brazil Current. At 19°S, Miranda and Castro Filho (1982) estimate maximum surface velocities on the order of 70 cm/sec (relative to 500 m) with a transport of about 6.5 Sv. Significant portions of the flow are confined to the surface waters, above 200 m and over the continental shelf (Peterson and Stramma 1991). The current intensifies as it heads south. A recirculation cell is evident south of 30°S and the transport estimates between 27°S and 33°S present a broad range from 9 to 27 Sv (Peterson and Stramma 1991). The Brazil Current meets a branch of the ACC flowing northward at around 35-38°S and deflects eastward to form the southern boundary of the gyre, the South Atlantic Current. On the eastern boundary, carrying cold waters from the Antarctic northward, the Benguela Current closes the surface circulation. The region where these two currents meet is complicated by the presence of the Agulhas retroflection water from the southern

Indian Ocean. The flow of Indian Ocean water around the southern coast of Africa does not appear to be continuous but estimates for the exchange between the two oceans in the region range from the fairly small value of about 3 Sv to the substantial rate of 15 Sv ( Peterson and Stramma (1991) from Shannon *et al.* 1989, and Gordon and Haxby 1990) The Benguela Current leaves the coast at about 30°S and heads northwest across the Atlantic basin. Between 28°S and 32°S transport estimates for the Benguela Current range from 15 Sv to 21 Sv (Svedrup *et al.* 1942, Wooster and Reid 1963, Fu 1981, Stramma and Peterson 1989 ). Along the African coast where there is an equatorward surface drift, upwelling of cool, deep waters is evident and reaches to 15°S (Peterson and Stramma 1991).

According to Reid (1989) the axis of the main gyre shifts to the south with depth so that it is centered at about 35°S at 1500 m. Below this the Mid-Atlantic Ridge and Rio Grande Rise act to confine the gyre to the Brazil Basin. Within this basin the deeper waters flow towards the equatorward along the edge of the ridge. Some of this water crosses into the eastern basin near the equator and journeys back to the southern regions along with water from the North Atlantic. The abyssal waters are not confined to a western boundary but spread across most of the basin floor. In the eastern Cape Basin, below about 3000 m the flow forms a cyclonic gyre.

The water masses found in the South Atlantic are often described by a set of 5 layers: bottom water, deep water, intermediate water, central and surface water. As in the other chapters, property sections have not been included in this paper. The reader is referred to the many sections and references available in Reid (1989), Peterson and Stramma (1991) and Gordon and Molinelli (1982).

### *Surface and Subsurface Water*

In the South Atlantic the depth of the pycnocline varies from about 400 m at the Subtropical Convergence, down to 600 m at 25°S and back up to about 300 m at 5°S. The character of the surface water is greatly affected by the surface circulation. There are high salinities at the southern tip of Africa and north of about 15°S. There are also high salinities within the main gyre itself with lower values towards the east. In the surface waters, oxygen decreases from south to north away from the high concentrations in the polar regions. Phosphate, which has higher concentrations in the ACC and fairly low values within the gyre, has a maximum in the east at about 15°S where the oxygen is lowest. Silica also tends to increase to the north with a maximum near the lowest oxygen concentrations.

Beneath the surface layer is a water mass associated with a subtropical salinity maximum known as Central Water. This water mass is distinguished by an almost linear T-S relationship between  $T=6^\circ$ ,  $S=34.5\text{‰}$  and  $T=19^\circ$ ,  $S=36\text{‰}$  (Tchernia 1980). It is thought to be formed through vertical convection at about 40° north and south. Due to the variety of source waters for the surface currents in the South Atlantic the characteristics of the surface and central water mass vary with location. In some regions they are one and the same.

### *Intermediate Water*

The intermediate water is distinguished by an oxygen maximum at about  $\sigma_\theta = 27.12$  at 45°S which sinks to about  $\sigma_\theta = 27.23$  at 15°S. Underlying the oxygen maximum is the salinity minimum which lies at about 1000 m at 30°S and rises to about 800 m beyond the equator (Reid 1989). Intermediate water flows northward along the western boundary south of 40°S and north of 25°S, but its path between these two latitudes, possibly around the perimeter of the main gyre is not certain (Reid 1989). The salinity minimum increases as it moves northward mixing

with the waters above and below. Tchernia (1980) quoting Wust gives an order of magnitude estimate of 9 Sv of Intermediate Water flowing north.

### *Deep Water*

The deeper waters of the South Atlantic are the result of the relatively warm, saline, oxygen rich and nutrient poor North Atlantic Deep Water mass flowing south and interleaving with the colder, fresher, nutrient rich Circumpolar Water (CPW) which has entered through Drake Passage. Fu (1981) distinguishes Upper CPW ( $\sigma_\theta = 27.4$  to  $\sigma_2 = 36.7$ ) from Upper NADW ( $\sigma_2 = 36.9$  to  $37.03$ ). But Reid (1989) indicates that it is often difficult to place precise definitions on the separation.

### *Bottom Water*

The lower layer of CPW is separated from the upper layer by the thick mass of NADW which extends to about 45.85 (Reid 1989) or 45.88 (Fu 1981) in  $\sigma_4$ . Like its upper counterpart it displays a characteristic oxygen minimum. The very deepest bottom waters (AABW) are formed in the Antarctic, mainly in the Weddell Sea. They are characterized by their low temperature. They are also fresh and rich in silica. The flow of the bottom water is highly affected by the topography but appears to flow northward across the entire Brazil Basin after passing through the Vema Channel at 30°S. It does not enter eastern basins (Reid 1989).

## **3.1.2 Review of Previous Heat Flux Results**

The deep water masses which are formed in the North Atlantic pass through the South Atlantic which acts as the link in the global thermohaline circulation for the eventual exchange of NADW with the rest of the World Ocean. This large movement of cold water southward is the reason it is expected that the South

Lat.	Date	Type	Reference	$10^{15}$ W
8°S	1981	d	Fu	0.18 to 0.41
8°S	1983	d	Roemmich	0.74
8°S	1986	m	Sarmiento	0.38
8°S	1986	m	Philander & Pacanowski	0.64
8°S	1985	m	Russel	0.7
15-16°S	1962	d	Bryan	0.63 to 1.3
15-16°S	1981	d	Fu	0.73 to 0.86
15-16°S	1985	i	Hsiung	0.2
15-16°S	1986	m	Sarmiento	0.37
20-21°S	1981	d	Fu	0.54
20-21°S	1985	i	Hsiung	0.15
20-21°S	1986	m	Sarmiento	0.40
20-21°S	1989	i	Hsiung <i>et al.</i>	-2.3 to 1.5
20-21°S	1985	m	Russel	0.5
24°S	1978	d	Bennett	0.65
24°S	1962	d	Bryan	0.33
24°S	1981	d	Fu	0.54
24°S	1983	d	Roemmich	0.61
24°S	1986	m	Sarmiento	0.44
25°S	1985	i	Hsiung	0.09
28°S	1981	d	Fu	0.83
28°S	1986	m	Sarmiento	0.27
30°S	1982	i	Hastenrath	.69
30°S	1985	i	Hsiung	.04
30°S	1985	m	Russel	0.8
32°S	1978	d	Bennett	0.16-0.68
32°S	1981	d	Fu	0.66-0.88
32°S	1990	d	Rintoul	0.25

Table 3.1: Estimates of northward heat transport in the South Atlantic Ocean. Type 'd' implies a direct estimate. Type 'i' implies an indirect estimate. Type 'm' implies model results. Much of this table is adapted from Peterson & Stramma (1991).

Atlantic should express a net equatorward heat flux and not the poleward flux expected in the other southern ocean basins. Table 3.1 illustrates that observation appears to support this theory of equatorward heat flux.

In spite of the observational agreement in the sign of the heat flux in the South Atlantic there is still, as in the other ocean basins, a fairly large range in the estimates of its magnitude. Bennett (1978) was able to obtain the range of 0.16 to 0.88 PW by varying the widths of the boundary currents. Peterson and

Stramma (1991) point to the ranges estimated by Bryan (1962) and Fu (1981) as an example of difference in values obtained by different investigators using different techniques, but the same data, to make the estimates. Bryan's value of 0.63 PW came from the Meteor data set. Fu obtained a value of 0.86 using this same data. Bryan's value 1.3 PW came from the IGY data set, from which Fu obtained a value of 0.73. Bryan did not quote errors for his values as he felt it would be impossible to estimate them objectively. He did state that the wind stress values used in the analysis were greatest source of uncertainty and that the inadequate sampling might also contribute to the uncertainty in the flux estimates. All Fu's standard errors were on the order of 0.2 PW. These errors calculated from the correlation coefficients between deviations of potential temperature and geostrophic velocity from their zonal averages do not include the uncertainty in the Ekman component which was considered to be negligible. So it appears that even the sources of error in these calculations is not agreed upon. Hsiung *et al.* (1989) cite computational uncertainties as one of the major reasons for the discrepancies found in the estimates but they also point to large seasonal variations as another major cause. The range in heat flux values quoted from Hsiung *et al.* (1989) in Table 3.1 is based on their extreme monthly values of  $-2.3 \pm 8$  PW for January to  $1.5 \pm 7$  PW for March. They also imply that although the Atlantic exhibits fairly large heat transports it does not dominate the global oceanic heat budget as both the Pacific and the Indian Oceans exhibit monthly maxima as great as those found in the Atlantic.

### 3.1.3 Description of the Data Used

In the South Atlantic we used data from the South Atlantic Ventilation Experiment (SAVE). The second leg of this experiment occupied a section which ran from 2°N, 356.4°E to 9°S, 11.4°E and then from 10.2°S, 12.7°E to 18.9°S, 322.1°E. we used the latter portion of this section crossing the Atlantic between South Africa



and South America and refer to it as the 15°S section. At ~ 30°S we combined data from legs 3 and 4 to produce a section which runs from 23.6°S, 318.7°E to 30°S, 15.3°E. We refer to this as the 30°S section. (see Fig. 1.3)

Table 1.3 gives the details on the various legs. The northern section was traversed in January of 1988 and the southern section combines data from February 1988 and January 1989. The station spacing ranged from a minimum of 9 km to a maximum of 188 km and averaged about 115 km for both sections. Details on the measurement methods and the data itself are available in the preliminary shipboard data report supplied by the Physical and Chemical Data Facility of Scripps Institute of Oceanography (1988).

Fig. 3.1 shows the zonally averaged profiles of potential temperature, salinity, oxygen, phosphate and silica at both latitudes based on the 18 layer model described in Table 1.8. In Fig. 3.1b the high salinity of the surface waters in the main South Atlantic gyre is evident at both latitudes, with increasing values towards the north as found by Reid (1989). The decrease in oxygen from south to north is also apparent though the associated increases in phosphate and silica are barely visible. Both phosphate and silica exhibit increased concentrations from west to east in the upper waters. In layer 3 at about 500 db, we find an oxygen minimum which based on its temperature and salinity would appear to be associated with the Central Water mass. At the 30°S the oxygen maximum of the Intermediate water appears at  $\sigma_\theta = 27.2$ . It is not apparent at 15°S. The underlying salinity minimum is centered just above a 1000 db at 30°S and has risen to about 800 db at 15°S as suggested by the literature. The salinity minimum has increased from south to north as might have been expected due to mixing with the waters above and below.

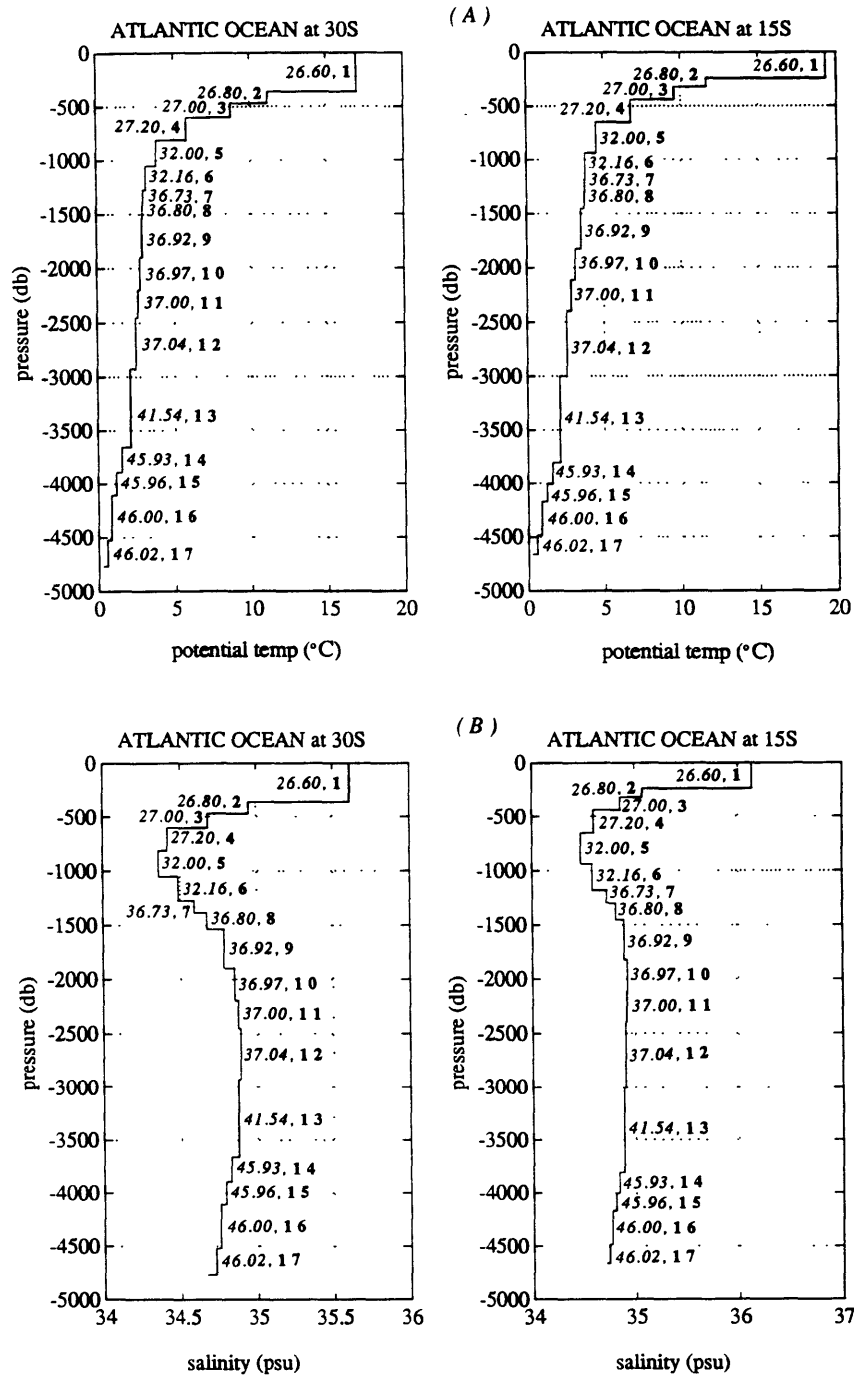
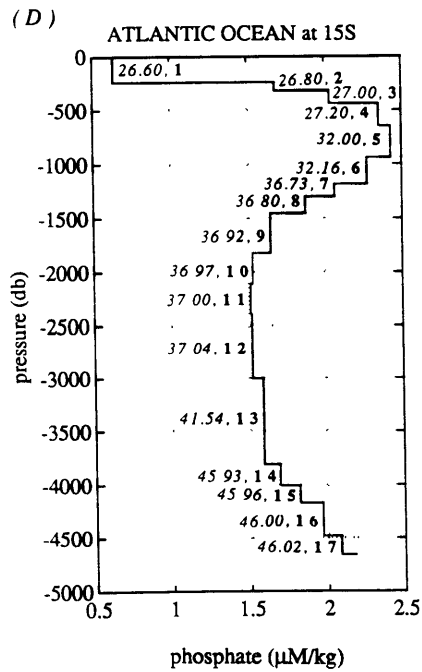
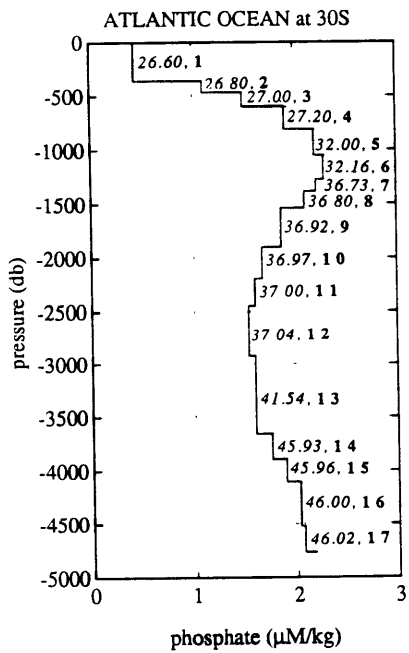
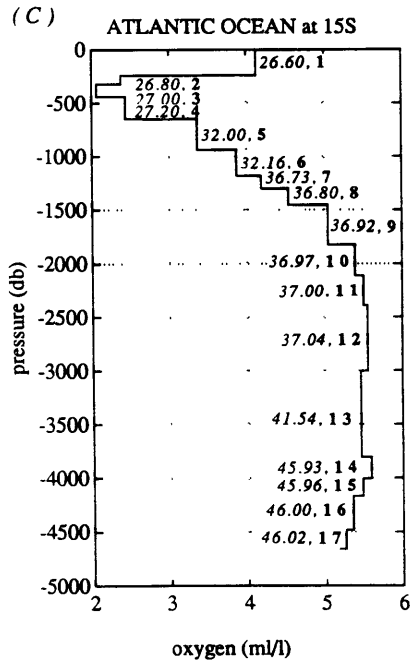
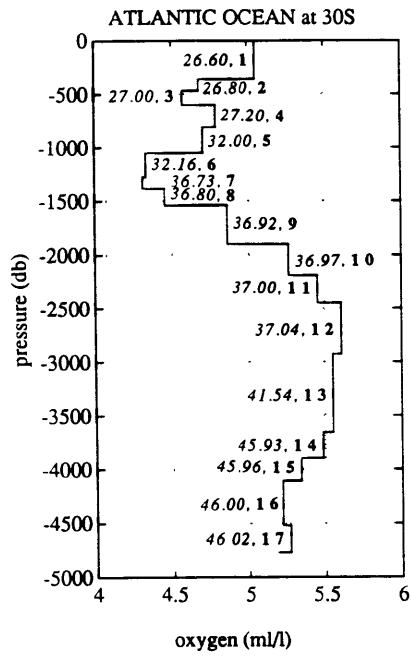
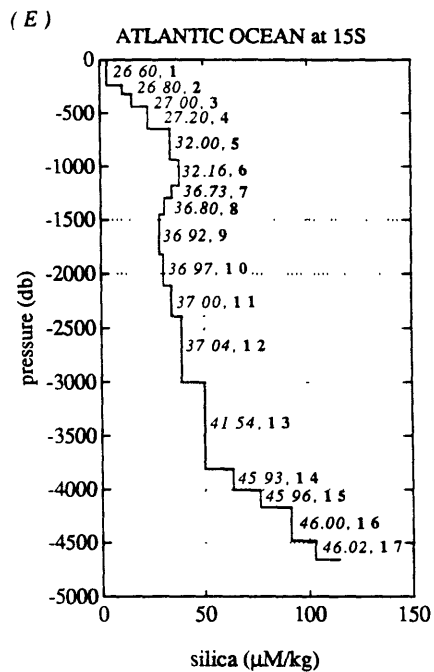
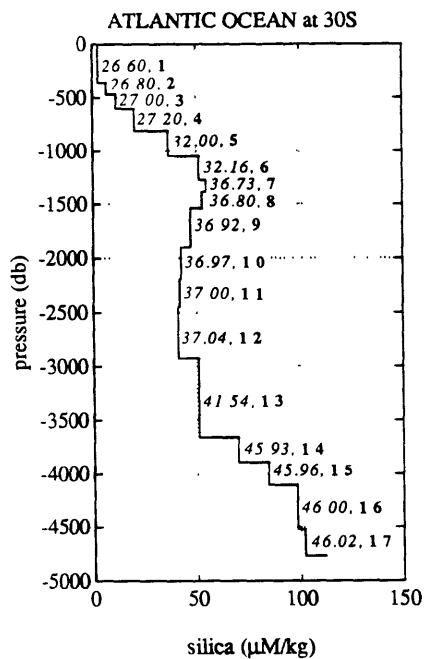


Figure 3.1: Zonally averaged profiles of temperature (a), salinity (b), oxygen (c), phosphate (d) and silica (e) for the Atlantic Ocean sections using the 18 layer model.





Between about 1000 db and 1400 db at 30°S there is an oxygen minimum and associated phosphate and silica maxima. This layer of water is fresher than the underlying water and thus has all the characteristics associated with the upper layer of CPW. These characteristics become confused with the Intermediate water at 15°S where the phosphate maximum has risen to ~800 db and the oxygen minimum is no longer visible. Below this the higher salinity and oxygen, and lower nutrient concentrations of the NADW extend down to about 3700 db. The lower salinity and increasing nutrient concentrations define the boundary between the NADW and the lower CPW and AABW which are seen at depth.

In the next section we use the information presented above on the water masses and circulation to examine the results of models which have been chosen to describe the South Atlantic Circulation.

## 3.2 Atlantic Ocean Models

### Models A1 & A1a - Conservation of Mass in Isopycnal Layers

The first model constructed for the South Atlantic sections is one in which mass is conserved in layers 2 through 18. The constraint in the surface layers is that the net Ekman convergence found in this region from wind stress data be balanced by a net geostrophic divergence. The top to bottom mass flux at each latitude is required to balance the *a priori* estimate of the Ekman flux. The Ekman flux values computed from the wind stress data of Han and Lee (1981) are shown in Table 1.6. Along the line at 30°S the Ekman flux normal to the section was computed to be  $-7.5 \pm 3.4 \times 10^9$  kg/sec in the annual mean. The Ekman flux normal to the 15°S section was  $-1.4 \pm 0.8 \times 10^9$  kg/sec, resulting in a net convergence of  $6.1 \pm 3.5 \times 10^9$  kg/sec in the region between the sections.

As in the Indian Ocean models, two initial reference levels were chosen in order to study the sensitivity of the solutions to variations in the initial estimate. The shallow initial reference level (SIRL) was taken to be  $\sigma_2 = 36.73$  (approximately 1300 m), the nominal division between the northward flow of Upper CPW and the southward flow of NADW. The deep initial reference level (DIRL) was given as  $\sigma_4 = 45.93$ , the division between the NADW flow and the reverse flow beneath it of Lower CPW and AABW. In order to more easily describe the circulation found by the models, in the following discussion we will use the term Intermediate Water or IW to indicate the combined flows of the Antarctic Intermediate Water and the Upper Circumpolar Water. We shall use the term Bottom Water or BW to refer to the combined flows of Lower Circumpolar Water and Antarctic Bottom Water.

There are 53 stations pairs representing the southern section and 47 describing the northern section. To determine the reference level velocities at each station pair and the cross-isopycnal transfers between each layer means finding a total of 118 unknowns. Applying the considerations discussed earlier, a rank of 15 was chosen for the A1 models. The rms reference level velocity at this rank is 0.7 cm/sec. The cross-isopycnal transfer terms are on the order of  $10^{-6}$  cm/sec and displayed similar characteristics to those found in the other oceans namely, decreasing magnitude with depth and oscillating sign. There was no apparent downwelling through the first interface as would be expected if the Ekman convergence were not completely balanced through horizontal geostrophic advection. As in our other models, most of the reference level velocities are not well resolved. The mean value of the diagonal of the resolution matrix,  $\mathbf{V}\mathbf{V}^T$  was 0.13. The equations describing the conservation in the deep layers were more important in producing the solution than the upper layer equations. This is most likely because the deeper layers tended to be thicker than the upper layers. The surface layer equation was used somewhat less than the others due to the uncertainty stemming from the Ekman flux estimates. The resolution of the solutions was compact in the sense described earlier, that is, the

solutions were the result of a weighted average of "true" velocities at nearby as opposed to distant stations pairs. Such compact resolution was also found in the South Atlantic by Fu (1981) and Rintoul (1988,1990).

The absolute velocity field for our best estimate model (discussed later) is shown in Fig. 3.2. At 15°S the Brazil current appears to be fairly distant from the western boundary and has a maximum velocity of only 15 cm/sec. There is a strong equatorward flow inshore of the Brazil Current and a counter-current to the west. At 30°S the Brazil current is much more obvious. Hugging the coast it attains poleward velocities of upto 43 cm/sec. There is a counter-current to the east of the Brazil Current at this latitude as well. On the eastern boundary of the basin the Benguela current is not nearly so obvious at either latitude. There are regions of equatorward flow at about 2°E and 8°E at 30°S and at about 4°E and 10°E at 15°S. The more shoreward of the two has maximum velocities of about 30 cm/sec. The northwesterly movement of the current is apparent but not obvious from these positions. Separating the two equatorward flows is poleward flow with maximum velocities of about 15 to 20 cm/sec. These velocities field are very similar to those found by Fu (1981) and Rintoul (1988) at similar latitudes.

Fig. 3.3 shows the zonally integrated mass transports in the individual layers of the two sections. Table 3.2 quantifies the mass transport within the various core layers for all the Atlantic models. In the surface layer at 30°S there is a net northward transport of  $6 \pm 4 \times 10^9$  kg/sec . At 15°S there is a net northward transport of  $4 \pm 9 \times 10^9$  kg/sec which implies that within the estimated uncertainty, the requirement that the Ekman convergence be balanced in the top layer by a net geostrophic divergence is consistent with the other model constraints.

Below the surface layer there is an equatorward flux at both latitudes down to about 1300 m. This flow of IW (*i.e.* contains by our definition both AAIW and Upper CPW) represents about  $7 \pm 7 \times 10^9$  kg/sec at 30°S and  $7 \pm 18$  at 15°S.

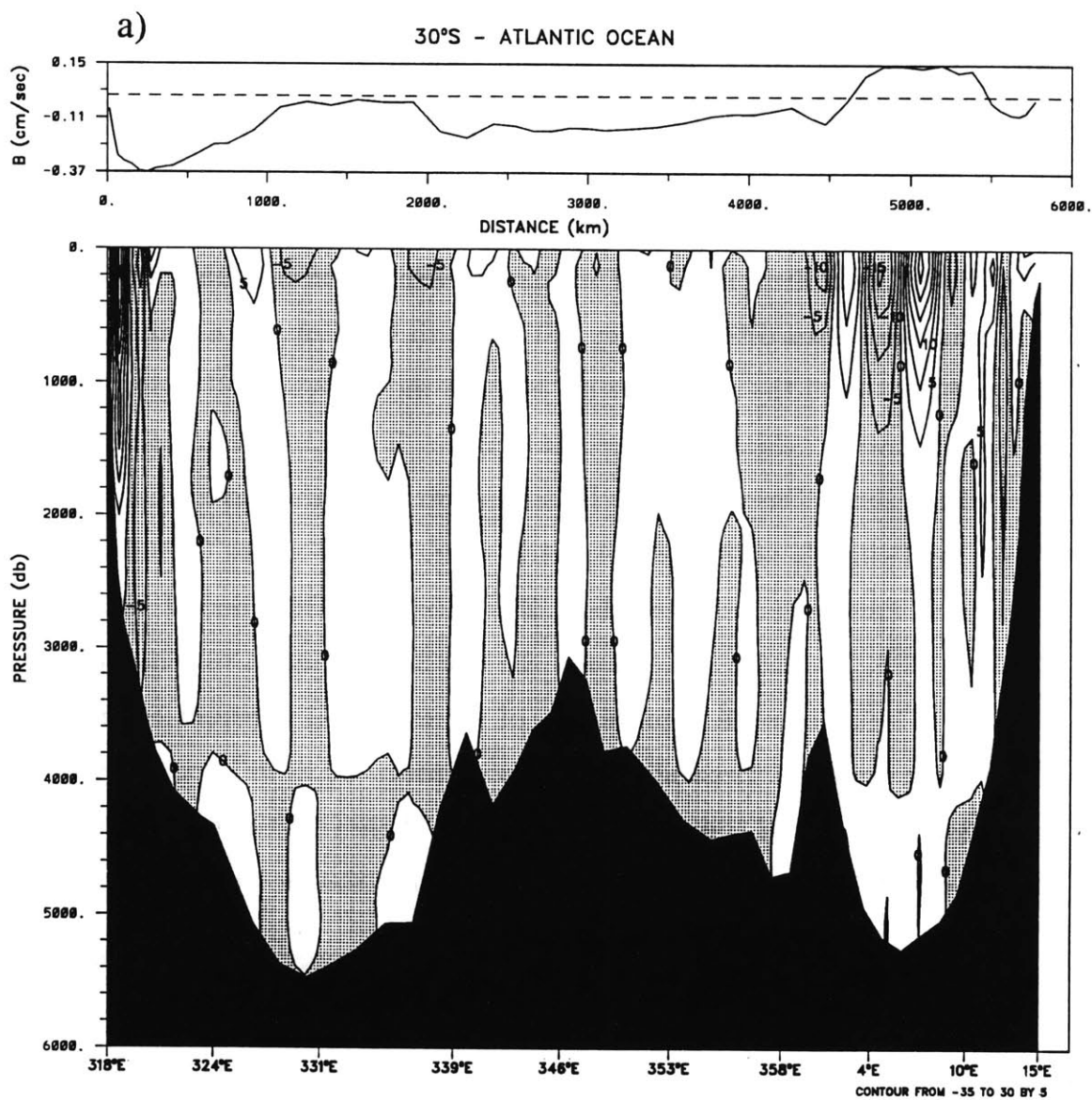
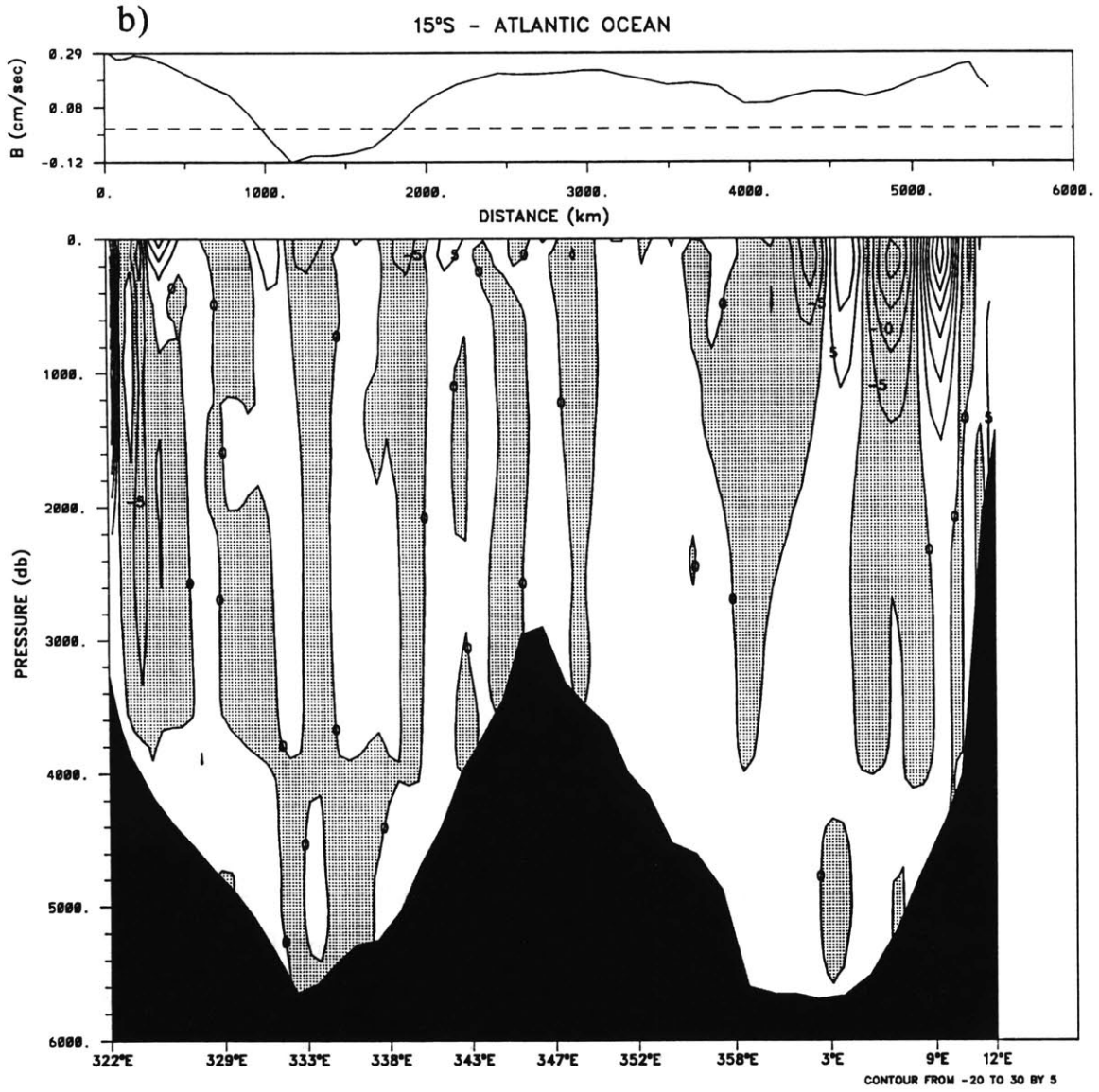


Figure 3.2: The absolute velocity field for our best estimate Atlantic Ocean model, A7a: (a) at 30°S, between South America and South Africa (b) at 15°S, between South America and South Africa. The value of the reference level velocity at  $\sigma_4 = 45.93$  is displayed at the top.





Water Mass	A1 DIRL	A2 DIRL	A3 DIRL	A4 DIRL	A5 DIRL	A6 DIRL	A7 DIRL
30°S Surface	7.0	6.8	6.8	6.5	6.9	8.0	7.3
30°S IW	9.3	9.1	9.6	9.5	11.2	14.1	9.6
30°S NADW	-20.7	-21.3	-19.6	-19.7	-19.0	-17.7	-18.2
30°S BW	4.3	5.3	3.2	3.6	0.9	-4.7	1.2

Water Mass	A1 SIRL	A2 SIRL	A3 SIRL	A4 SIRL	A5 SIRL	A6 SIRL	A7 SIRL
30°S Surface	5.6	5.4	5.0	4.6	4.7	7.1	6.1
30°S IW	6.6	6.3	7.4	6.9	7.2	12.9	6.4
30°S NADW	-17.9	-18.3	-14.2	-15.1	-14.9	-13.4	-19.5
30°S BW	5.8	6.6	2.1	3.6	3.0	-5.2	7.0

Water Mass	A1 DIRL	A2 DIRL	A3 DIRL	A4 DIRL	A5 DIRL	A6 DIRL	A7 DIRL
15°S Surface	4.1	4.2	3.7	4.1	4.0	3.8	4.2
15°S IW	11.3	10.9	11.3	10.9	11.9	20.2	14.0
15°S NADW	-20.4	-21.0	-18.9	-18.7	-17.2	-17.9	-24.7
15°S BW	5.1	6.0	4.0	4.1	1.5	-6.1	6.5

Water Mass	A1 SIRL	A2 SIRL	A3 SIRL	A4 SIRL	A5 SIRL	A6 SIRL	A7 SIRL
15°S Surface	3.5	3.6	3.3	3.4	3.4	5.2	3.6
15°S IW	6.5	6.2	7.1	6.3	6.9	14.6	8.8
15°S NADW	-16.7	-17.2	-14.0	-13.8	-13.9	-11.8	-9.8
15°S BW	6.8	7.6	2.8	4.2	3.8	-7.8	-2.6

Table 3.2: Transport in the core layers of the South Atlantic for each of the models run. All units are  $10^9$  kg/sec.

The poleward flow of NADW extending to  $\sim 3700$  m at  $30^\circ\text{S}$  and  $4200$  m at  $15^\circ\text{S}$  carries  $17 \pm 11 \times 10^9$  kg/sec at the northern latitude and has increased slightly to  $18 \pm 32 \times 10^9$  kg/sec at the southern latitude. The bottom waters show a increase in the opposite direction, from south to north of  $6 \pm 6$  to  $7 \pm 12 \times 10^9$  kg/sec . These values are quite similar to those reported by Rintoul (1988,1990) for his model using an initial reference level of 700 db (6 Sv of Surface Waters, 5 Sv of AAIW, -16 Sv of NADW and 5 SV of BW).

Turning to the results of the DIRL model, A1a (Fig. 3.4), we find that the solution size has decreased slightly. The rms reference level velocity is 0.6 cm/sec.

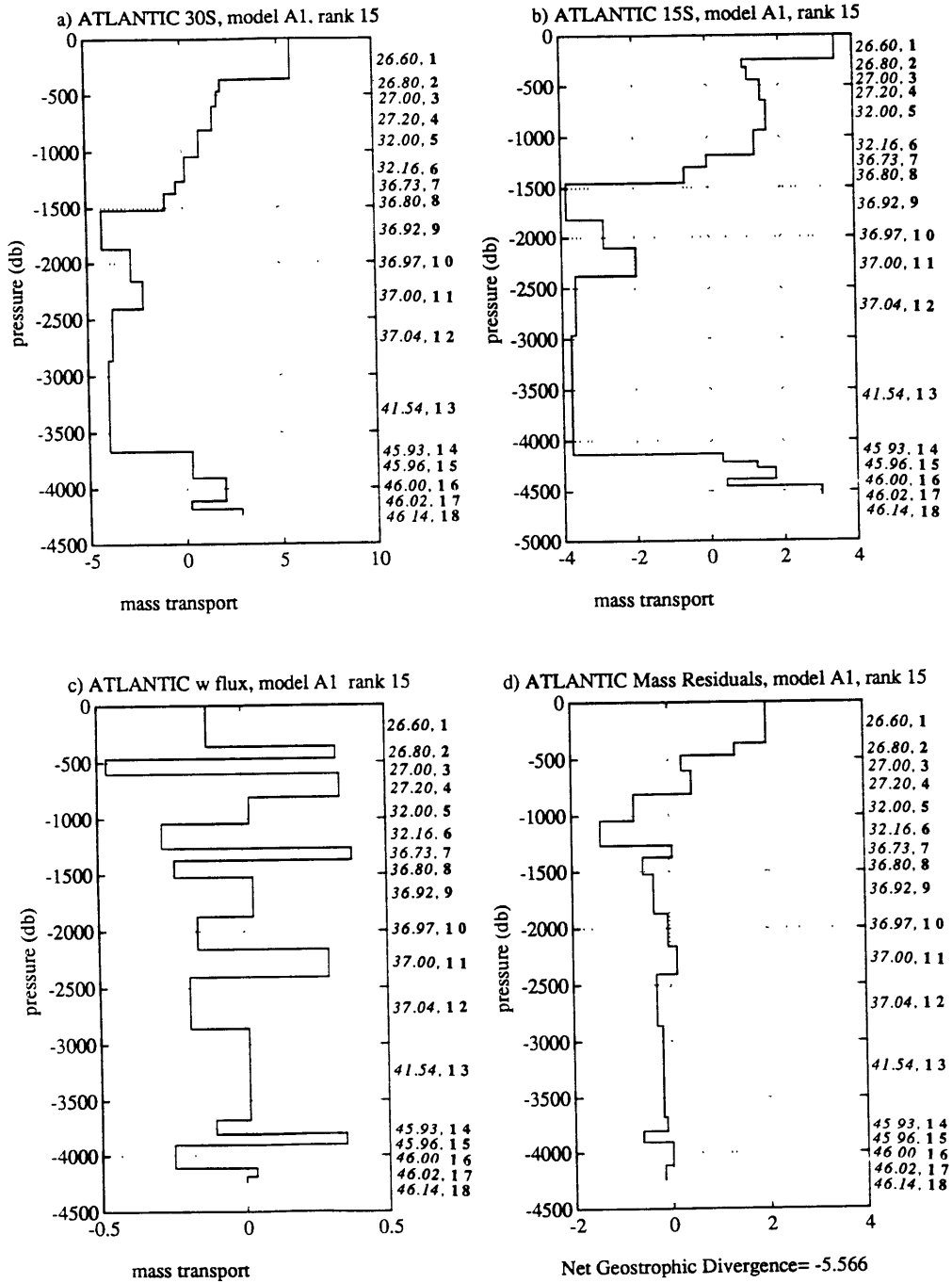


Figure 3.3: The zonally averaged mass transports from the SIRL model A1 for the two Atlantic sections: (a) at 30°S, (b) at 18°S. (c) Mass transport across isopycnals due to the vertical transfer terms. (d) Mass residuals within each layer after the transports due to (a), (b) and (c) have been summed. The Ekman component is included in the surface layer. The units are  $10^9$  kg/sec.

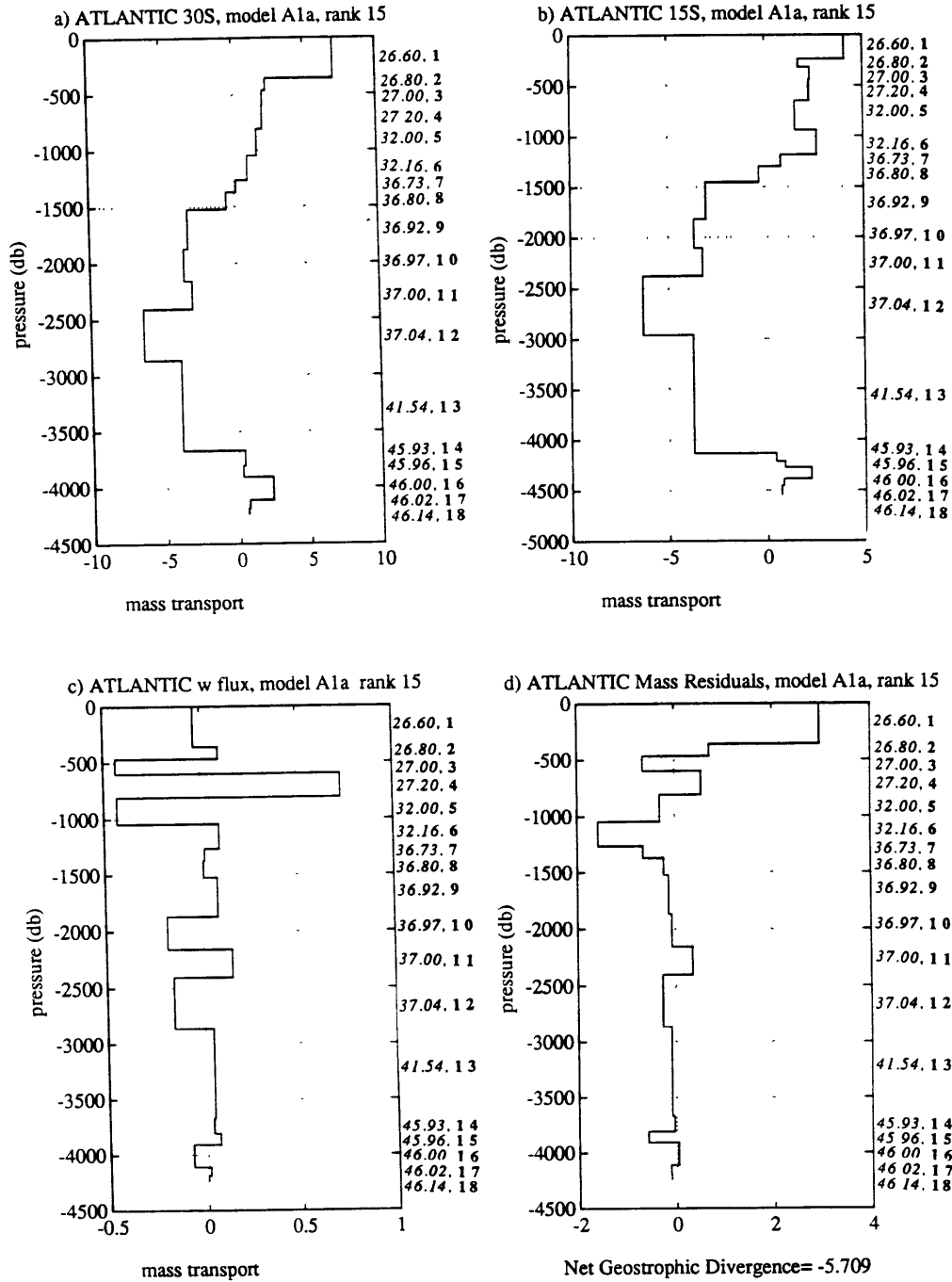


Figure 3.4: The zonally averaged mass transports from the DIRM model A1a for the two Atlantic sections: (a) at 30°S, (b) at 18°S. (c) Mass transport across isopycnals due to the vertical transfer terms. (d) Mass residuals within each layer after the transports due to (a), (b) and (c) have been summed. The Ekman component is included in the surface layer. The units are  $10^9$  kg/sec.

The reference level velocities themselves are not as smooth as those found at the shallower reference level. The character of the cross-isopycnal fluxes is unchanged. The character of the meridional mass transports in the various cores layers is also similar to those found in the SIRL model, but the magnitudes have changed. The equatorward flux of Intermediate Water has increased by about  $3 \times 10^9$  kg/sec at  $30^\circ\text{S}$  and has nearly doubled at  $15^\circ\text{S}$ . The transport of NADW has also increased, to approximately  $21 \times 10^9$  kg/sec at both latitudes. These changes are similar but more extensive than the changes found by Rintoul (1988,1990) for his standard model at  $32^\circ\text{S}$  with an initial reference level of 3500 db compared to the model using 700 db as the initial reference level.

### *Property Fluxes*

Since there are differences between the SIRL and DIRL models, corresponding differences in the property fluxes also exist. We shall discuss the property fluxes of the SIRL model as a baseline for later comparison with the DIRL results. Table 3.3 quantifies the integrated property fluxes for the two models.

Model A1 produces a fairly small equatorward heat flux of  $0.3 \pm 1.8$  PW at both latitudes. This value is comparable to the 0.25 Pw quoted by Rintoul (1988,1990) at  $32^\circ\text{S}$ . Hastenrath, Bennett, Fu and Russel all found values approximately twice as large near this latitude, but Hsuing (1985) and as mentioned above, Rintoul, found smaller values. At  $15^\circ\text{S}$  we once again fall at the low end of the range of previous estimates. The values at the two latitudes considered together indicate that neither a heat loss to nor a gain from the atmosphere is occurring between  $15^\circ\text{S}$  and  $30^\circ\text{S}$ , which is consistent with the finding of Fu (1981). Sarmiento's 1986 model results predicted a small gain of heat by the ocean between the two latitudes of  $13 \text{ W/m}^2$ . Bunker's (1982) map of net annual heat gain in the Atlantic indicate that a large portion of this region has no net annual heat gain.

	Model A1 SIRL	Model A1a DIRL	Std Error	Nullspace Error	Units
30°S Heat	0.3	0.4	1.7	0.1	PW
15°S Heat	0.3	0.4	1.9	0.1	
net conv.	0.0	0.0			
30°S Oxygen	-8	-18	145	8	10 <sup>9</sup> mL/sec
15°S Oxygen	9	24	469	15	
net conv.	-17	-42			
30°S Phosphate	-3	1	67	5	kmol/sec
15°S Phosphate	-3	-7	146	4	
net conv.	0	8			
30°S Silica	86	211	5271	348	kmol/sec
15°S Silica	369	169	6541	311	
net conv.	-282	42			
30°S PO38	-693	-720	9014	384	kmol/sec
15°S PO38	29	65	19880	401	
net conv.	-722	-785			
Ekman 15°S	-7.0	-7.1			10 <sup>9</sup> kg/sec
Ekman 30°S	-1.4	-1.4			

Table 3.3: Property fluxes for the Atlantic Ocean Models A1 and A1a which conserve mass in isopycnal layers. Positive flux values are northward. Positive convergence values imply that more of a tracer enters the region between the two sections than leaves. The standard and nullspace errors are defined in Appendix B. The standard error is the average for the two models

All the nutrient fluxes are small and quite indistinguishable from zero. We shall however, look at the fluxes and the associated patterns of convergence and divergence so that we may see how sensitive the values are to model changes.

Within this region we find a small net production of oxygen and an insignificant consumption of phosphate. The NADW carries about  $100 \times 10^9$  mL/sec of oxygen across each section, approximately three times the amount carried in the other core layers. Most of the divergence of oxygen appears to occur in the intermediate layers from about 500 to 1300 db ( $\sim 20$  mL/sec). The possible explanations for this production of oxygen at depth are: overturning within this region (an idea not supported by the literature), upwelling of NADW and AABW, perhaps occurring in the east coast regions or else simply that the divergence itself is simply not significant within the error ( $O(200$  mL/sec) and should not be considered real.

We find a net production of silica which occurs through out the water column below about 800 db. Although the NADW is rich in silica, its concentrations are not as great as found in the AABW. Its great volume allows the NADW mass to carry large amounts of the nutrients southward ( $\sim 670$  km/sec at  $30^\circ\text{S}$ ). Consistent with the findings of Broecker and Peng (1982), the bottom water, although it does not match the volume of NADW, carries nearly as much silica northward ( $\sim 555$  km/sec at  $30^\circ\text{S}$ ).

Model A1a, which uses the deeper initial reference level produces a more vigorous overturning cell and an increased heat flux at both latitudes of  $0.4 \pm 1.8$  PW. There is still no net heat gain by the ocean within the region. The net production of oxygen which has now doubled, is still contained primarily in the intermediate layers. The net flux of phosphate at the northern latitude has increased, while at the southern latitude remains small but with reversed sign. At  $15^\circ\text{S}$  this appears to be mainly due to the decrease in BW, going from the SIRL to the DURL model. At  $30^\circ\text{S}$  there is no obvious difference in any particular layer or set of layers which produces the change. Similar variations have occurred in the flux of silica leading to a very small net consumption within the box, which is at least consistent with the production of oxygen.

The first addition to the initial model was a set of equations describing conservation of salinity in isopycnal layers (models A2 and A2a). The integrated fluxes for these models are shown in Table 3.4. As expected from our experience in the other oceans, very little in the way of independent information was gained from this addition and the solutions remain essentially unchanged.

## Models A3 & A3a - Conservation of Silica in Isopycnal Layers

With the addition of silica conservation in the layers below the euphotic zone where consumption occurs and above the bottom<sup>1</sup> where production occurs, the rank of the solution increased by 1, indicating that some new, independent information has been gleaned. The character of the reference level velocities remained unchanged, although the rms values increased by about 0.1 cm/sec for both models. In these models it became apparent that most of the cross-isopycnal transfer was occurring in the intermediate and bottom layers with very little exchange occurring between the isopycnals throughout the extent of the NADW. This brings to mind the rather oversimplified picture of the South Atlantic circulation in which the NADW mass is moving to the south sandwiched between the intermediate and bottom waters with mixing only occurring at the boundaries between the different water masses. The most significant change which has occurred with the addition of the silica constraints is the decrease in magnitude of the overturning cell. The transport of NADW has decreased by  $3-4 \times 10^9$  kg/sec . Most of the corresponding decrease in northward flow occurs in the BW layers as there is actually a slight increase in the transport in the intermediate layers. The lowest layers now exhibit small amounts of poleward flow.

The effect on the property fluxes (Table 3.5) is most evident in the SIRL model which has undergone the greater change in the vertical structure of the mass transport. There is now a small net heat gain by the ocean between the two latitudes of about  $11 \text{ W/m}^2$ , which is not significant within the error of  $\sim 300 \text{ W/m}^2$ . The net production of oxygen in the region has not changed but there is now a corresponding consumption of both phosphate and silica as might be expected. The net divergence of PO<sub>38</sub> within the region has been converted to a small net convergence. As the DIRL model has not had to work quite so hard to meet the

---

<sup>1</sup>'Above the bottom' is defined as just below the depth of the Mid-Atlantic ridge.



	Model A2 SIRL	Model A2a DIRL	Std Error	Nullspace Error	Units
30°S Heat	0.3	0.4	1.7	0.1	PW
15°S Heat	0.3	0.4	1.8	0.1	
net conv.	0.0	0.0			
30°S Oxygen	-8	-18	141	6	10 <sup>9</sup> mL/sec
15°S Oxygen	12	28	457	12	
net conv.	-20	-46			
30°S Phosphate	-2	1	68	4	kmol/sec
15°S Phosphate	-4	-8	143	3	
net conv.	2	9			
30°S Silica	136	263	5290	292	kmol/sec
15°S Silica	411	187	6410	261	
net conv.	-275	76			
30°S PO38	-630	-651	9042	331	kmol/sec
15°S PO38	45	92	19600	381	
net conv.	-675	-743			
Ekman 15°S	-7.0	-7.1			10 <sup>9</sup> kg/sec
Ekman 30°S	-1.5	-1.5			

Table 3.4: Property fluxes for the Atlantic Ocean Models A2 and A2a which conserve mass and salt in isopycnal layers.

	Model A3 SIRL	Model A3a DIRL	Std Error	Nullspace Error	Units
30°S Heat	0.3	0.4	1.7	0.1	PW
15°S Heat	0.4	0.4	1.8	0.1	
net conv.	-0.1	0.0			
30°S Oxygen	-17	-19	160	3	10 <sup>9</sup> mL/sec
15°S Oxygen	4	21	493	11	
net conv.	-21	-40			
30°S Phosphate	3	1	84	2	kmol/sec
15°S Phosphate	-3	-6	147	3	
net conv.	6	7			
30°S Silica	311	234	6291	249	kmol/sec
15°S Silica	183	190	5782	228	
net conv.	128	44			
30°S PO38	-395	-678	9588	267	kmol/sec
15°S PO38	-242	124	19660	327	
net conv.	153	-802			
Ekman 15°S	-7.1	-7.1			10 <sup>9</sup> kg/sec
Ekman 30°S	-1.5	-1.5			

Table 3.5: Property fluxes for the Atlantic Ocean Models A3 and A3a which conserve mass, salt and silica in isopycnal layers.

requirement of silica conservation in isopycnal layers, the property fluxes for this model have not changed as drastically. Note that the previous DIRM models already estimated a small net convergence of silica within this region.

#### **Models A4 & A4a - Conservation of PO<sub>38</sub> in Isopycnal Layers**

In the next pair of models conservation of the combined quantity PO<sub>38</sub> (138O<sub>2</sub> + P) was required in the layers below the euphotic zone to the bottom. Once again an increase in the rank of 1 resulted. These constraints have the effect of increasing the reference level velocities slightly, more so in the SIRM model than in the DIRM model. In both models the transport of BW has increased but the effect is greater in the SIRM model which also produces an increased transport of NADW at 30°S. In both models there is a small increase in the convergence of silica, a decrease in the convergence of phosphate and a corresponding change in the PO<sub>38</sub>. In the SIRM model the estimated net gain of heat by the ocean within the region has increased slightly to about 15 W/m<sup>2</sup> (Table 3.6), but the error is still on the order of error of 300 W/m<sup>2</sup>.

Before drawing a final conclusion from our analysis of the South Atlantic, two more experiments appear to be appropriate. The first is to see if it is possible to remove the oxygen production at depth by requiring that oxygen be conserved below the surface layers (an equivalent requirement was made in the Pacific models). The second is to examine the solution when the heat flux is forced to be as great as the other values found in the literature.

#### **Models A5 & A5a - Conservation of Oxygen below the Surface**

To reduce the production of oxygen below the surface layers the SIRM model A5 reduces the strength of the overturning cell and in particular creates an equatorward flow in layer 13 (part of the NADW mass). In the DIRM models the same effect occurs though simultaneously the comparatively oxygen rich BW is reduced

	Model A4 SIRL	Model A4a DIRL	Std Error	Nullspace Error	Units
30°S Heat	0.2	0.4	1.8	0.1	PW
15°S Heat	0.3	0.4	1.6	0.1	
net conv.	-0.1	0.0			
30°S Oxygen	-18	-21	148	3	10 <sup>9</sup> mL/sec
15°S Oxygen	7	20	456	11	
net conv.	-25	-41			
30°S Phosphate	4	2	78	2	kmol/sec
15°S Phosphate	-4	-6	131	3	
net conv.	8	8			
30°S Silica	444	309	6063	235	kmol/sec
15°S Silica	262	223	5336	219	
net conv.	182	86			
30°S PO38	-269	-601	9375	255	kmol/sec
15°S PO38	-195	127	18300	310	
net conv.	74	-728			
Ekman 15°S	-6.9	-6.8			10 <sup>9</sup> kg/sec
Ekman 30°S	-1.6	-1.6			

Table 3.6: Property fluxes for the Atlantic Ocean Models A4 and A4a which conserve mass, salt, silica and PO38 in isopycnal layers.

by 75% at the southern section and by 60% at the northern section. Unfortunately, at neither section is the attempt very successful (see Table 3.7). Since nothing significant has been gained by the inclusion of the oxygen constraints they will be left out of the best estimate model. We conclude that the most likely source of this oxygen production at intermediate depths is upwelling of deep and bottom waters.

### Models A6 & A6a - Requiring a Larger Equatorward Heat Flux

Model A6 (SIRL) and A6a (DIRL) required net heat fluxes through the sections equal to the average of the higher values at the two latitudes reported by the others listed in Table 3.1. These mean values were  $0.9 \pm 0.3$  PW at 15/degrees S and  $0.8 \pm 0.1$  PW at 30/degrees S. Table 3.8 tabulates the integrated results. For both models, there is a production of oxygen, a consumption of nutrients and small gain of heat by the ocean within the region. Interestingly enough, the models show less sensitivity to the change in the initial reference level than any Atlantic model so far. Unfortunately the manner in which the circulation is changed in order to

	Model A5 SIRL	Model A5a DIRL	Std Error	Nullspace Error	Units
30°S Heat	0.2	0.4	1.8	0.1	PW
15°S Heat	0.4	0.4	1.7	0.1	
net conv.	-0.2	0.0			
30°S Oxygen	-19	-23	161	3	10 <sup>9</sup> mL/sec
15°S Oxygen	-1	8	553	5	
net conv.	-18	-31			
30°S Phosphate	4	2	84	2	kmol/sec
15°S Phosphate	-2	-3	163	2	
net conv.	6	5			
30°S Silica	399	183	6515	226	kmol/sec
15°S Silica	230	139	5643	211	
net conv.	169	44			
30°S PO38	-309	-704	10431	250	kmol/sec
15°S PO38	-284	20	20160	281	
net conv.	-25	-684			
Ekman 15°S	-6.5	-6.1			10 <sup>9</sup> kg/sec
Ekman 30°S	-1.6	-1.7			

Table 3.7: Property fluxes for the Atlantic Ocean Models A5 and A5a which conserve mass, salt, silica, PO38 and oxygen in isopycnal layers.

	Model A6 SIRL	Model A6a DIRL	Std Error	Nullspace Error	Units
30°S Heat	0.6	0.6	0.6	0.0	PW
15°S Heat	0.7	0.6	0.6	0.0	
net conv.	-0.1	0.0			
30°S Oxygen	-27	-32	239	3	10 <sup>9</sup> mL/sec
15°S Oxygen	10	21	642	8	
net conv.	-37	-52			
30°S Phosphate	-1	2	129	1	kmol/sec
15°S Phosphate	-15	-12	223	3	
net conv.	14	14			
30°S Silica	-514	-238	6017	110	kmol/sec
15°S Silica	-1250	-1005	8165	74	
net conv.	736	767			
30°S PO38	-1288	-1183	17100	106	kmol/sec
15°S PO38	-1568	-796	37325	167	
net conv.	280	387			
Ekman 15°S	-9.6	-10.6			10 <sup>9</sup> kg/sec
Ekman 30°S	-1.2	-1.2			

Table 3.8: Property fluxes for the Atlantic Ocean Models A6 and A6a which conserve mass, salt, silica and PO38 in isopycnal layers, and require larger equatorward heat fluxes through the sections.

meet the new constraint is not acceptable. To produce a greater equatorward heat flux the model has:

- increased the solution size,  $\mathbf{b}^T \mathbf{b}$  drastically,
- increased the transport of warmer surface and intermediate waters,
- decreased the flux of cooler NADW
- and has reversed the sign of the bottom water transport, so that it now flows towards the pole.

This solution with no net northward flow of AABW appears unreasonable in the face of our current understanding of the South Atlantic circulation and therefore, we conclude that the larger equatorward heat flux is not consistent with the data and the other model constraints. Rintoul (1990) reached the same conclusion for somewhat different reasons. In his model where an equatorward heat flux of 0.69 PW was required through a section at 32°S, the result was a much stronger meridional overturning cell with 27 Sv carried in the NADW layers. Although he states that the relative contributions made by each water mass to the cell remains about the same, which is true for the fractions of surface, intermediate and deep layers, the transport of bottom water though still equatorward has been reduced and only represents about 10% of the poleward flow as compared to the 30% it represented in the standard model. In the reduction of equatorward flowing bottom water his solution is similar to ours. He rejected the larger equatorward heat flux hypothesis based upon the need for larger reference level velocities, a near reversal of the Brazil Current and the deep western boundary currents and the stronger, meridional, vertical overturning cell. The change in our reference level velocities has reversed the flow of bottom water and we also reject the hypothesis of a larger equatorward heat flux based upon the unlikely circulation produced.

## Models A7 & A7a - Unconstrained growth of $w^*$ .

We have found the integrated fluxes of oxygen and nutrients are fairly sensitive to the initial reference level chosen for the models. In general the meridional overturning cell is stronger for the deeper initial reference level. The stronger overturning cell produces a larger production of oxygen and consumption of phosphate while at the same time reducing the consumption of silica. The consumption of silica, which was found in all the DIRL models, was only obtained in the SIRL models after the conservation of silica in isopycnal layers below the euphotic zone and above the bottom was included in the model constraints. There appears to be oxygen production at depth, but we were unsuccessful in the attempt to require even conservation within these layers, never mind consumption. This production may be due to coastal upwelling as seen by Peterson and Stramma (1991). The errors on the fluxes are large, so that as in the other oceans, an attempt was made to reduce the residuals by allowing the unconstrained growth of the  $w^*$  terms.

Making this change (model A7 and A7a), the cross-isopycnal transfer terms increased as in the other oceans by about an order of magnitude to about  $10^{-5}$  cm/sec. In the DIRL model, downwelling occurs in the uppermost layers with upwelling below this in the intermediate layers. The strongest downwelling ( $\sim 5 \times 10^9$  kg/sec) occurs between layers 13 and 14, at about 3600 m. In the SIRL model, upwelling occurs everywhere between layers 3 and 15, with the strongest downwelling ( $> 5 \times 10^9$  kg/sec) appearing between layers 16 and 17. The DIRL model gives an integrated solution similar to model A4 but with a reduced flow of bottom water at 30°S and an increased transport of NADW at 15°S. The SIRL model produces a stronger overturning cell, with a poleward flow of bottom water at 15°S. This BW transport reverses direction at the next higher rank. The property fluxes have changed somewhat (see Table 3.9), but even with the reduction in the error, none are distinguishable from zero except the heat flux at 15°S.

	Model A7 SIRL	Model A7a DIRL	Std Error	Nullspace Error	Units
30°S Heat	0.3	0.4	0.5	0.1	PW
15°S Heat	0.5	0.5	0.4	0.1	
net conv.	-0.2	-0.1			
30°S Oxygen	-7	-13	28	6	10 <sup>9</sup> mL/sec
15°S Oxygen	2	8	215	16	
net conv.	9	-21			
30°S Phosphate	-3	-2	16	4	kmol/sec
15°S Phosphate	-8	-3	33	5	
net conv.	5	1			
30°S Silica	174	29	1907	337	kmol/sec
15°S Silica	-403	13	2409	326	
net conv.	577	16			
30°S PO38	-682	-886	2386	344	kmol/sec
15°S PO38	-962	-75	4873	439	
net conv.	280	-811			
Ekman 15°S	-7.4	-7.4			10 <sup>9</sup> kg/sec
Ekman 30°S	-1.5	-1.5			

Table 3.9: Property fluxes for the Atlantic Ocean Models A7 and A7a which conserve mass, salt, silica and PO38 in isopycnal layers. These models both allow the vertical transfer terms to grow to the size of the reference level velocities, if necessary.

The character of the circulation is similar for all the models, though the magnitude of the overturning cell is different. It is difficult to choose a best estimate solution because we are unable say which mass and property fluxes are more realistic for this region. Choosing the A7 models (conservation of mass, salt, silica and PO38) as the most informed estimates, with the lowest standard error, we further take the deep initial reference level model (A7a) as our best estimate, because the solution size is smaller and because the DIRL models are, in general, less sensitive to the addition of new constraints.

The heat flux is not as sensitive to the choice of initial reference level as the other property fluxes. For the DIRL model A7a, we obtain an equatorward heat flux of  $0.4 \pm 0.4$  Pw at 30°S and  $0.5 \pm 0.3$  Pw at 15°S. Both these values fall on the low end of the range of values found by other investigators. An attempt to force a large heat flux through the sections failed as the resulting circulation was

not consistent with our understanding of the meridional, vertical overturning cell in the South Atlantic and in particular the path the Antarctic Bottom water.



## Chapter 4

### Conclusions

In this thesis we have used hydrographic data and inverse methods to examine the circulation in the southern regions of the Pacific, Indian and Atlantic Oceans. The main emphasis has been upon the determination of an upper limit on through flow between the Pacific and Indian Oceans via the Indonesian Archipelago and the heat transport at each of the sections.

It was found that using data from the South Pacific only, that the very largest through flow estimates of 20 Sv cannot be rejected. Much of the compensation for a net northward mass flux through the section in the South Pacific occurs in the deep and bottom layers. Increased through flow in turn produces an increased net northward transport of oxygen due to this greater transport of deep and bottom water. Although there is not a dramatic change in the temperature flux estimates for a large through flow model, the change leans systematically towards a net equatorward flux of temperature within the basin. The largest through flow estimates are also supported by the South Indian Ocean data set.

Combining the available information from both the Pacific and Indian Oceans, the results were similar to those found using the individual models, except that in the Pacific a greater proportion of the compensation occurred in the upper layers,

which in turn produced larger estimates for the already questionable equatorward temperature flux. As expected however, there is still a net poleward heat flux within these two basins. The magnitude of the net heat flux is not greatly affected by the magnitude of the through flow.

It is the conclusion of this thesis that the largest through flow estimates (upto 20 Sv) are indeed quite possible. But, the data used in these models do not contain enough information to place either an upper or lower bound on the estimate of the through flow. The seasonal and interannual variations which have been found by other investigators and which we are incapable of resolving using the present data set and analysis, leads us to further conclude that in the long term mean the estimate of 10 Sv through flow is most reasonable. The great variation in the magnitudes of the through flow found by other investigators (Table 1.1) is probably representative of the true range of the transport over shorter time scales. To more accurately assess the effect of any particular magnitude of the through flow on the circulation and property fluxes using this type of analysis, it would be useful to have sections which were occupied in similar seasons within the two basins. It would also be most useful to include data extending across the archipelago itself.

The Atlantic Ocean is the source of most of the deep and bottom waters found throughout the World Ocean. The North Atlantic Deep Water (NADW) mass is formed when relatively warm, saline water flows poleward in the North Atlantic through a region where the cooling effects of evaporation are strong. The resulting cold, salty water sinks into the deep ocean and NADW is formed. The NADW flows back out the North Atlantic at depth, through the South Atlantic and eventually is entrained in the flow of the Antarctic Circumpolar Current which carries it into the other ocean basins. For NADW to be formed, there must be a supply of upper layer waters to feed the formation process. As mentioned in Chapter 1 there are two possible (not mutually exclusive) paths for the circulation of NADW

as it passes out of the Atlantic to spread into the other ocean basins, eventually to return in the upper layers to feed formation, having undergone upwelling into the thermocline (Gordon 1986).

The cold water path allows the water to return through the Drake Passage into the South Atlantic at the relatively cold temperatures of AAIW and Subantarctic Mode Water. Gordon estimated that less than 25% of the water returned through this route. The warm water path expects the water to be returned around the southern tip of Africa from the retroflection region of the Agulhas Current. This water is warmer, coming mainly from the Indian Ocean thermocline.

Since a reasonably large Indonesian Passage through flow is supported by our data, the warm water path suggested by Gordon appears to be feasible. However, our data does not support a large (or in our best estimate solution, even significant) southward flow through the Mozambique Channel from the SEC as Gordon suggests. The water which intensifies the Agulhas Current in the south must come from the eastern side of Madagascar.

Our results cannot support or reject the hypothesis that significant portions of the Agulhas water actually makes into the South Atlantic to close the warm water route. Certainly it is reasonable to expect from the estimates of through flow provided by other authors and discussed in Chapter 3 that this path could maintain some importance in the circulation of NADW. However, since we were unable to force the larger heat flux estimates made by other observers through our sections in the South Atlantic, it appears that this data set supports the findings of Rintoul (1990) in which the importance of the cold water route in maintaining the global overturning cell and the formation process of NADW was significantly greater than the role played by the warm water route.

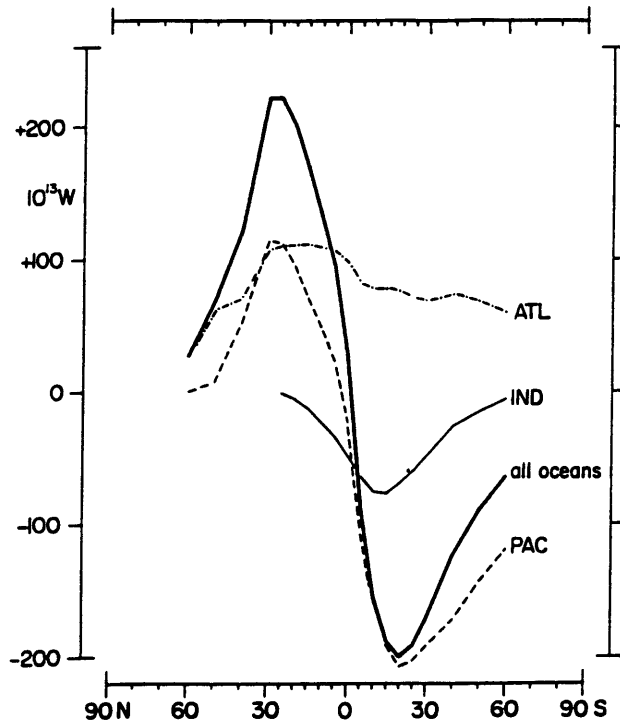


Figure 4.1: From Hastenrath (1982). Annual mean meridional heat transport within the oceans: Pacific (dashed), Atlantic(dash-dotted), Indian (thin solid), and all oceans combined (heavy solid). Northward transport positive, units in  $10^{13}$  W.

Combining the results of our best estimate solutions from the three different oceans (models PI and A7a), we find a net heat flux at  $\sim 30^{\circ}\text{S}$  of  $-1.1 \pm 1.7$  PW poleward, with small equatorward heat flux in the South Atlantic ( $0.4 \pm 1.4$  PW) and large poleward heat flux in the combined Pacific–Indian basins ( $-1.50 \pm 1.3$  PW), most of which can be attributed to the Indian Ocean. The standard error associated with this value is large and so it is not significantly different from zero, however, the major portion of this poleward heat flux has arisen from the Indian Ocean in which the fairly large negative value was a consistent result of all the models. Comparing this value to Figs. 4.1 and 4.2 (Figure 1 and 3 of Hastenrath (1982), respectively) it is seen to be lower than previous indirect estimates which places the northward heat transport by the oceans at this latitude at between about -1.5 and -2.0 PW.

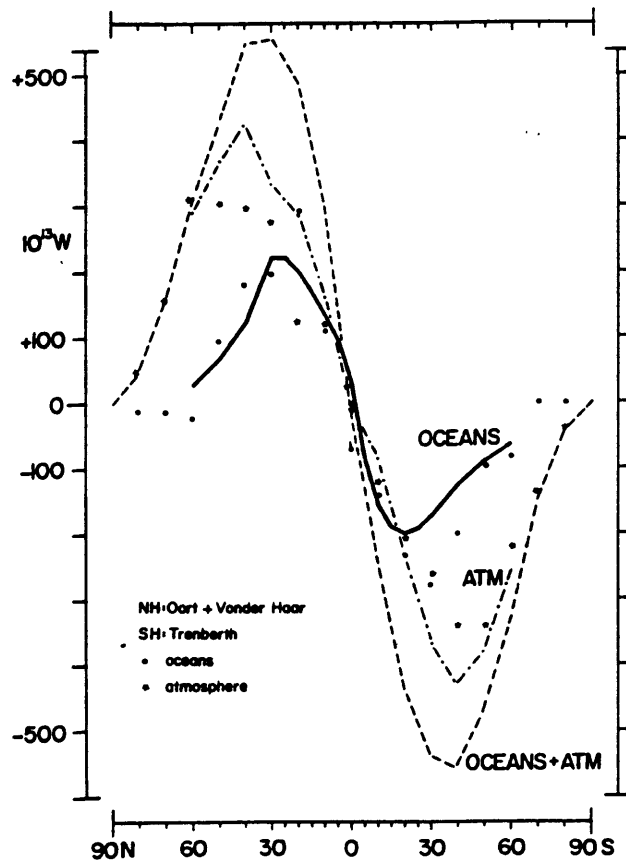


Figure 4.2: From Hastenrath (1982). Annual mean meridional heat transport within the ocean-atmosphere system (dashed line – from satellite measurements), within the oceans (solid line – from Fig. 4.1), and within the atmosphere (dashed-dotted line – residual). Estimates by Oort and Vonder Haar (1976) for the Northern Hemisphere and by Trenberth (1979) for the Southern Hemisphere are given as dots for the ocean and stars for the atmosphere.

Bennett's (1978) estimate at 32°S ranged from -1.46 to 2.27 PW depending upon the boundary current widths chosen. Hsuing (1985) estimated a global oceanic heat transport of -1.6 PW, which is dominated by a large southward heat flux in the Indian ocean as our value is. The value found here,  $-1.1 \pm 1.7$  PW is consistent with these previous estimates.

There are two ways in which the analysis of these data sets could be expanded:

- The information is available within the inverse results to draw some conclusions about the zonal circulation within these basins. Such an analysis would help explain the net meridional flow of water masses (or layers) as they have been described here and shed some more light on the property fluxes and the patterns of convergences and divergences. The oxygen and nutrient fluxes and how they are affected by the various model constraints could also be looked at in more detail. Examining the property content of the Benguela Current could allow something to be said about the amount of Indian Ocean thermocline water it contains and therefore about the closing of the warm water path around the southern tip of S. Africa.
- The errors in this analysis are large. To reduce the errors one must have greater confidence in the solutions (*i.e.* the *a priori* estimate of the uncertainties must be reduced). One cannot simply reduce this estimate without including some new information in the problem (as we did when we constrained the heat flux estimates) or changing some of the old physics or introducing some new physics in the problem since it would mean accepting uncomfortably large solution sizes. The inclusion of vertical mixing terms in the inverse equations might be one source of new physics. It is not clear that vertical mixing coefficients if they were included would be any more effective in reducing the errors than the vertical transfer terms. How such variables

should be weighted is not immediately obvious and would require some care since they would multiply derivatives of property concentrations as opposed to simply concentrations in the inverse equations. It is possible that they, like the cross-isopycnal transfer terms would oscillate in sign unless they were forced to be positive or allowed to be nearly fully resolved, further reducing the resolution of the reference level velocities. In either case interpretation would be difficult since they would be quantities which have been integrated both zonally and meridionally across the entire area. A fairly simple addition to models which would be helpful in reducing the initial uncertainties would be a section across the Mozambique Channel.

The inverse method has allowed us to calculate mass, heat and nutrient fluxes all three southern oceans by combining some different types of data and giving a simple method for comparing the results of a number of different models. It was found that in all three basins that although the salinity data did not, the nutrient data did provide information to the models independent of mass conservation. However, the results are not wholly satisfying as the size of our errors remains large and most of our results are not significantly different from zero. It is possible that in order to produce basin wide estimates of property fluxes more information is needed than can be found in two hydrographic sections. In particular, to better determine an upper bound on the Indonesian Archipelago through flow it would be useful to include data closer to the archipelago itself, as well as, data across the Mozambique Channel. A more systematic analysis of the how each element of physics is applied in the problem (including the various matrix weights) would shed some light on whether more data is needed or better expression of the physics itself is required.

## Appendix A

### Formulation of the Inverse Problem

#### A.1 Introduction

Inverse machinery takes as its input a model, which combines many, and ideally all, the pieces of information known about an under-determined system. It produces a *best estimate* of the solution, along with an estimate of the uncertainty in the solution and of the relative importance of the individual constraints imposed. Any method which can solve an ill-posed problem is an inverse method. A good one will allow the consistency of the model results to be tested. The inverse technique used here is the Singular Value Decomposition (SVD).

This appendix briefly reviews the inverse technique of the SVD as applied to an ocean system where the unknowns are the geostrophic reference level velocities and the horizontally averaged cross-isopycnal transfer terms. Appendix B gives some further details and a discussion of the error analysis, but the reader is referred to the numerous detailed discussions of this technique which can be found in the literature such as Wunsch (1978), Wunsch *et al.* (1983), Roemmich (1980), Rintoul (1988) and Wiggins (1972). The main purpose of this appendix will be to outline some of the specific choices which were made for the models used in this thesis,



including: the choice of density layers, row and column weights, initial reference levels and matrix rank.

## A.2 Inverse Basics

The inverse problem is designed to combine all the various pieces information known about a system into a single set of simultaneous equations which is then solved using the least squares technique of SVD. The model used here begins with a set of hydrographic sections with which one or more enclosed areas are defined. Around the perimeters of these areas are land, information about the temperature, salinity, oxygen and nutrients or some other data such as transport estimates of a boundary current or an Ekman flux contribution. The design of the model is based on this data and the following set of physical assumptions:

- The system is in a steady state and in hydrostatic and geostrophic balance so that the thermal wind equations apply to the problem.
- That a reasonable initial estimate can be made of reference level at which the velocities are relatively small, *ie.* a level at which it sensible to minimize the velocities.
- A set of equations describing the extent of conservation of mass and other properties within the areas can be written. These equations may include non-geostrophic components.
- A set of divisions can be defined in the vertical, in this case, isopycnal layers across which all transport is described in terms of a zonally averaged cross-isopycnal flow representing a variety of unresolved processes contributing to the net 'vertical' flux.

None of these assumptions is absolutely necessary to the definition of the inverse problem. Another completely different set, as long as they are justified by the data and the physics of the problem would be perfectly acceptable. The above assumptions represent the simplest system, believed to be consistent with true one, which makes full use of the available knowledge and data. Incompatibilities between the data and the physical constraints will be determined by the inverse. Lack of the appropriate physics will be evident as structure in the residuals.

The assumption of a steady, hydrostatic geostrophic balance allows the thermal wind equations to be written. These are then integrated to a reference level,  $z_0$ , to form the familiar dynamic method equations which describe the geostrophic velocity  $v_R$  normal to the section, relative to an unknown reference level, velocity,  $v_0$ .

$$P_z = -g\rho \quad fv = \frac{1}{\rho_0}P_x \quad fu = -\frac{1}{\rho_0}P_y \quad (\text{A.1})$$

$$fv_z = -\frac{g}{\rho_0}\rho_x \quad fu_z = \frac{g}{\rho_0}\rho_y \quad (\text{A.2})$$

$$v(z_R) - v(z_0) = \frac{-g}{f\rho_0} \int_{z_R}^{z_0} \rho_x dz \quad (\text{A.3})$$

$$u(z_R) - u(z_0) = \frac{g}{f\rho_0} \int_{z_R}^{z_0} \rho_y dz$$

There are a number of different methods for finding either the reference level velocity or an expected level of no motion which are well described in the literature. The inverse method allows one to find that reference level velocity which is consistent with *a priori* assumptions about the conservation of mass and other properties within the box by combining the equation A.3 with the integrated continuity

equation to give the following:

$$\begin{aligned}
& \sum_{j=1}^S \rho_{ij} \mathbf{a}_{ij}^S (\mathbf{v}_{ijR} + \mathbf{b}_j)^S \mathbf{C}_{ij}^S - \sum_{j=1}^N \rho_{ij} \mathbf{a}_{ij}^N (\mathbf{v}_{ijR} + \mathbf{b}_j)^N \mathbf{C}_{ij}^N + \\
& \sum_{j=1}^W \rho_{ij} \mathbf{a}_{ij}^W (\mathbf{v}_{ijR} + \mathbf{b}_j)^W \mathbf{C}_{ij}^W - \sum_{j=1}^E \rho_{ij} \mathbf{a}_{ij}^E (\mathbf{v}_{ijR} + \mathbf{b}_j)^E \mathbf{C}_{ij}^E - \\
& \mathbf{a}_i^{Htop} \mathbf{w}_i^{*top} \mathbf{C}_i^{Htop} + \mathbf{a}_i^{Hbot} \mathbf{w}_i^{*bot} \mathbf{C}_i^{Hbot} \approx 0, \quad (\text{A.4})
\end{aligned}$$

where,

$i, j$  are the layer and station pair indices, respectively

$H$  indicates the horizontal layer interface,

$top, bot$  indicate the top and bottom of the layer respectively,

$S, N, E, W$  indicate the southern, northern, eastern, and western boundaries of the layer, respectively,

$\mathbf{v}_R$  is the relative velocity,

$\mathbf{b}$  is the reference level velocity,

$\mathbf{w}^*$  is the cross-isopycnal transfer

$\mathbf{a}$  is the interface area ( vertical unless indicated otherwise ),

$\mathbf{C}$  is the property concentration

Such an equation can be written for each conserved property in each layer, as well as, for the top to bottom transport. Separate equations can be written for the flux across individual sections. The right hand side can be written to include

a non-geostrophic component. This set of equations is then manipulated into the form:

$$\sum_j \rho_j \mathbf{a}_j \mathbf{C}_j \mathbf{b}_j - \mathbf{a}^{Htop} \mathbf{C}^{Htop} \mathbf{w}^{*top} + \mathbf{a}^{Hbot} \mathbf{C}^{Hbot} \mathbf{w}^{*bot} \approx - \sum_j \rho_j \mathbf{a}_j \mathbf{v}_{jR} +$$

*Ekman Component + Known Flux through the Box etc ...*, (A.5)

which can in turn be written,

$$\mathbf{A} \mathbf{b} + \mathbf{n} = -\mathbf{\Gamma}, \quad (\text{A.6})$$

where, the elements of the  $\mathbf{A}$  matrix are  $\int_B^T \rho_{ij} \mathbf{a}_{ij} \mathbf{C}_{ij} dp$ ,  $\mathbf{b}$  is the vector of unknown reference level velocities and the cross-isopycnal transfer terms.  $\mathbf{\Gamma}$  is the vector of known relative velocity transports plus other optional right hand side elements.

The SVD seeks the solution which minimizes the objective function:

$$J = (\mathbf{A} \mathbf{b} + \mathbf{\Gamma})^T (\mathbf{A} \mathbf{b} + \mathbf{\Gamma}) + \mathbf{b}^T \mathbf{b}, \quad (\text{A.7})$$

that is, the residuals and the solution size. The SVD decomposes the  $\mathbf{A}$  matrix such that  $\mathbf{A} = \mathbf{U} \mathbf{\Lambda} \mathbf{V}^T$ . The solution vector  $\mathbf{b}$  is given by:

$$\mathbf{b} = \mathbf{U}^T \mathbf{\Lambda}^{-1} \mathbf{V} (-\mathbf{\Gamma}) \quad (\text{A.8})$$

or

$$\mathbf{b} \approx \sum_{l=1}^k \frac{\mathbf{u}_l (-\mathbf{\Gamma})}{\lambda_l} \mathbf{v}_l, \quad (\text{A.9})$$

where,  $k$  is the matrix rank, the choice of which will be discussed later in this appendix. The vectors  $\mathbf{u}_l$  and  $\mathbf{v}_l$  are the individual columns of the  $\mathbf{U}$  and  $\mathbf{V}$  matrices.

It is assumed from the beginning that there is no one correct answer to this problem. We are not taking an snapshot of an instantaneous ocean circulation, but rather looking at what might be thought of as time average picture. We are seeking solutions which are consistent with the observed data and our assumptions about the physics which governs the problem. The solution will therefore, depend upon

---

Depth/pressure	db
Temperature	°C
Salinity	‰
Oxygen	ml/l
Phosphate	μmoles/kg
Silicate	μmoles/kg
PO38	μmoles/kg

---

Table A.1: Units of variables for all sections used throughout this thesis.

which equations we choose to use, how those equations are weighted relative to one another and ultimately upon how the *best estimate* of the solution is chosen. The next section discusses choices made for this research.

### A.3 Formulation of the Equations

#### A.3.1 Data Preparation

All the oceanographic data used in this research comes from hydrographic sections, with the exception of the 18°S Indian Ocean section which has CTD, 2 decibar, temperature and salinity measurements. References in which details concerning the field preparation of the data are given in the individual chapters where the data are used. The units for each of the different types of variables are given in Table A.1. All the data have been converted to these same units.

The hydrographic data have been interpolated onto a set of 37 standard depths ranging from 0 to 8000 db. By averaging the values 20 db above and below each of the standard depths the CTD data have computed for these same depths. Where necessary the data have been extrapolated down to the deepest standard depth above the observed bottom.

The relative geostrophic velocities are computed using data on the standard depths, except in the case of the CTD data. For these, the geostrophic velocities are computed at the two decibar intervals and then averaged onto the standard depths as above. The velocities were extrapolated down to the deepest common depth by retaining the isopycnal slope at the deepest common depth down to the bottom.

The  $\mathbf{A}$  matrix elements,  $A_{ij} = \int_B^T \rho_{ij} \mathbf{a}_{ij} \mathbf{C}_{ij} dp$  associated with the individual  $\mathbf{b}_j$ 's are constructed from the integrated standard depth values which have been interpolated to the depth of the individual layers used in the integral. The layer boundary values which are used in the  $\mathbf{w}^*$ ,  $\mathbf{A}$  matrix elements are also interpolated from the values at the standard depths.

### A.3.2 Choice of Isopycnal Layers

Each enclosed area in the inverse calculation is divided into a set of layers in the vertical. Within these layers, it is expected that mass and other properties will be approximately conserved. To minimize the flow between the layers they are defined by potential density surfaces, in order that the buoyancy force may oppose the cross-isopycnal flow.

The neutral surface, defined as that in which the gradient normal to the surface is always parallel to the buoyancy force (McDougall 1987) might be a more accurate choice. Here a compromise is made, in which rather than computing neutral surfaces, the pressure reference level is allowed to change as a bounding isopycnal surface expresses large vertical variations. The difference in pressure between the isopycnal surface and its reference pressure never exceeds 500 db. In this way, it approximates the neutral surface which by definition will be the same as the isopycnal surface at the reference pressure. The error introduced by this approximation is expected to be much less than the measurement error (Rintoul 1988).

The density layers used in section 1.2 were those provided by the inverse calculation of Wunsch *et al.* (see Fig. 1.1). They were chosen to emphasize the water masses expected in the South Pacific as defined by Reid (1965,1973, 1981) and Warren (1973,1981). The layers used in the rest of this thesis (Table 1.8) have been chosen to allow recognition of the variety of water masses found in all the southern oceans. As a result, some of these layers are empty in some of the individual ocean models. The water masses within potential density layers are discussed in more detail for each ocean as they built into the model.

### A.3.3 Choice of Equation Weightings

The problem has been reduced to the simple form  $\mathbf{A}\mathbf{b} + \mathbf{n} = -\mathbf{\Gamma}$ . However, before this equation is solved, it is desirable to perform some weighting upon its components. Without such weighting the SVD will have the unfortunate tendency to produce solutions,  $\mathbf{b}_j$ :

- in which equations ( $\mathbf{A}$  matrix rows) containing the larger coefficients have been used to a greater extent than those containing the smaller coefficients,
- which are proportional in magnitude to the corresponding elements (columns) of the matrix  $\mathbf{A}$ .

The first of these biases is removed through the weighting of the constraint equations, that is, the rows of the  $\mathbf{A}$  matrix. The row weighting performs two functions. To remove artificially large or small coefficients which are due to the arbitrary units in which the various concentrations are measured, each row is divided by the mean value of the associated concentration. This prevents, for instance, the salinity coefficients from being 35 times the size of the mass coefficients. The second use of the row scaling is to allow weighting by the expected error in the various

equations. A simple example of this is: given two equations with coefficients of equal magnitude, but in which one of the equations has an expected uncertainty of 1 and the second an expected uncertainty of 100, we would wish to downweight the second equation in order that it does not have as much effect on the solution as the first.

The row weights are defined by the matrix  $\mathbf{S}^{-1/2}$ , where  $\mathbf{S} = \sigma^2 \bar{\mathbf{C}}^2$ ,  $\bar{\mathbf{C}}$  is the diagonal matrix of mean concentrations,  $\sigma^2$  is the problem variance.  $\mathbf{S}$  is essentially the covariance matrix for the observations. The fact that our  $\mathbf{S}$  is diagonal implies the assumption that the noise in each of the equations is uncorrelated. There are most likely correlations between the neighbouring layers and a more complicated form could certainly be used if more detailed knowledge of the covariance functions were available. The use of the covariance matrix indicates that an *a priori* estimate of the noise in observations has been made. An *a posteriori* estimate of the the problem variance can be made from the problem residuals:

$$\sigma^2 = \sum_{j=1}^M \frac{(\mathbf{A}\mathbf{b} + \mathbf{\Gamma})^2}{M - k}. \quad (\text{A.10})$$

The resulting estimate of  $\sigma^2$  made from the problem residuals ought to be of similar magnitude to that initially estimated in order for the problem to be consistent (Wiggins 1972). If the residuals are much smaller than expected from the estimated variance in the observations then it is possible to conclude that the observation error was overestimated or even that the model is wrong. On the other hand, if the residuals are very large compared to the estimated observation variance then not only is it likely that the observation error was underestimated, it is also possible that the model itself is not adequate to explain the data. Residuals which retain recognizable structure or trends are a good indication of the latter.

Rintoul (1988) gives a good discussion of the possible sources of observational error in this problem. These include errors in navigation, measurement, interpola-



tion and extrapolation. Following his example, the layer equations in all our models are expected to approximate conservation to within 2 Sv, while the top to bottom equations are given an expected error of 1 Sv. There may be other uncertainties in particular layers or sets of layers, due for instance, to outcropping, making it necessary to further downweight particular equations. When such extra downweighting occurs, it is explicitly noted in the text.

The second bias listed above, that which causes the solutions  $\mathbf{b}_j$  to be proportional to the corresponding elements of the matrix  $\mathbf{A}$  is avoided by scaling the columns of  $\mathbf{A}$  by the square roots of the lengths of the columns<sup>1</sup>. This is necessary to prevent stations pairs which are widely spaced from producing larger values of  $\mathbf{b}_j$  than pairs which are more closely spaced. In most of our models we also applied a depth weighting to downweight the shallower stations, which also have a tendency to produce larger values of  $\mathbf{b}_j$ . This is discussed in greater detail in Chapter 1, where an example is given.

The weighting performed, the SVD will now solve the system:

$$\begin{aligned} \mathbf{A}'\mathbf{b}' + \mathbf{n} &= -\mathbf{\Gamma}' & (\text{A.11}) \\ \mathbf{A}' &= \mathbf{S}^{-1/2}\mathbf{A}\mathbf{W}^{-1/2} \\ \mathbf{\Gamma}' &= \mathbf{S}^{-1/2}\mathbf{\Gamma} \\ \mathbf{b}' &= \mathbf{W}^{1/2}\mathbf{b}. \end{aligned}$$

### A.3.4 Choice of Initial Reference Levels

The SVD attempts to not only minimize the residuals,  $(\mathbf{A}\mathbf{b} + \mathbf{\Gamma})^T(\mathbf{A}\mathbf{b} + \mathbf{\Gamma})$  but also the solution size,  $\mathbf{b}^T\mathbf{b}$ . It is, therefore, necessary to choose an initial reference level where it is expected that the *true* velocities are zero, or more reasonably,

---

<sup>1</sup>The column lengths are always calculated after all the other weights have been applied.

simply small. The method of choosing a so called level of no motion has grown into an art in itself, with a variety of possibilities having been put forth by equally as many oceanographers. Good discussions of these various methods can be found in Pond and Pickard (1983), Rintoul (1988), Schott and Stommel (1978) and Wunsch (1977,1978). The best decision which can be made, applies all the *a priori* knowledge or beliefs about the ocean circulation to the problem so that at the very least, the clearly irrational choices are avoided.

In choosing the initial reference levels for this research we have done exactly this, applying all we know about each particular section to the choice and then considering what happens if that choice is varied. In most cases, we will use deep isopycnals for the initial choice; the sections in the Indian Ocean are the exception and are discussed in Chapter 2.

### **A.3.5 Choice of the Best Estimate of the Solution**

As the system is under-determined, there are an infinite number of solutions to the ocean circulation problem as it is expressed here, that is, there are always more unknowns than independent equations. It is therefore, necessary to provide other criteria by which the choice of the *best estimate* solution will be made. This is done through the selection of the matrix rank, which is to say, how many of the given equations are independent. This choice determines number of SVD singular values will be used in determining the solution  $\mathbf{b}$ , (equation A.9). The singular values are given in decending order of magnitude; the higher the rank, the smaller the value of  $\lambda$ . The smaller values of  $\lambda$  which approach zero can cause the solution size to increasae dramatically. However, leaving out too many singular values results in an overly smooth solution, containing little information about the true structure and under-utilizing the precious little knowledge we do have about the system.

There are three guidelines to the choice of rank, *i.e.* the number of eigen vectors to be used in forming the solution:

- One can look for a jump in the magnitude of the singular values. The smaller singular values act to increase the solution size (see equation A.9).
- One can compare the relative sizes of the solution,  $\| \mathbf{b}^T \mathbf{b} \|$  and the residuals,  $\| \mathbf{A} \mathbf{b} + \mathbf{\Gamma} \|$ , looking for the estimate in which the residuals are acceptably small, while the solution has not become unreasonably large.
- One can look at the absolute size of the residuals as compared to the initial estimate of the problem uncertainty.

In our models, we have used all three of the above to determine the appropriate rank. However, when first two guidelines do not point to an obvious choice, the last one has been used as the deciding factor. If the solution is extremely rank sensitive, it is indicative of considerable noise associated with the higher wavenumbers. Thus including the higher wavenumbers, means the smaller singular values will cause large differences in the solutions. In most cases, nearby ranks do not give significantly different solutions.

The resolution matrices furnish practical information about the solution at a given rank. They also provide a method of comparing solutions at different ranks. The resolution matrices are  $\mathbf{V}\mathbf{V}^T$  and  $\mathbf{U}\mathbf{U}^T$ . They are derived in the following manner:

$$\begin{aligned}\mathbf{A}\mathbf{b} &= -\mathbf{\Gamma} \\ \mathbf{A}^T\mathbf{A}\mathbf{b} &= \mathbf{A}^T(-\mathbf{\Gamma}) \\ \hat{\mathbf{b}} &= \mathbf{A}^T(\mathbf{A}\mathbf{A}^T)^{-1}(-\mathbf{\Gamma})\end{aligned}$$

using  $\mathbf{A} = \mathbf{U}\mathbf{\Lambda}\mathbf{V}^T$  gives

$$\begin{aligned}\hat{\mathbf{b}} &= \mathbf{V}\mathbf{\Lambda}^{-1}\mathbf{U}^T(-\mathbf{\Gamma}) \\ \hat{\mathbf{b}} &= \mathbf{V}\mathbf{\Lambda}^{-1}\mathbf{U}^T(-\mathbf{A}\mathbf{b}_{\text{true}}) \\ \hat{\mathbf{b}} &= \mathbf{V}\mathbf{V}^T\mathbf{b}_{\text{true}}\end{aligned}\tag{A.12}$$

$$\begin{aligned}-\hat{\mathbf{\Gamma}} &= \mathbf{A}\hat{\mathbf{b}} \\ -\hat{\mathbf{\Gamma}} &= \mathbf{A}\mathbf{V}\mathbf{\Lambda}^{-1}\mathbf{U}^T(\mathbf{A}\mathbf{b}_{\text{true}}) \\ -\hat{\mathbf{\Gamma}} &= \mathbf{U}\mathbf{U}^T(-\mathbf{\Gamma})_{\text{true}}\end{aligned}\tag{A.13}$$

so at any particular rank,  $k$ :

$$\hat{\mathbf{b}} = \mathbf{V}_k\mathbf{V}_k^T\mathbf{b}_{\text{true}}$$

and

$$-\hat{\mathbf{\Gamma}} = \mathbf{U}_k\mathbf{U}_k^T(-\mathbf{\Gamma})_{\text{true}}$$

where,  $\hat{\mathbf{b}}$  and  $\hat{\mathbf{\Gamma}}$  are the estimates of the solution and residuals found from the SVD and  $\mathbf{b}_{\text{true}}$  and  $\mathbf{\Gamma}_{\text{true}}$  are the unknown true solutions, and  $\mathbf{U}_k$  and  $\mathbf{V}_k$  are the matrices containing the first  $k$  vectors of  $\mathbf{U}$  and  $\mathbf{V}$  respectively.

The resolution matrix  $\mathbf{V}\mathbf{V}^T$  in equation A.12, shows how the estimated values  $\hat{\mathbf{b}}$  are related to the true solution  $\mathbf{b}_{\text{true}}$ . Examination of the diagonal of the resolution matrix gives a sense of how much of the true solution was captured. A resolution matrix  $\mathbf{V}_k\mathbf{V}_k^T = \mathbf{I}$ , the identity matrix, indicates that the system is

full rank and the problem is therefore, fully-determined. A compact resolution is one in which the estimates,  $\hat{\mathbf{b}}_j$  are local averages of the true solution. In this case the elements of  $\mathbf{V}_k\mathbf{V}_k^T$  whose values are closest to unity will be grouped around the diagonal.

The matrix  $\mathbf{U}\mathbf{U}^T$  can be used to describe how much any particular equation of observation was used, relative to the others, in determining the solution. The sum of the diagonal elements of the  $\mathbf{U}_k\mathbf{U}_k^T$  is equal to the matrix rank. The interpretation of a diagonal element of  $\mathbf{U}\mathbf{U}^T$  corresponding to a particular equation approaching unity, is that the equation contributed fully and independently to the determination of the solution.

## Appendix B

### Error Analysis

This appendix contains some detail on how the error analysis for this problem was approached. The method is the same as that presented in the appendix of WHG. It is only repeated here for clarity and to correct some of the misprints<sup>1</sup> in the 1983 text which is often referenced.

The actual or *true* velocity field in a hydrographic section can be written as the sum of the relative velocity from the thermal wind equations,  $\mathbf{v}_R$  based upon an initial reference level, the velocity at that reference level,  $\mathbf{b}$  from equation A.9, other velocity components such as Ekman, leakage, *etc* ...,  $\mathbf{v}_E$  and the component due to the null-space vectors,  $\mathbf{v}_N$ :

$$\begin{aligned}\mathbf{v} &= \mathbf{v}_R + \mathbf{v}_E + \mathbf{b} + \mathbf{v}_N \\ &= A_1 + A_2 + A_3 + A_4\end{aligned}\tag{B.1}$$

Hence, the flux of any particular property  $C$  across the zonal section can be written:

$$F_c = B_1 + B_2 + B_3 + B_4.\tag{B.2}$$

---

<sup>1</sup>It has been confirmed that these were misprints and that the code used in the 1983 analysis was correct.

$B_1$  is the flux due to the relative velocity,

$$B_1 = \sum_{j=1}^J \int_{-D_j}^0 C_j(\mathbf{z}) \rho_j(\mathbf{z}) \mathbf{v}_{Rj}(\mathbf{z}) dz \Delta \mathbf{x}_j. \quad (\text{B.3})$$

$B_2$  is the flux due to the other velocity components,

$$B_2 = \sum_{j=1}^J \int_{-D_j}^0 C_j(\mathbf{z}) \rho_j(\mathbf{z}) \mathbf{v}_{Ej}(\mathbf{z}) dz \Delta \mathbf{x}_j. \quad (\text{B.4})$$

$B_3$  is the flux due to the reference level velocity,

$$B_3 = \sum_{j=1}^J \int_{-D_j}^0 C_j(\mathbf{z}) \rho_j(\mathbf{z}) dz \mathbf{b}_j \Delta \mathbf{x}_j. \quad (\text{B.5})$$

$B_4$  is the flux due to the null-space vectors, those components of the *true*  $\mathbf{b}$ , which cannot be included in the model, because no information about them is available.

$$B_4 = \sum_{j=1}^J \int_{-D_j}^0 C_j(\mathbf{z}) \rho_j(\mathbf{z}) dz \mathbf{v}_{Nj} \Delta \mathbf{x}_j. \quad (\text{B.6})$$

Here,  $J$  is the number of station pairs in the section,  $j$  is the index to the individual stations,  $D_j$  is the depth a station pair,  $\Delta x_j$  is the spacing between the stations in the pair.

Let  $\hat{C}_j = \Delta x_j \int_{-D_j}^0 C_j \rho_j dz$ , then,

$$\begin{aligned} B_3 &= \mathbf{C}^T \mathbf{b} \\ &= \mathbf{C}^T \left( \sum_{l=1}^k \alpha_l \mathbf{V}_l \right) \\ &= \sum_{l=1}^k \alpha_l \mathbf{C}^T \mathbf{V}_l \end{aligned} \quad (\text{B.7})$$

and

$$B_4 = \sum_{l=k+1}^N \alpha_l \mathbf{C}^T \mathbf{Q}_l. \quad (\text{B.8})$$

There are a number of sources of error in total flux  $F_c$ .

- The errors in  $B_1$  (flux due to relative velocity) can be due to:
  1. the noise in the hydrographic observations.
  2. the deviation of a particular section from the average, if  $F_c$  is interpreted as a time average
- The errors in  $B_2$  (flux due to other velocity components) can be due to:
  1. direct observational errors in the wind stress
  2. direct observational errors in the leakage rates or boundary current transports
- The errors in  $B_3$  (flux due to the reference level velocity) like  $B_1$  can be due to: can be due to:
  1. the noise in the hydrographic observations.
  2. the deviation of a particular section from the average, if  $F_c$  is interpreted as a time average
  3. the fact that  $\mathbf{b}$  may not be representative of the true reference level velocity field
- The errors in  $B_4$  (flux due to the unknown null-space vectors) can be due to:
  1. the noise in the hydrographic observations.

Given the same data and model constraints  $B_4$ , represents the difference between any one estimate of the flux and any other. This is because the set of vectors  $\{\mathbf{V}_l \mathbf{Q}_l\}$  form a complete set.

As shown in Appendix A, the SVD actually solves the problem,

$$\mathbf{A}'\mathbf{b}' + \mathbf{n} = -\mathbf{\Gamma}'.$$



The row weighting matrix  $\mathbf{S}$ , is defined in such a way that the elements of  $\mathbf{S}^{-1/2}\mathbf{\Gamma}$  have the same units and therefore, the same noise variance;  $\langle \mathbf{S}^{1/2}\mathbf{\Gamma} \rangle$ . As is often done, we have chosen to regard all units in the SVD as belonging to  $\lambda$ , leaving  $\mathbf{U}$  and  $\mathbf{V}$  unitless. In our case  $\lambda$  has units  $\text{km}^2$  (assuming that  $\rho \approx 1$ ). One needs to be careful that this is indeed the case. Weighting the matrix without regard for units can create confusing results. By our definition, the column weights  $\mathbf{W}^{-\frac{1}{2}}$  have no units, so that quantities such as  $\hat{\mathbf{C}}$  and  $\hat{\mathbf{C}} \mathbf{W}^{-\frac{1}{2}}$  have the same dimensions, namely concentration x  $\text{km}^2$ .

By way of example for the more complicated flux case, we first show the derivation for the unnormalized<sup>2</sup> solution variance  $\langle \mathbf{b}_i \mathbf{b}_j \rangle$ .

$$\begin{aligned}
\mathbf{b}'_j &= \sum_{l=1}^k \frac{\mathbf{U}_l^T(-\mathbf{\Gamma})}{\lambda_l} \mathbf{V}_{lj} \\
\langle \mathbf{b}'_i \mathbf{b}'_j \rangle &= \sum_{l=1}^k \sum_{m=1}^k \frac{\mathbf{V}_{li} \mathbf{V}_{mj}}{\lambda_l \lambda_m} \langle \mathbf{U}_l^T(-\mathbf{\Gamma}) \mathbf{U}_m^T(-\mathbf{\Gamma}) \rangle. \\
&= \sigma^2 \sum_{l=1}^k \sum_{m=1}^k \frac{\mathbf{V}_{li} \mathbf{V}_{mj}}{\lambda_l \lambda_m} \delta_{lm} \\
&= \sigma^2 \sum_{l=1}^k \frac{\mathbf{V}_{li} \mathbf{V}_{lj}}{\lambda_l^2}.
\end{aligned}$$

Since,

$$\mathbf{b}_j = (\mathbf{W}^{-\frac{1}{2}} \mathbf{b}')_j,$$

we can write,

$$\langle \mathbf{b}_i \mathbf{b}_j \rangle = \sigma^2 \sum_{l=1}^k \frac{(\mathbf{W}^{-\frac{1}{2}} \mathbf{V}_1)_i (\mathbf{W}^{-\frac{1}{2}} \mathbf{V}_1)_j}{\lambda_l^2} \quad (\text{B.9})$$

---

<sup>2</sup>In our notation:

- the unnormalized or unrotated variables are  $\mathbf{A}, \mathbf{b}, \mathbf{\Gamma}, \hat{\mathbf{C}}$
- the normalized or rotated variables are  $\mathbf{A}', \mathbf{b}', \mathbf{\Gamma}', \hat{\mathbf{C}}'$ .

Where, we have assumed,

$$\delta_{lm}\sigma^2 = \langle \mathbf{U}_l^T(-\Gamma)\mathbf{U}_m^T(-\Gamma) \rangle$$

In our most of models we have taken,

$$\begin{aligned} \sigma^2 &= \sum_{l=k+1}^M \frac{[\mathbf{U}_l^T(-\Gamma)]^2}{M - k} \\ &= \sum_{l=1}^M \frac{[\mathbf{A}\mathbf{b} + \Gamma]^2}{M - k}. \end{aligned}$$

Following the same steps, the variance of the flux of  $\hat{\mathbf{C}}$  belonging to the term  $B_3$  can be derived:

$$\begin{aligned} G^2 &\equiv \text{variance } \mathbf{F}_c = \langle (\sum_i \hat{\mathbf{C}}_i \mathbf{b}_i)^2 \rangle \\ &= \langle (\sum_i \hat{\mathbf{C}}_i \mathbf{b}_i)(\sum_j \hat{\mathbf{C}}_j \mathbf{b}_j) \rangle \\ &= \left\langle \sum_i \sum_j \left( \hat{\mathbf{C}}_i \sum_l \frac{\mathbf{U}_l^T(-\Gamma)}{\lambda_l} (\mathbf{W}^{-\frac{1}{2}} \mathbf{V}_1)_i \right) \times \left( \hat{\mathbf{C}}_j \sum_m \frac{\mathbf{U}_m^T(-\Gamma)}{\lambda_m} (\mathbf{W}^{-\frac{1}{2}} \mathbf{V}_m)_j \right) \right\rangle \\ &= \sum_i \sum_j \hat{\mathbf{C}}_i \hat{\mathbf{C}}_j \sum_l \sum_m \frac{(\mathbf{W}^{-\frac{1}{2}} \mathbf{V}_1)_i (\mathbf{W}^{-\frac{1}{2}} \mathbf{V}_m)_j}{\lambda_l \lambda_m} \langle \mathbf{U}_l^T(-\Gamma)\mathbf{U}_m^T(-\Gamma) \rangle \\ &= \sigma^2 \sum_i \sum_j \hat{\mathbf{C}}_i \hat{\mathbf{C}}_j \sum_l \frac{(\mathbf{W}^{-\frac{1}{2}} \mathbf{V}_1)_i (\mathbf{W}^{-\frac{1}{2}} \mathbf{V}_1)_j}{\lambda_l} \end{aligned} \quad (\text{B.10})$$

It is the square root of this value,  $G$ , which is referred to as the standard error associated with the flux.

To estimate the error in B4, that due to the lack of knowledge concerning the null-space vectors, we use the fact that the vectors  $\mathbf{V}_1$  and  $\mathbf{Q}_1$  form a complete orthonormal set. thus we can write:

$$\hat{\mathbf{C}} = \sum_{l=1}^k (\hat{\mathbf{C}}^T \mathbf{V}_1) \mathbf{V}_1 + \sum_{l=k+1}^J (\hat{\mathbf{C}}^T \mathbf{Q}_1) \mathbf{Q}_1. \quad (\text{B.11})$$

Using equation B.8 and assuming  $\mathbf{Q}_l^T \mathbf{Q}_m = \delta_{lm}$ , we can write the squared magnitude of  $B_4$ :

$$|B_4|^2 = \left| \sum_{l=k+1}^J \alpha_l \hat{\mathbf{C}}^T \mathbf{Q}_l \right|^2.$$

To take the weighting matrix  $\mathbf{W}^{-\frac{1}{2}}$  into account, let  $\mathbf{H} = \mathbf{W}^{-\frac{1}{2}} \hat{\mathbf{C}}$ , so that,

$$\begin{aligned} |B_4|^2 &= \left| \sum_{l=k+1}^J \alpha_l \mathbf{H}^T \mathbf{Q}_l \right|^2 \\ &\leq \sum_{l=k+1}^J |\alpha_l|^2 |\mathbf{H}^T \mathbf{Q}_l|^2 \\ &\leq \sum_{l=k+1}^J |\alpha_l|^2 (\mathbf{H}^T \mathbf{Q}_l \mathbf{Q}_l^T \mathbf{H}) \\ &\leq \left( \sum_{l=k+1}^J \alpha_l^2 \right) \sum_{l=k+1}^J (\mathbf{H}^T \mathbf{Q}_l \mathbf{Q}_l^T \mathbf{H}) \\ &\leq \left( \sum_{l=k+1}^J \alpha_l^2 \right) (\mathbf{H}^T \mathbf{Q}_l \mathbf{Q}_l^T \mathbf{H}) \\ &= \left( \sum_{l=k+1}^J \alpha_l^2 \right) \mathbf{H}^T \mathbf{H} \left( \frac{\mathbf{H}^T \mathbf{Q}_l \mathbf{Q}_l^T \mathbf{H}}{\mathbf{H}^T \mathbf{H}} \right) \\ &\equiv \left( \sum_{l=k+1}^J \alpha_l^2 \right) \mathbf{H}^T \mathbf{H} \Delta \end{aligned} \tag{B.12}$$

The 'null-space' error given in the tables is the magnitude by which  $F_c$  would change were the velocity vector ( $A_3 + A_4$ ) to change by 1 cm/s rms. It is not absolutely necessary to calculate the null-space vectors, since  $\Delta$  can be defined in terms of  $\mathbf{V}$ :

$$\Delta = \frac{\mathbf{H}^T \mathbf{Q} \mathbf{Q}^T \mathbf{H}}{\hat{\mathbf{C}}^T \hat{\mathbf{C}}} \tag{B.13}$$

$$\mathbf{Q} \mathbf{Q}^T + \mathbf{V} \mathbf{V}^T = 1 \tag{B.14}$$

so

$$\begin{aligned}\Delta &= \frac{\mathbf{H}^T(\mathbf{1} - \mathbf{V}\mathbf{V}^T)\mathbf{H}}{\mathbf{H}^T\mathbf{H}} \\ &= 1 - \frac{\mathbf{H}^T\mathbf{V}\mathbf{V}^T\mathbf{H}}{\mathbf{H}^T\mathbf{H}}\end{aligned}$$

$\mathbf{H}^T\mathbf{V}\mathbf{V}^T\mathbf{H}$  is the squared projection of  $\mathbf{H}$  onto the range of  $\mathbf{A}$ . If  $\Delta$  should vanish, which would either imply that the problem were fully determined so that there were no null-space, or that  $\mathbf{H}$  were completely orthogonal to the null-space, then the uncertainty due to  $B_4$  would be zero. It is usually found that the projection of  $\mathbf{H}$  onto the null-space is non-zero, but small.

Recreating the example given by WHG, using values found in this text, we can show that a small projection onto the null-space implies that reasonable changes in the computed flux estimates, would require unreasonable changes in the reference level velocities.

The units of  $\alpha_l$ , the expansion coefficients are km/sec. Therefore, an rms null-space velocity of 1 cm/sec gives:  $\sum_{l=k+1}^J |\alpha_l|^2 = 1 \times 10^{-10} \text{ (km}^2/\text{sec}^2) / \text{(cm/sec)}$  rms null-space velocity.

Consider the heat flux equation at 43°S for model P3 at rank 26:

$$J - k = 211 - 26 = 185$$

$$\Delta = 0.009$$

$$\mathbf{H}^T\mathbf{H} = 1.098 \times 10^7 .$$

An rms null-space velocity of 1 cm/sec, will produce a heat flux less than or equal to  $[(185 \times 10^{-10}) \text{ km}^2/\text{sec}^2 \times (0.009) \times (1.098 \times 10^7) \text{ }^\circ\text{C}^2\text{km}^4]^{1/2}$

$$= 4.2 \times 10^{-2} \text{ km}^3 \text{ }^\circ\text{C}/\text{sec}$$

$$= 4.2 \times 10^6 \text{ m}^3/\text{sec}$$

$$= 1.8 \times 10^{14} \text{ W}$$

The bulk formula calculations have produced heat flux values on the order of a 1 PW. There would have to be an increase of  $10^{15}/1.8 \text{ cm/sec} = 6 \text{ cm/sec}$  in the rms reference level velocity to produce so large a heat flux. This value, although not out of the realm of possibility, appears unlikely<sup>3</sup> and therefore, unless there is reason to change the constraints used in the inverse, heat flux values of such magnitude must be considered inconsistent with our data.

---

<sup>3</sup>The rms reference level velocities for all the Pacific models were less than 1 cm/sec.

## Appendix C

### Column Weighting for 18°S Section

This appendix explains how the disparity in the flux uncertainties of the two sections in the Indian Ocean led to an extra column weighting for the stations in the 18°S section.

The uncertainty in the flux at the 31°S section in the Indian Ocean was calculated as:

$$\begin{aligned}\sigma_{31} &= (\sigma_{section}^2 + \sigma_{ekman_{31}}^2)^{1/2} \\ &= (1^2 + 2.2^2)^{1/2} \\ &= 2.69\end{aligned}$$

where:

$\sigma_{section}$  is the 1 Sv error within which we have assumed we can compute a flux across a section,

$\sigma_{ekman_{31}}$  is the error assigned to the Ekman transport at 31°S, estimated from the variance in the annual wind stress values across the section.

The uncertainty in the flux at the 18°S section in the Indian Ocean was calculated as:

$$\begin{aligned}
 \sigma_{31} &= (\sigma_{section}^2 + \sigma_{ekman18}^2 + \sigma_{mozambique}^2)^{1/2} \\
 &= (1^2 + 7.6^2 + 13.5^2)^{1/2} \\
 &= 15.52
 \end{aligned}$$

This disparity in the flux uncertainties had an undesired affect on the relative solution sizes at the two latitudes. Given a section with an uncertainty of the order of about  $1-4 \times 10^9$  kg/sec , as is the case in the two Pacific sections, the column norm weights tend to be dominated by the flux equation values. In other words, the column norm weight tends to make the flux equations order 1, while making the elements of layer constraints quite a bit less than 1. As long as this is true for both sections there is no problem.

In the 18°S section, the column norms are not dominated by the flux equations due of the large uncertainty in the fluxes. This occurs because the rows have already been divided by their uncertainty before the column norms are computed. As a result the elements in the rows of the **A** matrix associated with the layers tend to be of order 1. In the 31°S section, as the Pacific, these elements are  $\ll 1$ . Since the 18°S columns contains larger values than the 31°S columns, the SVD tends to use the 18°S data first as it can make relatively large changes in the residuals for relatively small cost in the solution size. As explained in Chapter 2, this results in larger, better resolved  $\mathbf{b}_j$  at 18°S, with smaller, less well resolved  $\mathbf{b}_j$  at 31°S.

This is not the affect desired from the column normalization. We see no physical reason for the solution to be larger in one section compared to the other. This is the same as saying, we see no reason for the 18°S section to be better resolved than the 31°S section. The decision was therefore made, to downweight the 18°S

section by a factor which would produce solutions of similar resolution for both sections.



## REFERENCES

- Baumgartner, A. and E. Reichel (1975) *The World Water Balance*. Elsevier Scientific Pub. Co., N.Y., 179 pp.
- Bennett, A. F. (1978) Poleward heat fluxes in southern hemisphere oceans. *J. Phys. Oceanogr.*, **8**, 785–798.
- Berner E.K. and R.A. Berner (1987) *The Global Water Cycle*. Prentice–Hall, Inc., Englewood Cliffs, New Jersey pp. 397.
- Boland F.M. and B.V. Hamon (1970) The East Australian Current 1965–1968. *Deep Sea Res.*, **17**, 777–794.
- Broecker, P.G. and T.H. Peng (1982) *Tracers in the Sea*. Lamont-Doherty Geological Observatory, Columbia University, Palisades, N.Y., 690 pp.
- Bryan K. (1962) Measurements of meridional heat transport by ocean currents. *J. Geophys. Res.*, **67**, 3403–3414.
- Bryan K. (1982) Poleward heat transport by the ocean: observations and model. *Ann. Rev. Earth Planet. Sci.*, **10**, 15–38.
- Bryden, H.L., D.H. Roemmich and J.A. Church (1990) Heat transport across 24°N in the Pacific. Accepted for publication in *Deep Sea Res.*
- Bunker A.F. (1988) Surface energy fluxes of the South Atlantic Ocean. *Monthly Weather Review*, **116**, 809–823.
- Carissimo, B.C., A.H. Oort and T.H. Vonder Haar (1985) Estimating the meridional energy transports in the atmosphere and ocean. *J. Phys. Oceanogr.*, **15**, 82–91.
- Coachman, L.K. and K. Aargaad (1988) Transports through the Bering Strait: annual and interannual variability. *J. Geophys. Res.*, **93** (C12), 15,535–15,539.
- Duncan C.P. (1970) The Agulhas Current, Phd Dissertation, University of Hawaii, 76 pp.
- Fiadiero, M.E.M., (1975) Numerical modelling of tracer distribution in the deep Pacific Ocean. Ph.d. thesis, University of California, San Diego, 226 pp.
- Fiadiero, M.E.M. and H. Craig (1978) Three–dimensional modeling of tracers in the deep Pacific Ocean: I. Salinity and oxygen. *J. Mar. Res.*, **36**, 326–355.

- Fine, R.A. (1985) Direct evidence using tritium data for throughflow from the Pacific into the Indian Ocean. *Nature*, **315**, 478–480.
- Fonesca, T. (1989) An overview of the poleward undercurrent and upwelling along the Chilean Coast. *Poleward Flows along Eastern Ocean Boundaries*. In: *Coastal and Estuarine Studies*, **34**. S.J. Neshyba, Ch.N.K. Mooers, R.L. Smith and R.T. Barber (Eds.), Springer-Verlag, New York, NY, 203–218.
- Fu, L. (1986) Mass, heat and freshwater fluxes in the South Indian Ocean. *J. Phys. Oceanogr.*, **16**, 1683–1693.
- Fu, L. (1981) The general circulation and meridional heat transport of the subtropical South Atlantic determined by inverse methods. *J. Phys. Oceanogr.*, **11**, 1171–1193.
- Georgi, D.T. and J.M. Toole (1982) The Antarctic Circumpolar Current and the oceanic heat and freshwater budgets. *J. Mar. Res.*, **40**(Suppl.), 183–197.
- Godfrey, S. and T.J. Golding, (1981) The Sverdrup relation in the Indian Ocean, and the effect of Pacific-Indian Ocean through flow on Indian Ocean circulation and an the east Australian Current. *J. Phys. Oceanogr.*, **11**, 771–779.
- Godfrey, S. and Ridgeway (1984) Seasonal behavior and possible mechanism of Leeuwin Current, Western Australia. *Trop. Ocean Atmos. Newsletter*, **26**, 16–17.
- Gordon, A.L. (1985) Indian–Atlantic transfer of thermocline water at the Agulhas retroflection. *Science*, **227**, 1030–1033.
- Gordon, A.L. (1986) Interocean exchange of thermocline water. *J. Geophys. Res.*, **91**, 5037–5046.
- Gordon, A.L. and W.F. Haxby (1990) Agulhas eddies invade the South Atlantic: evidence from Geosat altimeter and shipboard conductivity–temperature–depth survey. *J. Geophys. Res.*, **95**, 3117–3125.
- Gordon, A.L. and Molinelli (1982) *Southern Ocean Atlas*. Columbia University Press, New York.
- Han, Y–J., and S.W. Lee (1981) A new analysis of monthly mean wind stress over the global ocean. *Climatic Research Institute Report No. 26*, Oregon State University, 148 pp.
- Harris, T.F.W. (1972) Sources of the Agulhas Current in the spring of 1964. *Deep Sea Res.*, **19**, 633–650.

- Hastenrath, S. (1980) Heat budget of the tropical ocean and atmosphere. *J. Phys. Oceanogr.*, **10**, 159–170.
- Hastenrath, S. (1982) On meridional heat transports in the world ocean. *J. Phys. Oceanogr.*, **12**, 922–927.
- Hogg, N.G., P. Biscaye, W. Gardner and W.J. Schmitz, Jr. (1982) On the transport and modification of Antarctic Bottom Water in the Vema Channel. *J. Mar. Res.*, **40** (Suppl.), 231–263.
- Hsuing J. (1985) Estimates of global oceanic meridional heat transport. *J. Phys. Oceanogr.*, **15**, 1405–1413.
- Hsuing J., R.E. Newell and T. Houghtby (1989) The annual cycle of oceanic heat storage and oceanic meridional heat transport. *Quart. J. Roy. Meteor. Soc.*, **115**, 1–28.
- Lutjeharms J.R.E. and H.R. Valentine (1984) Southern Ocean thermal fronts south of Africa. *Deep Sea Res.*, **31** (12), 1461–1475.
- Luyten J. and H. Stommel (1982) Recirculation reconsidered. *J. Mar. Res.*, **40**(Suppl.), 407–426.
- McCartney M. (1977) Subantarctic Mode Water, *A Voyage of Discovery*, M. Angel (ed.), Pergamon Press, 103–119.
- McDougall, T.J. (1987) Thermobaricity, cabbeling and water-mass conversion. *J. Geophys. Res.*, **92**, 5448–5464.
- Metzl, N., B. Moore and A. Poisson (1990) Resolving the intermediate and deep advective flows in the Indian Ocean by using temperature, salinity, oxygen and phosphate data: the interplay of biogeochemical and geophysical tracers. *Palaeoeco., Palaeoclim., Palaeoecol.* **89**, 81–111.
- Minster J-F and M. Boulahdid (1987) Redfield ratios along isopycnal surfaces – a complementary study. *Deep Sea Res.*, **34** 1981–2003.
- Miranda L.B. and B.M. Castro Filho (1982) Geostrophic flow conditions of the Brazil Current at 19°S. *Ciencia Interamericana*, **22**, 44–48.
- Murray, S.P. and D. Arief (1988) Throughflow into the Indian Ocean through Lombok Strait. *Nature*, **333**, 444–447.
- Oort, A, H., and T.H. Vonder Haar (1976) On the observed annual cycle in the ocean-atmosphere heat balance over the northern hemisphere. *J. Phys. Oceanogr.*, **6**, 781–800.

- Peterson R.G. and L. Stramma (1991) Upper-level circulation in the South Atlantic Ocean. *Progress in Oceanography*, **26**, (1), 1–73.
- Philander and Pacanowski (1986) The mass and heat budget in a model of the tropical Atlantic Ocean. *J. Geophys. Res.*, **91**, 14212–14220.
- Pond S. and G.L. Pickard (1983) *Introductory Dynamical Oceanography*, Pergamon Press, New York, 329 pp.
- Pickard, G.L. and W.J. Emery (1982) *Descriptive Physical Oceanography*, Pergamon Press, New York, 249 pp.
- Piola, A.R. and A.L. Gordon (1984) Pacific and Indian Ocean upper-layer salinity budget, *J. Phys. Oceanogr.*, **14**, 747–753.
- Physical and Chemical Data Facility (1988) South Atlantic Ventilation Experiment, Preliminary Shipboard Physical and Chemical Data Report. Pub. No. 225, Scripps Institute of Oceanography, University of California, San Diego.
- Redfield, A.C., B.H. Ketchum and F.A. Richards (1963) The influence of organisms on the composition of sea-water. *The Sea*, Vol. **2**, M.N. Hill (ed.), Interscience, New York, NY, 26–77.
- Reid, J.L., Jr. (1965) Intermediate waters of the Pacific Ocean. *Johns Hopkins Oceanogr. Stud.*, **5**, 96 pp.
- Reid, J.L., Jr. (1973) Transpacific hydrographic sections at Lats 43°S and 28°S: The *Scorpio* Expedition -III. – Upper water and a note on southward flow at mid-depth. *Deep Sea Res.*, **20**, 39–49.
- Reid, J.L., Jr. (1981) On the mid-depth circulation of the world ocean. *Evolution of Physical Oceanography*, The MIT Press, Cambridge, pp. 70–111.
- Reid, J.L., Jr. (1986) On the total geostrophic circulation of the South Pacific Ocean, flow patterns, tracers and transports. *Progress in Oceanography*, **16**, 1–61.
- Reid, J.L., Jr. (1989) On the total geostrophic circulation of the South Atlantic Ocean, flow patterns, tracers and transports. *Progress in Oceanography*, **23**, (3), 149–244.
- Rintoul S.R. (1988) Mass, heat and nutrient fluxes in the Atlantic Ocean determined by inverse methods. Ph.D. thesis, MIT/WHOI, 287 pp.
- Rintoul S.R. (1991) South Atlantic Interbasin Exchange. *J. Geophys. Res.*, **96**, 2675–2692.

- Roemmich D., (1983) The balance of geostrophic and Ekman transports in the tropical Atlantic Ocean. *J. Phys. Oceanogr.*, **13**, 1534–1539.
- Roemmich D., (1980) The application of inverse methods to problems in ocean circulation. Ph.D. thesis, MIT/WHOI, 193 pp.
- Russel G.L., J.R. Miller and L.C. Tsang (1985) Seasonal oceanic heat transports computed from an atmospheric model. *Dyn. Atmos. Ocean.*, **9**, 253–271.
- Sarmiento (1986) On the north and tropical Atlantic heat balance. *J. Geophys. Res.*, **91**, 11677–11689.
- Saetre, R. and A.J. Da Silva (1984) The circulation of the Mozambique Channel. *Deep Sea Res.*, **31**, (5), 485–508.
- Schott, F., and H. Stommel (1978) Beta-spirals and absolute velocities in different oceans. *Deep Sea Res.*, **25**, 961–1010.
- Smith, R.L., A. Huyer, J.S. Godfrey and J.A. Church (1991) The Leeuwin Current off western Australia, 1986–1987. *J. Phys. Oceanogr.*, **21**, 323–345.
- Stommel, H. and A.B. Arons (1960) On the abyssal circulation of the world ocean-II. An idealized model of the circulation pattern and amplitude in oceanic basins. *Deep Sea Res.*, **6** 217–233.
- Stommel, H., E.D. Stroup, J.L.Reid and B.A. Warren (1973) Transpacific hydrographic sections at Lats 43°S and 28°S: The *Scorpio* Expedition -I. Preface. *Deep Sea Res.*, **20**, 1–7.
- Svedrup, H.U., M.W. Johnson and R.H. Fleming (1942) *The Oceans – Their Physics, Chemistry and General Biology*. Prentice-Hall, Englewood Cliffs, NJ, 1087 pp.
- Talley L. (1984) Meridional heat transport in the Pacific Ocean. *J. Phys. Oceanogr.*, **14**, 231–241.
- Tchernia P. (1980) *Descriptive Regional Oceanography*. Pergamon Press, New York, 253 pp.
- Thompson R.O.R.Y. (1984) Observations of the Leeuwin Current off Western Australia. *J. Phys. Oceanogr.*, **14**, 623–628.
- Thompson R.O.R.Y. and G.Veronis (1980) Transport calculations in the Tasman and Coral Seas. *Deep Sea Res.*, **27**, 303–323.

- Toole, J.M. and M.E. Raymer (1985) Heat and fresh water budgets of the Indian Ocean - revisited. *Deep Sea Res.*, **32**, (8), 917–928.
- Trenberth, K.E. (1979) Mean annual poleward energy transport by oceans in the Southern Hemisphere. *Dyn. Atmos. Oceans*, **4**, 57-64.
- Tsuchiya P. (1986) Thermostads and circulation in the upper layer of the Atlantic Ocean. *Progress in Oceanography*, **16**, 235–267.
- Warren, B.A., (1973) Transpacific hydrographic sections at Lats 43°S and 28°S: The *Scorpio* Expedition -II. Deep Water. *Deep Sea Res.*, **20**, 9–38.
- Warren, B.A., (1976) Structure of deep western boundary currents. *Deep Sea Res.*, **23**, 129-142.
- Warren, B.A., (1981a) The deep circulation of the world ocean. *Evolution of Physical Oceanography*, The MIT Press, Cambridge, pp. 6–41.
- Warren, B.A., (1981b) Transindian hydrographic section at Lat. 18°S: Property Distributions and circulation in the South Indian Ocean. *Deep Sea Res.*, **28a**, (8), 759–788.
- Weare, B.C., P.T. Strub and M.D. Samuel (1981) Annual mean surface heat fluxes in the tropical Pacific Ocean. *J. Phys. Oceanogr.*, **11**, 705–717.
- Weaver, A.J. (1990) Ocean currents and climate. *Nature*, **347** 432.
- Wiggins, R.A (1972) The general linear inverse problem: Implication of surface waves and free oscillations for earth structure. *Rev. Geophys. Space Phys.*, **10**, 251–285.
- Wooster, W.S. and J.L. Reid (1963) Eastern boundary currents. *The Sea*, Vol. **2**, M.N. Hill (ed.), Interscience, New York, NY, 253-256.
- Wunsch, C. (1978) The general circulation of the North Atlantic west of 50°W determined from inverse methods. *Rev. Geophys. Space Phys.*, **16**, 583–620.
- Wunsch, C., D. Hu and B. Grant (1983) Mass, heat and nutrient fluxes in the South Pacific Ocean. *J. Phys. Oceanogr.*, **13**, 725–753.
- Wyrtki, K. (1961) Physical oceanography of the Southeast-Asian Waters. NAGA Rep. No. 2. Scripps Institution of Oceanography, 195 pp.
- Wyrtki, K. (1973) *Physical oceanography of the Indian Ocean, ecological studies, analysis and synthesis*, **3**, B. Zeitzshel ed., Springe-Verlag, 18–36.

Wyrтки, K. (1987) Indonesian through flow and the associated pressure gradient. *J. Geophys. Res.*, **92**, 12941-12946.

Wyrтки, K. (1988) *Oceanographic Atlas of the International Indian Ocean Expedition*, Amerind Publishing Co., New Dehli.